The Pennsylvania State University

The Graduate School

Department of Aerospace Engineering

AN INVESTIGATION OF PERFORMANCE BENEFITS AND TRIM REQUIREMENTS OF A VARIABLE SPEED HELICOPTER ROTOR

A Thesis in

Aerospace Engineering

by

Jason H. Steiner

Submitted in Partial Fulfillment
of the Requirements
for the Degree of

Master of Science

August 2008

The thesis of Jason Steiner was reviewed and approved* by the following:

Farhan Gandhi
Professor of Aerospace Engineering
Thesis Advisor

Robert Bill
Research Associate , Department of Aerospace Engineering

George Leisuietre
Professor of Aerospace Engineering
Head of the Department of Aerospace Engineering

*Signatures are on file in the Graduate School

ABSTRACT

This study primarily examines the main rotor power reductions possible through variation in rotor RPM. Simulations were based on the UH-60 Blackhawk helicopter, and emphasis was placed on possible improvements when RPM variations were limited to ± 15% of the nominal rotor speed, as such limited variations are realizable through engine speed control. The studies were performed over the complete airspeed range, from sea level up to altitudes up to 12,000 ft, and for low, moderate and high vehicle gross weight.

For low altitude and low to moderate gross weight, 17-18% reductions in main rotor power were observed through rotor RPM reduction. Reducing the RPM increases rotor collective and decreases the stall margin. Thus, at higher airspeeds and altitudes, the optimal reductions in rotor speed are smaller, as are the power savings. The primary method for power reduction with decreasing rotor speed is a decrease in profile power. When rotor speed is optimized based on both power and rotor torque, the optimal rotor speed increases at low speeds to decrease rotor torque without power penalties. Optimization at high flight speeds shows that both power- and torque-weighted optimums occur at the same rotor speeds. This trend is independent of vehicle gross weight. For very high gross weight and high altitude operations, the flight envelope can be expanded by increasing the rotor speed, preventing rotor stall.

Shaft torque was not seen to increase appreciably for moderate and high speed flight, with only a small increase in low speed flight. Main rotor collective pitch was seen to increase as rotor speed decreased to maintain thrust. In addition to main rotor collective pitch, main rotor longitudinal cyclic pitch was seen to increase at moderate to high cruise speeds when the rotor RPM was reduced. Blade coning also increased as RPM decreased due to reduction in centrifugal force, though first harmonic flapping angles remained nearly the same.

TABLE OF CONTENTS

LIST OF FIGURES

LIST OF TABLES

LIST OF SYMBOLS

θ	Local blade pitch
α	Local angle of attack
ψ	Rotor azimuth angle
β	Rotor flapping angle
ϕ_l	Local inflow angle
I_β	Blade flapping moment of inertia
θ_0	Collective pitch
θ_{1C}	Lateral cyclic pitch
θ_{1S}	Longitudinal cyclic pitch
β_0	Rotor coning angle
β_{1C}	Longitudinal flapping angle
β_{1S}	Lateral cyclic flapping
α_{wl}	Fuselage angle of attack
α_{shaft}	Shaft angle of attack
ϕ	Vehicle roll angle
ϕ_{tr}	Tail rotor roll angle offset
μ	Main rotor advance ratio
μ_{tr}	Tail rotor advance ratio
$[^*]$	Frequency non-dimensionalized by rotor speed
S_{ht}	Tail planform area
D_{ht}	Horizontal Tail Drag
L_{ht}	Horizontal Tail Lift
$L_{fuselage}$	Fuselage lift
$D_{fuselage}$	Fuselage Drag
R	Main rotor radius
R_{tr}	Tail rotor radius
Ω	Main rotor speed (rad / s)
Ω_{tr}	Tail rotor speed (rad / s)

ACKNOWLEDGEMENTS

There are many people that I need to thank for their patience, support and encouragement in undertaking my graduate education. First I would like to thank my advisor, Dr. Gandhi, for giving me the opportunity to continue my focus on rotorcraft technology at the graduate level. His knowledge and ideas have allowed me to take the next step in my life, and to hopefully advance the state of rotorcraft technology. I would also like to thank Dr. Bob Bill for his assistance throughout the process, from helping with the understanding of helicopter drive systems to proofreading and helping to improve my thesis. I would like to thank my manager at the Boeing V/STOL Wind Tunnel for his patience inletting me pursue this degree and for keeping my job open while I was away. Of course, none of this would have been possible without the funding support of the Office of Naval Research who sponsored this project.

I need to thank all of my fellow graduate students who have had an impact on this research and my life over the last two years. I want to thank Jamie Bluman helping make this helicopter model work and for helping me work through the problems. Oliver Leon and Eui Sung Bae were very helpful in ensuring my results made sense, and how to improve them. I would also like to thank Dr. Horn, Wei Guo, and Zihni Saribay for comparing notes and helping me see the overall picture.

Lastly I want to thank my family and friends for all their help. I could never have accomplished this without their encouragement. To my mother LouAnn and brother Trevor, I want to say thank you! Special thanks and acknowledgement go out to Russ Rufino, Pam Montanye, Conor Marr, Mihir Mistry and Sean Marlow for all the troubleshooting, proofreading, editing, and friendship they have provide

Chapter 1

Introduction

Helicopter power requirements are a major source of interest and research. Unlike their fixed wing counterparts, helicopters must produce both lift and drag through the rotor. This active thrust production results in a much higher power to weight ratio than that of an airplane. Also unlike an airplane's lift, helicopter lift cannot be increased simply by increasing airspeed, because collective pitch is the primary means of increasing rotor thrust. Rotor blade stall enforces the maximum thrust. The ability to simultaneously reduce helicopter required power in some portions of the flight envelope and to expand the flight envelope by delaying the onset of rotor stall would be a valuable contribution to the industry. The most straightforward and practical way to achieve both of these goals is to vary the main rotor rotational speed for different flight conditions.

Background of Variable Speed Rotors

The idea of changing the rotor speed on a helicopter is not a new idea. In fact it is commonly seen today, but not in manned helicopters: Radio-controlled helicopters have used variable rotor speed to increase thrust for a long time. The famous science fiction writer Robert A. Heinlein refers to increasing rotor speed to generate additional thrust for a rapid takeoff in his novel *Gulf*. Aside from this application in entertainment there has been some significant progress in understanding and applying variable rotor speeds in helicopter design. The previous research in the area of variable speed rotors falls into a few well-defined areas: conventional helicopters, tilt-rotors, slowed-rotor compound helicopters and also as an actuation mechanism for variable span rotors.

Optimum Speed Rotor

The most significant research to date into variable speed rotors is the Optimum Speed Rotor by Abraham Karem [1]. This details a helicopter design implementing a power-optimized rotor speed throughout the flight envelope. The patent is for a lightweight helicopter with a tailored rotor planform and twist distribution that provides for significant power reduction over much of the flight envelope. It also shows that the flight envelope is extended to higher speeds in forward flight due to the lower power requirements.

One aspect of this patent that must be noted is that the physical rotor design used was much larger than the baseline helicopter. This makes it likely that some portion of the observed power reduction is due directly to the changes in blade planform, twist and length. Since the baseline rotor is a rectangular planform rotor with minimal Twist, a single change in geometry could yield power improvements, and a combination of these could yield large improvements. With a larger rotor diameter, a slower rotor speed would produce the same tip speed. The patent shows that the range of tip speed, normalized by the baseline, ranges from 0.48 to 1.0. This very large range is difficult to grasp unless one understands that the larger rotor diameter, and thus rotor planform area, is so much larger that the rotor can still produce the required lift and thrust even with such a dramatically reduced rotor speed. Despite the undefined impacts of the change in geometry, the benefits are significant enough to warrant more studies on variable rotor speed for a conventional helicopter.

Variable Span Rotor

Variable rotor speed has also been discussed by Prabhakar et al [2] in his paper on variable span rotor blades. The rotor rotational speed change is used as an actuator by varying the centrifugal force of the outer portion of a

telescoping blade which is restrained by a linear spring. Thus, as the rotor speed is increased, the centrifugal force will increase as well, resulting in blade extension. Similarly, the reduction in rotor speed would result in a reduced diameter. This concept is especially useful with the addition of a locking mechanism that would allow the rotor to be spun up to a high rotational speed; after locking the blade in place, the rotor could be slowed down to take advantage of the power reductions.

Though the paper primarily addresses the effects of varying rotor diameter, it does include results relating to performance solely as a function of rotor speed in hovering flight. The first observed effect of variable RPM with a fixed span is that it is possible to fly with a significantly reduced tip speed in hover. Since the onset of stall is sufficiently far from the baseline weight at the baseline rotor speed, reducing the rotor speed of this model still allowed the vehicle to hover without stalling. This is an important observation because most airfoils used for helicopter rotors have little profile drag sensitivity to angle of attack while not approaching the stall angle. Thus, reducing the rotor speed would, in theory, reduce profile power. The paper does not address this condition directly but alludes to the possible power reduction through lower rotor speeds by showing that increasing rotor speed with a fixed span will increase power required above the baseline for the same thrust requirements.

Bell-Boeing V-22 Osprey

In addition to the research performed for a conventional helicopter design discussed above, the principles of variable rotor speed have been implemented on the Bell – Boeing V-22 Osprey. This tiltrotor design takes advantage of variable rotor speed to make the prop-rotors more efficient in forward flight. Since the rotor is, in essence, responsible for helicopter performance in low speed flight and acts as a propeller in forward flight, the rotational speed is critical to optimize performance. For the V-22, the rotor speed is reduced from 412 RPM when the

vehicle is in hover mode to 333 RPM in airplane mode. This yields a more efficient propeller for forward flight. This rotor speed reduction is the result of a decrease in engine speed.

Compound Helicopters

Compound helicopters show a marked improvement when using a slowed rotor in forward flight. Compound helicopters are a hybrid between an airplane and a helicopter. In hover and low speed flight, compound helicopters use the main rotor for lift and thrust. In high speed flight, the wings provide the lift, and an auxiliary propulsion method is used for forward thrust. In this high speed situation the rotor is no longer productive and becomes a significant source of drag. According to Floros and Johnson [3], reducing the rotor speed reduces rotor drag significantly, allowing for higher forward speeds and lower power requirements. Jay Carter, in a presentation to the 2003 AHS Annual Forum [4], detailed a design for a slowed rotor compound called the “Carter Copter.” This design utilizes a wing for lift in forward flight and auxiliary propellers to provide the thrust and anti-torque. The compound has a maximum advance ratio of 0.83 with the rotor spinning at 115 RPM. These advance ratios are much higher than would be expected for any conventional helicopter, but it shows that reducing rotor speed can result in impressive performance gains.

Helicopter Controls

Rotor speed variation and control can also be used to augment the traditional swashplate-based helicopter controls. A study by Chen [5] addressed the increased effectiveness of conventional controls in a helicopter with a varying rotor speed. Tankori and Rock [6] discussed the implementation of a rotor speed control as an additional control system parameter and its use in maneuvering.

According to Chen [5], the responsiveness of a helicopter to a fixed set of control inputs is dependent upon the rotor speed. Specifically, increasing rotor RPM improves the response of the aircraft to control inputs. Chen stipulates that a variable speed rotor has a better gust response than a typical constant RPM model. He also addresses a possible negative attribute of variable speed rotors: vibration. The first torsional mode of the aircraft frame is affected by variation in rotor speeds as this mode is influenced by the gearbox torque response. This presents a possible problem in designing a variable speed rotor, but does not make such a concept impossible.

Using rotor control as an additional control parameter, as shown in Tankori and Rock [6], shows a marked improvement in response time for a bob-up maneuver. This concept requires a rotor speed control loop dependent on rotor torque, to control the rotor speed as a function of the control system. This shows promise for designing more nimble and agile VTOL aircraft in the future. Another implementation of a variable rotor speed for vehicle control is introduced by Yoshizaki [7]. This study uses a variable rotor speed coupled with a moving center of gravity to control the aircraft. This control method replaces the traditional swashplate controls. It was found that varying the rotor speed of a pitch indexed lightweight helicopter between 500 and 600 RPM can replace collective pitch control through the swashplate.

Slowing the rotor in forward flight has its own control-related issues. A NASA wind tunnel study conducted on high advance ratio rotors showed that at advance ratios in excess of approximately 0.93, rotor controls became inverted relative to low advance ratio flight [8]. This means that to increase thrust at these speeds, the collective would actually be lowered. At advance ratios at or around 0.92 it was revealed that the rotor had little or no response to control inputs. In such a case, the rotor is essentially uncontrollable without the ability to vary the speed.

Stability

While the benefits of a variable speed rotor with regards to power and control systems have been addressed, such a helicopter would be of little use if the vehicle was not stable at advance ratios higher than the typical 0.35. Floros and Johnson [9] examine the effects of variable rotor speed and high advance ratio flight using simple helicopter models, rigid blade analysis and elastic blade analysis in CAMRAD II.

The analysis concerns flap stability and the effect of high speed forward flight on flap damping. Teetering, gimbaled and articulated rotors were examined, with varying levels of pitch flap coupling. Rigid blade analysis, using both a linear model and more rigorous analysis in CAMRAD II showed that teetering rotors were the most stable design. Articulated rotors had more instability, but this could be minimized by increasing pitch flap coupling through the δ_3 angle. An angle of 30 degrees resulted in the best stability maps. The gimbaled rotor showed more stability problems than either the teetering or articulated design. Instability occurred for this rotor at an advance ratio of 1.5 for no pitch flap coupling. The maximum advance ratio again occurred at a δ_3 angle of 30 degrees, but this allowed only a maximum advance ratio of 2. Elastic analysis of the teetering rotor revealed a more complex stability situation. When elastic blade motion was included in the analysis, the vehicle became unstable in flapping at an advance ratio of 1.5, unlike the rigid blade model. This does not change with varying torsional frequencies, making such an advance ratio an effective stability boundary in the case of a typical blade. The authors suggest that using a much stiffer blade may push the boundary to a higher ratio.

Proposed Concept

The concept of a variable speed rotor applied to a conventional UH-60 helicopter model will be investigated using a trim simulation program. The effect

of a variable speed main rotor will on rotor power will be investigated. It is expected that rotor speed will have large effects on main rotor power. The combination of rotor speed and airspeed is an essential component in predicting main rotor power and also forms the basis of developing optimal rotor speed schedules and patterns. Vehicle airspeed will range from hover to 180 knots.

Vehicle weight and operating altitudes are also important factors in helicopter performance. As gross weight increases, the rotor must produce more thrust, thus increasing the amount of power consumed. At high altitudes, the available engine power decreases while the air density decreases, making rotor stall more likely.

The helicopter model will employ a conventional swashplate control system, so the impact of varying rotor speed on control a parameters will be monitored. Main rotor collective and cyclic pitch will be emphasized. These parameters are the core control parameters to a conventional aircraft and it is expected that varying rotor speed will result in these values changing. Since reduced rotor speed increases the likelihood of blade stall, non-linear airfoil data will be used

Chapter 2

Model and Analysis Methods

Basic Helicopter Model

Operating Requirements

Helicopters are amazingly versatile vehicles. They can take off and land vertically, carry heavy loads from one place to another - either inside or outside of the aircraft - and quickly and precisely carry passenger to remote destinations. This is because the helicopter actively produces all of the requisite thrust and lift through the rotor, unlike a conventional fixed-wing aircraft. No runways are needed for takeoff and landing, and helicopters are capable of hovering in place instead of flying a holding pattern. These capabilities come at a price, however, as the helicopter must rely on complicated aerodynamic environments and sophisticated mechanical systems.

One of the difficulties in helicopter design is that the helicopter must maintain lift, forward thrust, and attitude control though the main rotor in hover and in forward flight regimes. This results in design compromises so that the helicopter can operate with good efficiency in all relevant ranges. Otherwise it would perform very well in one area, like forward flight, while suffering in another, like hover. Advances in modeling and blade tailoring have made it easier to design aircraft that perform better in certain regimes, but there are still compromises to accommodate the varied operating environments.

The focus of this research is to reduce the effects these compromises have on helicopter performance by allowing rotor speed to vary. This additional

operating parameter could make operation at off-design airspeeds and altitudes more efficient with the existing rotor and fuselage designs.

Model

The helicopter model is based on the design parameters and the aerodynamic properties and of the UH-60A. The model was developed at the Vertical Lift Research Center of Excellence at The Pennsylvania State University in conjunction with James Bluman [10]. The model is aimed at predicting the important properties of the helicopter with versatility and minimal computation time.

This helicopter was chosen for its conventional design and utility uses. The helicopter is widely used in the military for various different missions including carrying external cargo such as Humvees and transporting troops inside the operating theater. By allowing the helicopter to operate more efficiently in all conditions, the usefulness of this vertical lift platform could be expanded.

Aerodynamic Environment

The helicopter rotor experiences aerodynamic phenomena that do not occur with fixed-wing airplanes. On an airplane, the lifting surfaces - the wings and canard or tail - experience relatively constant air velocities that are primarily dependent upon the airspeed. The rotor blades produce lift by rotating and thus induce their own airspeed over the airfoils. The velocity distribution is more complicated. In hover, the encountered airspeeds are symmetric about the rotor hub. The local airspeeds on the blade are linearly increasing based on distance from the center of rotation as in Equation 2.1. Equation 2.2 shows that local airspeed ceases to be symmetric as the forward speed of the aircraft adds to the

local airspeed on the advancing blade, or subtracts from the local airspeed on the retreating blade.

$$V_{local} = (\Omega R)(r), (0 \le r \le 1) \quad \text{Eq. 2.1}$$

$$V_{local} = (\Omega R)(r + \mu \sin\psi) \quad \text{Eq. 2.2}$$

This non-uniformity of airspeed across the blade, in hover and in forward flight, results in an even more widely varying dynamic pressure. Since lift is proportional to the dynamic pressure, the lift shows large variations along the blade. This results in large differentials in lift near the blade tips, which causes the formation of strong tip vortices. These vortices, as well as the bound vorticity about the blade, result in an inflow velocity based on the rotor thrust. This is modeled for this study using momentum theory, which provides a uniform inflow velocity across the rotor disk as shown in Equation 2.3. This method applies to the average inflow through the rotor disk in hover or forward flight. In the case of forward flight, where μ > 0, the inflow ratio is solved iteratively using a Newton-Raphson method. Also for forward flight, a linear inflow model is applied using Equations 2.4 and 2.5, resulting in an inflow ratio distribution across the disk and azimuth as shown in Equation 2.7. Applying Prandtl tip loss, an empirical correction shown in Equation 2.6, increases the accuracy of this method by increasing the inflow velocity near the blade tips, thereby reducing the section lift as in Equation 2.8.

$$\lambda_0 = \frac{C_T}{\sqrt{\lambda_0^2 + \mu^2}} + \mu \tan(\alpha_{WL} + \alpha_{shaft}) \quad \text{Eq. 2.3}$$

$$\chi = \tan^{-1}\left(\frac{\mu}{\lambda_0}\right) \quad \text{Eq. 2.4}$$

$$K_X = \left(\frac{15\pi}{23}\right)\tan\left(\frac{\chi}{2}\right) \quad \text{Eq. 2.5}$$

$$F = \frac{2}{\pi}\cos^{-1}\left(\exp\left[\frac{(r-1)N_b\sqrt{1+1/\lambda^2}}{2}\right]\right) \quad \text{Eq. 2.6}$$

$$C_l = C_l^{Interpolated} \cdot F \qquad \text{Eq. 2.8}$$

$$\lambda(r,\psi) = \lambda_0(1 + r * K_X \cos(\psi)) \qquad \text{Eq. 2.7}$$

Rotor Force and Moment Calculations

Due to the nature of the helicopter, the largest and most important forces and moments are produced by the rotor. This environment is complex, both from an aerodynamic perspective and from a mechanical standpoint. Airflow in the rotor plane varies at a 1/rev rate and linearly across the rotor blade, while inflow velocity varies non-uniformly across the rotor disk. The control inputs from the swashplate act at a 1/rev frequency, while vehicle attitude is steady. The out-of-plane motion of rotor flapping also adds to the complexity by changing the angles at which rotor lift and drag act by altering the out-of-plane velocities due to the rotor motion. Since flapping affects the out-of-plane air velocity, an estimate of rotor flapping angles, and thus flapping rates, is needed. The closed-form flapping solutions for the first harmonic flapping motion are shown in Equations 2.9 through 2.11.

$$\beta_0 = \frac{\gamma}{\upsilon_\beta^2}\left[\frac{\theta_0}{8}\left(1+\mu^2\right) - \frac{\mu^2}{60}\theta_{tw} - \frac{\lambda}{6}\right] \quad \text{Eq. 2.9}$$

$$\beta_{1S} = \frac{\left(\theta_{1C} + \frac{\upsilon_\beta^2 - 1}{\gamma/8}\theta_{1S}\right)}{\left[1+\left(\frac{\upsilon_\beta^2-1}{\gamma/8}\right)^2\right]} \quad \text{Eq. 2.10}$$

$$\beta_{1C} = \frac{\left(-\theta_{1S} + \frac{\upsilon_\beta^2 - 1}{\gamma/8}\theta_{1C}\right)}{\left[1+\left(\frac{\upsilon_\beta^2-1}{\gamma/8}\right)^2\right]} \quad \text{Eq. 2.11}$$

The first step in calculating any rotor forces and moments is to calculate the relative airflow velocities and angles. Equations 2.12, 2.13, and 2.14 show the calculation of relative velocity and inflow angle, which will affect the angle of attack in subsequent steps. Equation 2.15 shows the calculation for the local Mach number based on the relative velocities.

$$\frac{U_T}{\Omega R} = r + \mu\sin\varphi \quad \text{Eq. 2.12}$$

$$\frac{U_P}{\Omega R} = \lambda + r\overset{*}{\beta} + \mu\sin\beta\cos\varphi \quad \text{Eq. 2.13}$$

$$\phi = \tan^{-1}\left(\frac{U_P}{U_T}\right) \quad \text{Eq. 2.14}$$

$$M_{local} = \frac{\sqrt{U_T^2 + U_P^2}}{V_{sound}} \quad \text{Eq. 2.15}$$

With the relative air velocities in place, the angle of attack can be calculated based on the collective and cyclic pitch, azimuth angle, twist angle and inflow angle (ϕ). The local pitch for the airfoil is a combination of collective, cyclic pitch, rotor azimuth angle and rotor twist rate as shown in Equation 2.16. The twist of the rotor is non-linear and is calculated by interpolating values from the helicopter parameters, as described in Appendix B. The resulting angle of attack is calculated using Equation 2.17. The lift, drag and pitching moment coefficients of the airfoil section are calculated using a 2-D interpolation based on angle of attack, α, and local Mach number for the SC-1095 and SC-1095R8 airfoil shapes. The type of airfoil varies between these two contours over the length of the rotor blade.

$$\theta = \theta_0 + \theta_{1C}\cos(\psi) + \theta_{1S}\sin(\psi) + \theta_{TW}(r) \qquad \text{Eq. 2.16}$$

$$\alpha = \theta - \phi \qquad \text{Eq. 2.17}$$

The interpolated coefficient values are then used to calculate the section lift, drag and moment values as in Equations 2.18 through 2.21. Since the airfoil coefficients are interpolated, they account for the effects of retreating blade stall.

$$V^2 = \left(\frac{U_T^2 + U_P^2}{\Omega^2 R^2}\right) \qquad \text{Eq. 2.18}$$

$$\frac{dL}{dr} = V^2\left(C_l\cos\phi - C_d\sin\phi\right) \qquad \text{Eq. 2.19}$$

$$\frac{dD}{dr} = V^2\left(Cd\cos\phi + C_l\sin\phi\right) \qquad \text{Eq. 2.20}$$

$$\frac{dM}{dr} = V^2 * C_M \qquad \text{Eq. 2.21}$$

These base force and moment values form the basis for all of the other rotor forces and moments. Integrating these along the rotor blade and around the rotor azimuth allows the calculation of the three rotor forces: thrust, drag and side

force, as well as the three rotor moments: pitching moment, rolling moment, and torque. This model uses non-dimensionalized coefficients to calculate rotor forces and moments in an effort to maintain generality for other helicopter models. Thus, the force coefficients are calculated in Equations 2.22, 2.23, and 2.24.

$$C_T = \frac{N_b}{4R\pi^2}\iint \frac{dL}{dr} c(r)\, dr d\psi \qquad \text{Eq. 2.22}$$

$$C_H = \frac{N_b}{4R\pi^2}\iint \left[\frac{dD}{dr}\sin(\psi) - \beta\cos(\psi)\frac{dL}{dr}\right] c(r)\, dr d\psi \qquad \text{Eq. 2.23}$$

$$C_Y = \frac{N_b}{4R\pi^2}\iint \left[-\frac{dD}{dr}\cos(\psi) - \beta\sin(\psi)\frac{dL}{dr}\right] c(r)\, dr d\psi \qquad \text{Eq. 2.24}$$

The rotor moment coefficients are calculated similarly. The most obvious difference is that the lift terms are transferred by the distance from the flap hinge to the hub, whereas torque is transmitted through the radial distance from the hub. Equations 2.25 through 2.27 show the rotor moment coefficients.

$$C_{MX} = \frac{N_b}{4R\pi^2}\iint \left[\frac{dL}{dr}\left(e_{flap}\right)\sin(\psi) - \beta\left(r - e_{flap}\right)\cos(\psi)\frac{dD}{dr} - \frac{dM}{dr}\cos(\psi)\right] c(r)\, dr d\psi \qquad \text{Eq. 2.25}$$

$$C_{MY} = \frac{N_b}{4R\pi^2}\iint \left[-\frac{dL}{dr}\left(e_{flap}\right)\cos(\psi) - \beta\left(r - e_{flap}\right)\sin(\psi)\frac{dD}{dr} - \frac{dM}{dr}\sin(\psi)\right] c(r)\, dr d\psi \qquad \text{Eq. 2.26}$$

$$C_Q = \frac{N_b}{4R\pi^2}\iint \frac{dD}{dr} rc(r)\, dr d\psi \qquad \text{Eq. 2.27}$$

In order to make these forces and moments compatible with the helicopter fuselage parameters, the values must be converted back to unit quantities. The simulation program uses imperial units by default but will work with metric units as well if the constants are changed accordingly. Equations 2.28 through 2.33 convert the non-dimensional rotor coefficients to dimensional values (in this case pounds and foot-pounds).

$$T = C_T\left(\rho\pi\Omega^2 R^4\right) \quad \text{Eq. 2.28}$$

$$H = C_H\left(\rho\pi\Omega^2 R^4\right) \quad \text{Eq. 2.29}$$

$$Y = C_Y\left(\rho\pi\Omega^2 R^4\right) \quad \text{Eq. 2.30}$$

$$M_X = C_{MX}\left(\rho\pi\Omega^2 R^5\right) \quad \text{Eq. 2.31}$$

$$M_Y = C_{MY}\left(\rho\pi\Omega^2 R^5\right) \quad \text{Eq. 2.32}$$

$$Q = C_Q\left(\rho\pi\Omega^2 R^5\right) \quad \text{Eq. 2.33}$$

The rotor power limit for this model was loosely based on the UH-60M. The maximum allowable horsepower for the engine at sea level was 4000 HP. The available power of the engine decreased with altitude according to Equation [2.34].

$$P_{avail} = (4000HP)\frac{\rho_{alt}}{\rho_{SL}} \quad \text{Eq. 2.34}$$

Rotor Motion

The most fundamental concept in helicopter design is that the vehicle produces lift and thrust through rotating blades. This rotation produces the airflow over the blades, whereas a fixed-wing aircraft would rely on forward flight to produce the airflow for lift. This means that helicopter rotors, being significantly smaller than a comparable airplane, must spin quickly to make up for the reduced size while still producing enough lift.

This rotation, however, is not the only motion that the rotor must undergo. The rotor blades also have their own periodic and transient motion. First and foremost among these motions is rotor flapping. This phenomenon is driven by the balance of aerodynamic and inertial, or centrifugal, forces. The centrifugal forces are proportional to the square of the rotational speed and do not change

appreciably with changes in airspeed or altitude. Variation in rotor speed, however, can have a large impact on this force. The aerodynamic forcing varies widely within the flight envelope. This drives the change in rotor flapping angles at different airspeeds and altitudes. The increased thrust requirements in forward flight, as well periodicity, result in a cyclic variation of flapping angles. For the study at hand, only the steady state and first harmonic flapping motions are examined. Closed form solutions are used to estimate the values for the first pass through the solver, but after that, the calculated values are used until convergence. Since this system is not solvable using closed form solutions for a real airfoil and rotor blade, a Galerkin method is used to find the flapping angles. The equation of motion for rotor flapping and coning is found in Equation 2.35.

$$\overset{**}{\beta} + \upsilon_\beta^2 \beta = \frac{M_\beta^{aero}}{I_\beta \Omega^2} = \overline{M}_\beta \qquad \text{Eq. 2.35}$$

By moving the non-dimensionalized flapping moment to the left-hand side of the equation, a correct flapping solution would yield zero. Since this scheme minimizes an error, the equation becomes Equation 2.36.

$$\overset{**}{\beta} + \upsilon_\beta^2 \beta - \overline{M}_\beta = \varepsilon \qquad \text{Eq. 2.36}$$

By assuming only first harmonic motion for flapping, the solution of these equations becomes simpler. The three equations that describe the three flapping angles, β_0, β_{1C}, and β_{1S}, can be written as in Equations 2.37, 2.38, and 2.39. In these equations, the previous values for flapping angles are used, except in the first pass, where the closed-form solutions are used. Using a minimization function in Matlab, the error functions, denoted as ε_0, ε_{1c}, and ε_{1S}, are reduced. When these errors are close to zero, the solution has converged to the correct flapping angles.

$$\upsilon_\beta^2 \beta_0 - \frac{\rho c(r) R^4}{4\pi I_\beta} \iint \frac{dL}{dr} d\psi = \varepsilon_0 \qquad \text{Eq. 2.37}$$

$$\left(\upsilon_\beta^2 - 1\right)\beta_{1C} - \frac{\rho c(r) R^4}{2\pi I_\beta} \iint \frac{dL}{dr} \cos\psi d\psi = \varepsilon_{1C} \qquad \text{Eq. 2.38}$$

$$\left(\upsilon_\beta^2 - 1\right)\beta_{1S} - \frac{\rho c(r) R^4}{2\pi I_\beta} \iint \frac{dL}{dr} \sin\psi d\psi = \varepsilon_{1S} \qquad \text{Eq. 2.39}$$

Balance of Forces and Moments

The next major step is to calculate the balance of forces and moments on the helicopter. The most complicated force and moment calculations are found in the rotor. The remaining loads are more straightforward, as shown below.

The horizontal tail in the rear of the helicopter provides a significant amount of pitch control in forward flight. It performs this duty despite being subjected to a complicated slew schedule and rotor wake interactions. Since this model does not calculate advanced effects of the rotor wake, an empirical model is used to match the rotor slew schedule to flight test and CAMRAD-II results through a wake skew angle, χ_{HT}, as discussed in Bluman [10]. With that relation in place, Equation 2.40 is used to calculate the slew angle, which is not to be confused with skew angle. Combined with the skew angle and the waterline pitch of the helicopter, the resulting tail incidence angle is shown in Equation 2.41. Lift and drag coefficients are calculated using interpolation methods as they are for the rotor blade airfoils. These yield the tail lift, drag and pitching moment effects on the fuselage given in Equations 2.42, 2.43, and 2.34.

$$\alpha_{slew} = 1437.2\mu^2 - 760.19\mu + 99.302, \mu > 0.1 \quad \text{Eq. 2.40}$$

$$\alpha_{ht} = \alpha_{slew} - \alpha_{WL} - \chi_{ht} \quad \text{Eq. 2.41}$$

$$L_{ht} = \tfrac{1}{2}\rho V_\infty^2 S_{ht} C_L^{HT} \quad \text{Eq. 2.42}$$

$$D_{ht} = \tfrac{1}{2}\rho V_\infty^2 S_{ht} C_D^{HT} \quad \text{Eq. 2.43}$$

The fuselage shape also affects the force and balance equations. The fuselage is obviously a source of drag, especially at high speeds and high angles of attack. The body provides a fair amount of lift as well. The lift and drag relations of this airframe are based on a polynomial fit from Yeo [11]. The lift and drag values can be found in Equations 2.44 and 2.45. With these forces in hand, the vehicle force and moments can then be summed as shown in Equations 2.46 through 2.51.

$$\mathrm{L}_{\mathrm{fuselage}} = \tfrac{1}{2}\rho \mathrm{V}_\infty^2 (1.0239\alpha_{WL}^5 + 12.841\alpha_{WL}^4 - 39.558\alpha_{WL}^3 - 30.214\alpha_{WL}^2 + 106.09\alpha_{\mathrm{WL}} - 0.709) \quad \text{Eq. 2.44}$$

$$\mathrm{D}_{\mathrm{fuselage}} = \tfrac{1}{2}\rho \mathrm{V}_\infty^2 \left(35.14 + 0.0440896\alpha_{\mathrm{WL}}^2\right) \quad \text{Eq. 2.45}$$

$$\sum F_X = D_{fuselage} + H\cos\left(\alpha_{WL} + \alpha_{shaft}\right) - T\sin\left(\alpha_{WL} + \alpha_{shaft}\right) + D_{ht} \quad \text{Eq. 2.46}$$

$$\sum F_Y = T\sin\phi + Y\cos\phi + T_{tr}\cos\left(\phi_{TR} - \phi\right) + L_{ht}\sin\phi \quad \text{Eq. 2.47}$$

$$\sum F_Z = L_{fuselage} + T\cos\left(\alpha_{WL} + \alpha_{shaft}\right) - Y\sin\phi + H\sin\left(\alpha_{WL} + \alpha_{shaft}\right) + L_{ht}\cos\phi - W + T_{TR}\sin\left(\phi_{TR} - \phi\right) \quad \text{Eq. 2.48}$$

$$\sum M_X = M_{XR} + \mathrm{T}_{\mathrm{TR}}\cos\left(\phi_{\mathrm{TR}} - \phi\right)\left(z_{TR} - z_{CG}\right) - z_{CG}W\sin\phi - M_{ZR}\sin\alpha_{shaft} \quad \text{Eq. 2.49}$$

$$\sum M_Z = M_{ZR} + T_{TR}\cos\left(\phi_{TR} - \phi\right)\left(x_{TR} + x_{CG}\right) + L_{ht}\sin\left(\phi\right)\left(x_{ht} + x_{CG}\right) \quad \text{Eq. 2.50}$$

$$\sum M_Y = M_{YR} + W\left(x_{CG}\right)\cos\alpha - L_{ht}\left[\left(x_{ht} + x_{CG}\right)\cos\alpha + z_{ht}\sin\alpha\right] + W\left(h_{CG}\right)\sin\alpha - T_{TR}\sin\left(\phi_{TR} - \phi\right)\left(x_{TR} + x_{CG}\right) - D_{fuselage}\left(\cos\alpha_{WL}\right)z_{CG} + D_{fuselage}\left(\sin\alpha_{WL}\right)x_{CG} + D_{ht}\left[z_{ht}\cos\alpha_{WL} - z_{ht}\cos\alpha_{WL}\right] - L_{fuselage}x_{CG} \quad \text{Eq. 2.51}$$

Simulation Model

All of the mathematical relations shown above set the stage for simulating helicopter performance in a computer program. The simulation uses the above equations and parameters to balance the vehicle forces and moments at a given airspeed. When the model is propulsively trimmed, the control parameters, rotor power and other aerodynamic data are recorded.

Program Outline

The simulation program used for this research generates helicopter trim parameters across a wide range of helicopter configurations. The most notable of these parameter changes is rotor speed which is generally held constant for a conventional, manned helicopter. Airspeed of the helicopter is also of vital importance, as the effects of variable rotor speed on helicopter performance have to be studied for the entire airspeed range of the typical vehicle. Rotorcraft weight and operating altitudes are two additional parameters that are varied over the course of the simulations.

The simulation works by trimming the helicopter model at the given rotor speed, airspeed, altitude and gross weight. Using a linearized, quasi-closed-form helicopter model such as found in elementary rotorcraft courses, a rough guess of trim attributes such as main rotor collective and cyclic pitch, vehicle attitude, tail rotor collective and rotor flapping parameters are generated. The actual forces and moments are calculated and summed using these assumptions. This yields the error. Perturbing the system once for each of the control parameters yields a Jacobian matrix, which is applied to the trim parameters to progressively decrease the error to zero. This is the trim result, and then the vehicle is re-trimmed at the next airspeed step, up to 180 knots. Then the rotor speed is

reduced and the process repeated. This process is repeated over a range of altitudes and gross weights for completeness.

Basic Trim

The basic trim routine mentioned above is a simpler version of the major simulation code. Starting from a guess for trim conditions and basic rotor and fuselage parameters, the forces and moments are summed and used to generate a Jacobian matrix to reduce the deviation from zero to within a small tolerance. An estimated solution to rotor flapping is also calculated during this step using Equations 2.9, 2.10, and 2.11. The resulting trim estimate is then passed to the calling function, in this case the main simulation code.

Flapping Calculations

The next step involves solving the actual rotor flapping based on control parameters. The routine calculates the flapping moment of the rotor blade across the rotor span and around the azimuth. Using a first order harmonic assumption, the steady and cyclic terms of rotor flapping are calculated. Solving the equations of motion yields the deviation from trim. The corresponding values are then used as the baseline to generate a Jacobian resulting from perturbations to generate a linearized model. Applying this iteratively eventually yields the correct flapping values for the given control settings and operating parameters.

Force and Moment Calculations

Once the estimated trim parameters are calculated and the corresponding flapping values are known, the forces and moments along the blade and around

the azimuth are calculated. This is done using a numerical trapezoidal integration along the rotor blade at any given azimuth angle. This is integrated over the range of azimuth angles, from 0 degrees to 360(1- $1/N_{psi}$) degrees, where N_{psi} is the number of azimuth angles used. This results in the rotor forces and moments in the hub reference frame. Passing these values to the fuselage reference frame through the shaft and disk tilt angles allows the rotor forces and moments to be resolved with the fuselage forces.

The most important fuselage force that is calculated is fuselage drag. This drag calculated using a model from Yeo [11]. The drag is heavily influenced by the angle of attack of the airframe and is represented using a second order polynomial function. The lift and drag components from the horizontal tail, modeled using a NACA 0012 airfoil, are translated to moments at the center of mass. Tail rotor thrust is calculated using momentum theory inflow and tail rotor collective.

Trim Procedure

The results from the summation of forces should be zero for a trimmed solution. Thus, solving for the trim parameters is simply a zero-finding algorithm. Using a six-by-six Jacobian matrix to develop the linearized relationships between control inputs and the force summations, the routine multiplies the inverse of the matrix with the current force summation.

Analysis Methods

Output from Simulation

The output from the trim simulation code is in the form of data grids. These grids contain data from each of the rotor speed and airspeed combinations for a given rotorcraft altitude and gross weight. The rotor speed range varies from 360 RPM to 180 RPM and the airspeed ranges from hover to 180 knots forward speed. Grid information is generated for all relevant parameters including the control parameters for the aircraft (collective and cyclic pitch, pitch and roll attitudes and tail rotor pitch), rotor flapping angles, and rotor inflow ratios for the main and tail rotors. Main rotor total power, induced power, profile power and torque are also measured and are the most important aspect of the output.

Examining Trends

The most basic analysis of the resulting data is visual inspection of the trends that appear with variation in rotor speed. To this end, contour plots are created to show any obvious trends and limits. These basic trends, as discussed in Chapter 3, give a hint of what a more in-depth look would reveal. It also allows the planning of an optimization method to find the best performance characteristics of the aircraft with variable rotor speed.

Optimization

The goal of this research program is to develop an understanding of what benefits can be gained from varying rotor speed on a conventional helicopter, and what requirements this entails. As such, some method of evaluating the

resulting data needs to be considered. Since performance, namely power reduction, is the focus of this study, it is also the primary evaluation criteria.

The first step is to evaluate all of the currently available data from the grids to determine what the minimum power is for a given gross weight, altitude and airspeed. This yields a schedule of rotor speeds that would yield the minimum main rotor power in 10 RPM increments. This method does not account for rotor torque changes, which for a cornerstone of understanding variable speed rotor behavior. To account for rotor torque, an optimization routine is used to find the minimum power, including a penalty due to torque increases. The first step for this is to evaluate the results with respect to power and torque using a normalized weighting function. Equation 2.52 shows this weighting function. WT is the relative weighting of torque compared to power.

$$F_{EVAL} = (1 - WT)\frac{P_{opt}}{P_{base}} + WT\frac{Q_{opt}}{Q_{base}} \qquad \text{Eq. 2.52}$$

For low weighting values, rotor power is the most important parameter, whereas at high weighting values, rotor torque is the most important. Using this function as the optimizing condition, a line search method is employed at each airspeed condition based on the method of Belegundu and Chandraputla [12]. The initial three-point pattern is acquired by using similar means as the discrete optimization previously performed. In this case, the grid data is evaluated based on the weighting function and a three-point pattern, where the central value is lower than either of the other two outside values, is identified. Then the quadratic fit methods are applied, eventually resulting in the weighting-function optimized rotor speeds for the airspeed, gross weight, and altitude combination.

Chapter 3

UH-60 results

The goal of this research was to analyze, document, and understand the effects of varying rotor speed of a conventional helicopter. Of primary interest was main rotor power, since power reduction is one of the most prominent areas of current and past helicopter research. As helicopters require much more power to fly compared to fixed-wing aircraft, power reduction plays a key role in expanding the current uses of helicopters as part of the world's aircraft fleet. Aside from power reductions, other key parameters were also examined, including: expansion or reduction of the flight envelope due to variable rotor speeds, the effect of varying rotor speed on main rotor torque, and thus tail rotor thrust. Understanding the physics behind these effects was also a major component as simulation as off-the-cuff predictions mean little without a valid explanation. The results presented in this section are for the UH-60 model detailed in Chapter 2. Three gross weights are discussed along with changes in altitude between sea level and 12,000 ft. Key results are also shown for different airspeeds corresponding to low speed, cruise, and high speed forward flight.

Baseline Weight

The majority of the work for this thesis took place using a UH-60 model with a gross weight of 18,300 lbs. This corresponds to the middle weight range of the aircraft and thus gives a good representation of the aircraft as a whole. For now, the discussion will focus on this weight. The effects of varying rotor weight are discussed later. Since helicopters are much more likely to be used for low-altitude operations than a fixed-wing aircraft. The discussion of helicopter performance starts at sea level.

In order to inspire confidence in the model used for this research, a comparison of flight test data, CAMRAD-II predictions and the current model are depicted. Main rotor power and trim characteristics are shown below in Figure 3.1. The flight test and CAMRAD-II data are taken from Yeo et al [11].

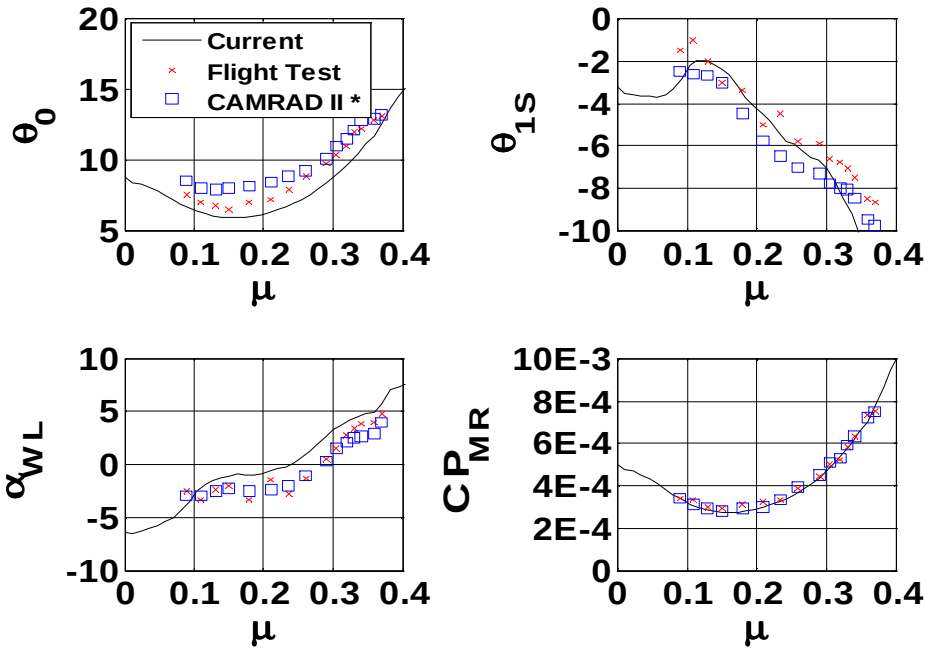

Figure 3.1: Model Validation with Flight Test and CAMRAD II results

The collective and cyclic pitch values predicted by the current analysis code fit well with the results from flight test and CAMRAD-II. A comparison of the collective pitch values show that the simulation was within one degree of the flight test data and two degrees of the CAMRAD II data for most of the range. There was a stronger correlation at μ = 0.1, but this did not change significantly with airspeed. Longitudinal cyclic pitch results agree within 0.5 degrees for much of the airspeed range. Low speed and very high speed values diverge slightly, but not more than 1 degree from the trim results. Vehicle pitch attitude shows the same trends with respect to airspeed, though the trim simulation yielded values approximately 1 degree larger for the cruise speed range. Main rotor power, the

primary focus of this research, shows a very close match to the previous data and predictions. The resulting power coefficients compare very well, implying that this trim simulation is sufficient to predict main rotor power for the given airspeed ranges.

Sea Level Results

Figure 3.1 shows the power contour in horsepower for the baseline gross weight at sea level, along with the three main forward flight regions. Low speed flight includes hover up to 40 knots. Cruise flight includes speeds from 40 knots to 130 knots. High speed continues from 130 to 180 knots at sea level. It will later be seen that the flight envelope will change based on altitude and gross weight; however these definitions will be used throughout the rest of this chapter.

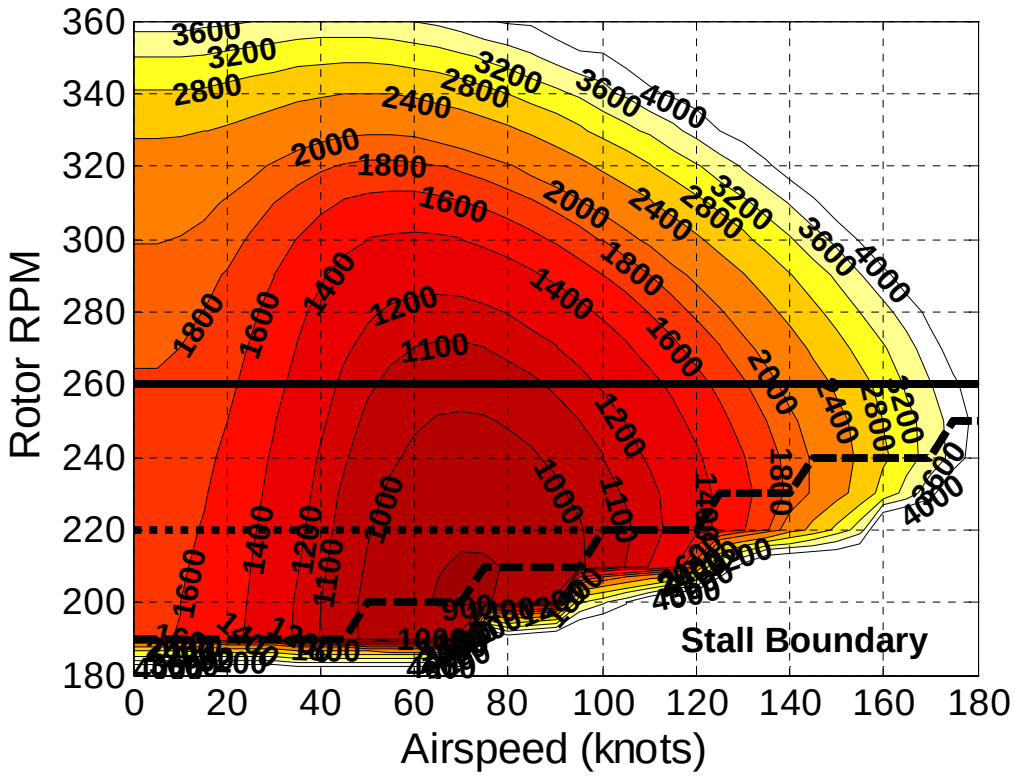

Figure 3.1: Main Rotor Power Contours, 18,300 lbs Gross Weight, Sea Level

The black line in this figure represents the baseline rotor speed of 258 RPM. This is equivalent to a tip speed of about 700 ft/s. There is little expansion in the sea level flight envelope obtained by reducing the rotor speed; however significant power reductions can be seen across the flight speed range. The white outer areas correspond to places where the rotor cannot trim or where the required power of the main rotor would exceed the engine capability.

In low speed flight, the power contour shows that there is a slight decrease in main rotor power required for a reduced main rotor speed. These power decreases are not large enough to justify RPM reduction, especially when the torque change is brought into the equation, as will be seen later. Additionally, the literature suggests that using a momentum theory based inflow model does not

have sufficient fidelity for low speed flight. Preliminary research at Penn State confirms that rotor speed reduction does not result in power reductions in hover, though results have not been published. Some steps were made to alleviate this problem, namely the inclusion of a Prandtl tip loss factor. This helps account for the tip effects, but is not enough to inspire confidence in the hover power predictions. In summary, the low speed benefits of reducing main rotor speed are not confidently predicted, nor do they yield a significant power benefit.

Cruise speed, on the other hand, shows tremendous potential for a variable speed rotor. As Figure 3.1 depicts, there is a large sensitivity to rotor speed in the 80 to 120 knot range. At this point in the flight envelope, even small changes in RPM can yield significant power reductions. Power can be reduced by over 150 HP here if the rotor speed is reduced enough. The lower boundary of rotor speed, approximated by the blue line, is due to rotor stall. In these cases, the reduced rotor speed is simply unable to produce enough thrust to maintain trim. This region is very important in helicopter operation, and thus a power reduction in cruise could have a very important impact on the future of helicopter operations.

In high speed flight significant power benefits can be seen. While the change in rotor speed does not result in an expansion of the flight envelope, it still yields some decrease in power, except at the very limits of forward flight. The contour plot also reveals that the baseline RPM of the aircraft is only slightly higher than the true optimum rotor speed for high speed flight.

Looking at the breakdown of induced and profile power provides a glimpse into the workings of the helicopter. Figure 3.2, shows the main rotor induced power contours, similar to the total power contours in Figure 3.1. The general trends around the baseline rotor speed show that induced power is largely independent of rotor speed. This insensitivity is due to the fact that regardless of

rotor speed, the rotor must produce the same amount of thrust. The induced power, being a direct result of rotor thrust, will stay roughly the same.

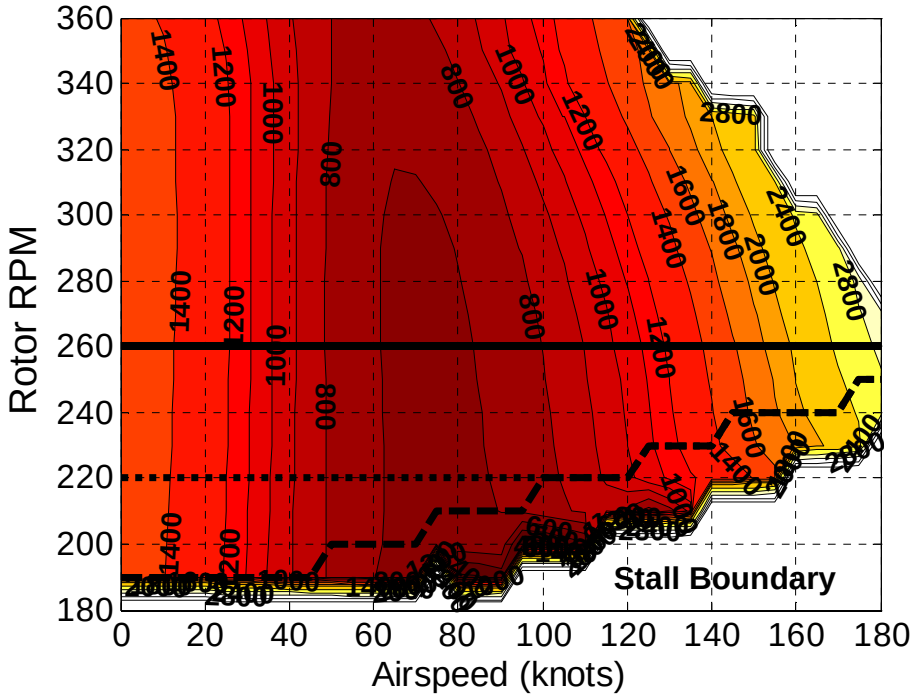

Figure 3.2: Main Rotor Induced Power Profiles, 18,300 lbs Gross Weight, Sea Level

Profile power, in contrast to induced power, shows a high sensitivity to rotor speed. Figure 3.3 shows that the profile power contour lines are nearly horizontal for low speeds. This implies that even a small change in rotor speed can have a profound effect on the profile power. This also implies that the total main rotor power reductions seen by reducing rotor speed are the result of this decreasing profile power. As airspeed increases, the rotor profile power increases as well. The ability of the rotor to show this marked decrease in profile power as a result of decreasing rotor speed arises from the ratio of airfoil lift to drag. When the airfoil is operating at an angle of attack that is far from the stall limit, the drag coefficient is not sensitive to the angle of attack. This is seen in Figure 3.4 where the drag coefficient of the airfoil remains nearly constant at

0.008. With a quasi-constant drag coefficient with respect to the rotor speed, it is inherently obvious that a decrease in rotor speed, and thus dynamic pressure, would result in power savings.

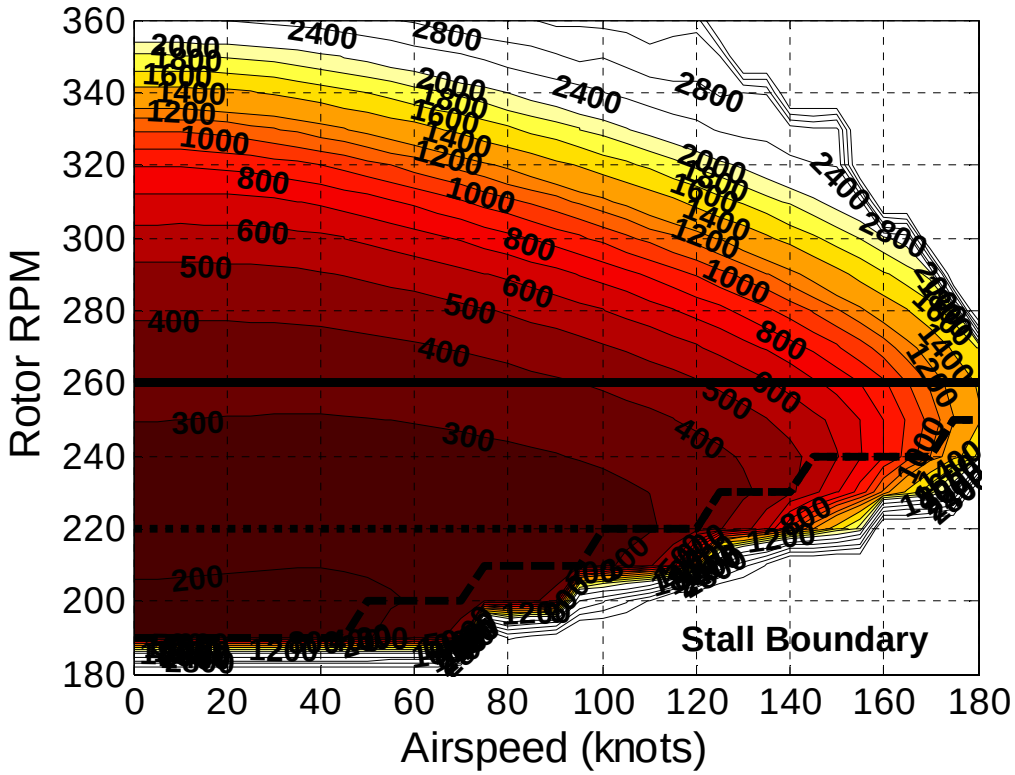

Figure 3.3: Main Rotor Profile Power Contours, 18,300 lbs Gross Weight, Sea Level

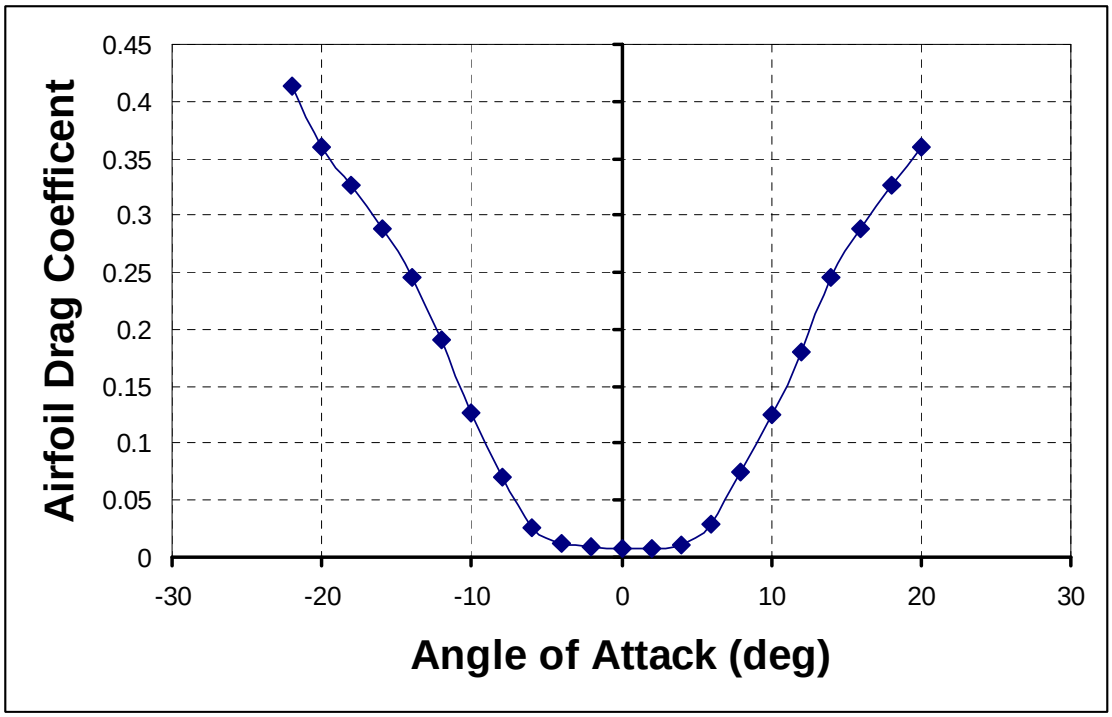

Figure 3.4: SC1095 Airfoil Drag Coefficient vs. Angle of Attack, Mach = 0.6

In order to make use of the power reductions discussed above, some type of optimal RPM schedule must be used. This was addressed in two different ways for this study. The first method was to use the parametric results that generated the contour plot in Figure 3.1 to find the RPM for minimum power. While this is not a true optimum because it is limited to discrete values, it provides a valuable look at the general trends that the rotor should follow to minimize power. Another aspect of this that is looked at is the impact of using variable-speed engine control vs. a variable speed transmission. Since continuously variable speed transmission technology has yet to be proven for helicopter applications, the ability to justify variable rotor speed with engine speed limitations is important. This research assumes that an engine can be operated within 15% of the baseline RPM without suffering significant reductions in efficiency.

Figure 3.5 shows the optimum RPM profile for minimum power at the baseline weight of 18,300 lbs. at sea level. The trend shows that for low to moderate speed flight, the lower the rotor RPM, the lower the rotor power. The unrestricted optimum, which assumes a variable speed transmission is utilized, shows that flying the rotor just above the edge of rotor stall minimizes power. When the rotor speed is limited by the assumption of only engine control, the same trend applies: fly the rotor as slowly as possible without reaching rotor stall. In this case, the minimum speed is 220 RPM or rotor stall, whichever is greater.

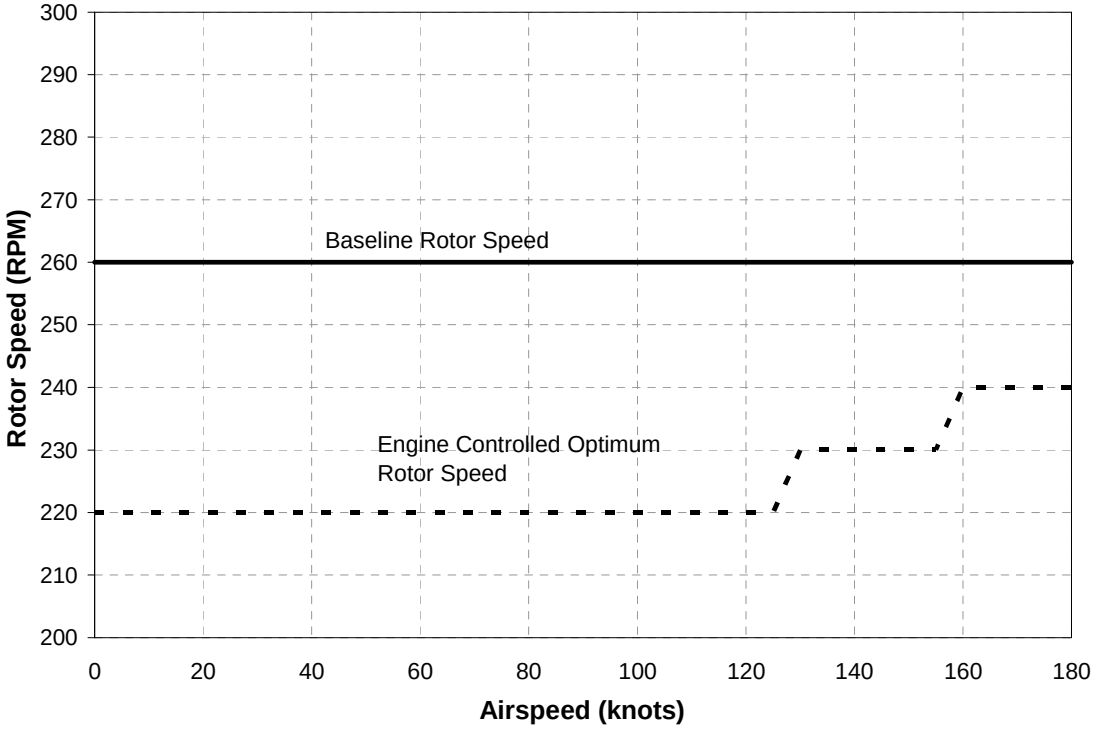

Figure 3.5: Optimum RPM Schedule vs. Airspeed, 18,300 lbs Gross Weight, Sea Level

This discrete optimum does not address the issue of increased rotor torque. To look at both power and torque together, the optimization routine mentioned in Chapter 2 was used to find the optimum RPM corresponding to a torque weighted function at each airspeed. This is a true optimum in the sense that it is not limited to discrete values. This routine was carried out to see the

effect that torque weighting has on the overall optimum RPM. Torque weighting values from zero (power only) to 100% (torque only) were evaluated. The resulting RPM profiles are shown below in Figure 3.6. The trend for the power-only optimum generally follows the discrete values above. When torque is added as an additional parameter, the trend shifts such that the rotor speed of hover and low-speed flight is equal to or higher than the nominal RPM. This is because, as mentioned previously, the power benefits in this regime are minimal for even significant RPM changes. Thus a decrease in rotor speed will result in a noticeable *increase* in shaft torque with a slight power reduction. This is apparent when looking at the low-speed sections of Figure 3.6 where the optimum rotor speed for the 100% torque weighted case is *higher* than the baseline. Looking at Figure 3.7 shows that at this weight value and airspeed, the required power is larger than the baseline requirements. For smaller weight values, with a larger emphasis on power instead of torque, the power levels will decrease. Weight values of 0% and 25% show this phenomenon well, as they result in lower power requirements with a reduced rotor speed. The torque curves in Figure 3.8 show the reverse, namely that power-weighted rotor speeds result in increased torque at low speeds, but converge as speed increases. High speed torque is roughly the same regardless of rotor speed, thus yielding power reductions.

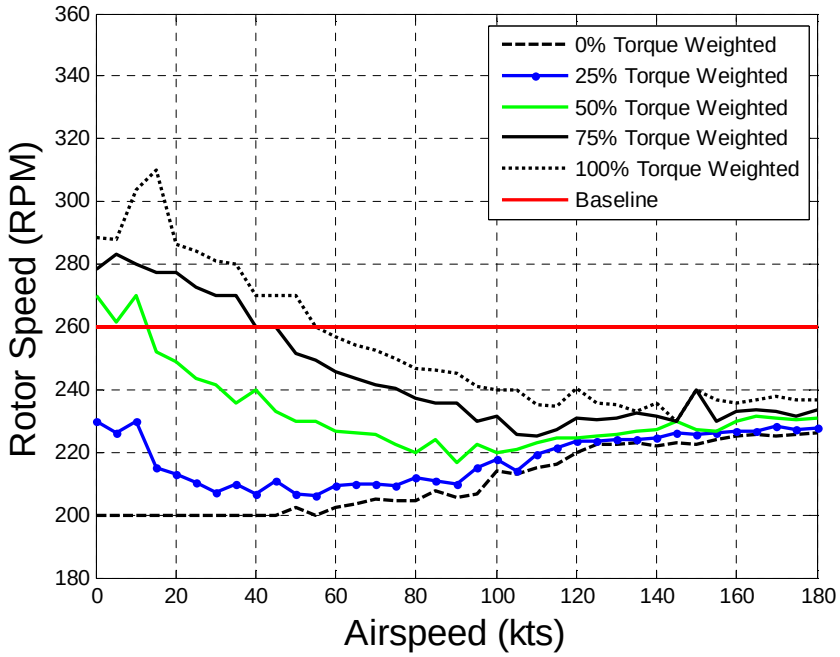

Figure 3.6: Torque Weighted Optimum RPM Schedules, 18,300 lbs Gross Weight, Sea Level

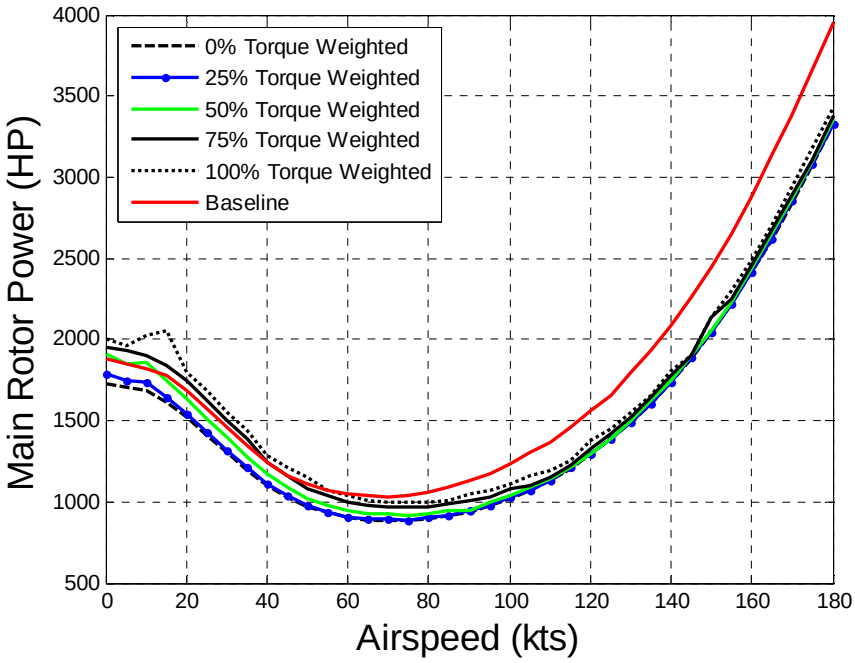

Figure 3.7: Torque Weighted Optimum Power Profiles, 18,300 lbs Gross Weight, Sea Level

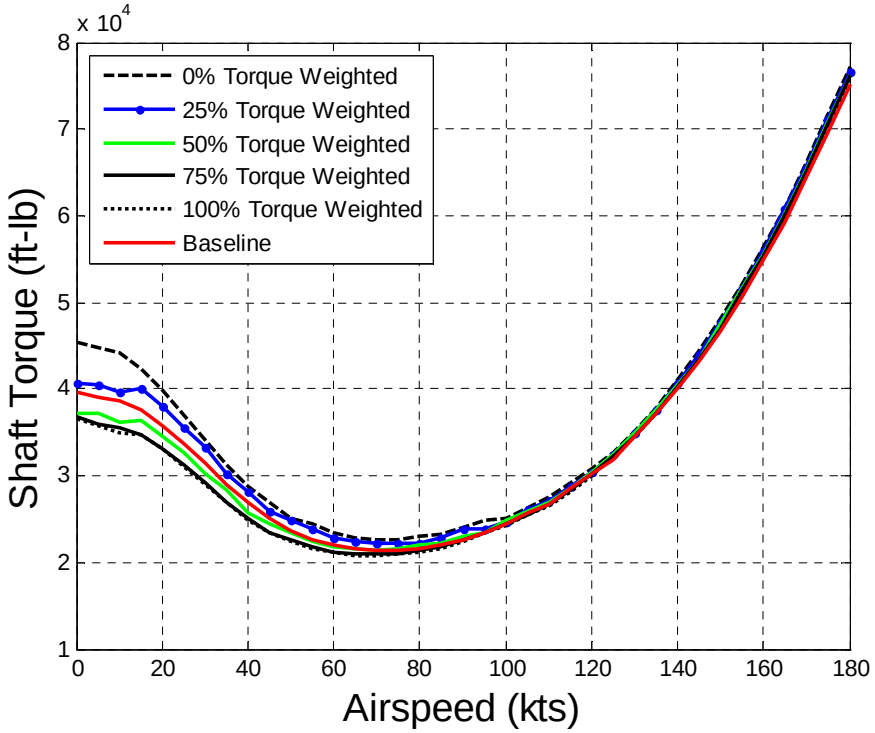

Figure 3.8: Torque Weighted Optimum Torque Profiles, 18,300 lbs Gross Weight, Sea Level

With the changing rotor speeds that are the focus of this study, the trim parameters of the helicopter would have to change to keep the aircraft in propulsive trim. From basic aeronautics, reducing the local speed relative to the airfoil will reduce the sectional lift for the same lift coefficient. Since $\mathbf{C_l}$ is directly dependent on the pitch of the airfoil, the pitch must increase to maintain lift. Thus, reducing rotor speed, and thus local blade speeds, would imply that the collective pitch of the rotor would have to increase. The contour plot of collective pitch in Figure 3.9 shows that this is the case. As rotor speed is reduced, the collective increases. This relationship determines the lowest usable rotor speed, as increasing collective will eventually result in rotor stall. This is shown on the plot.

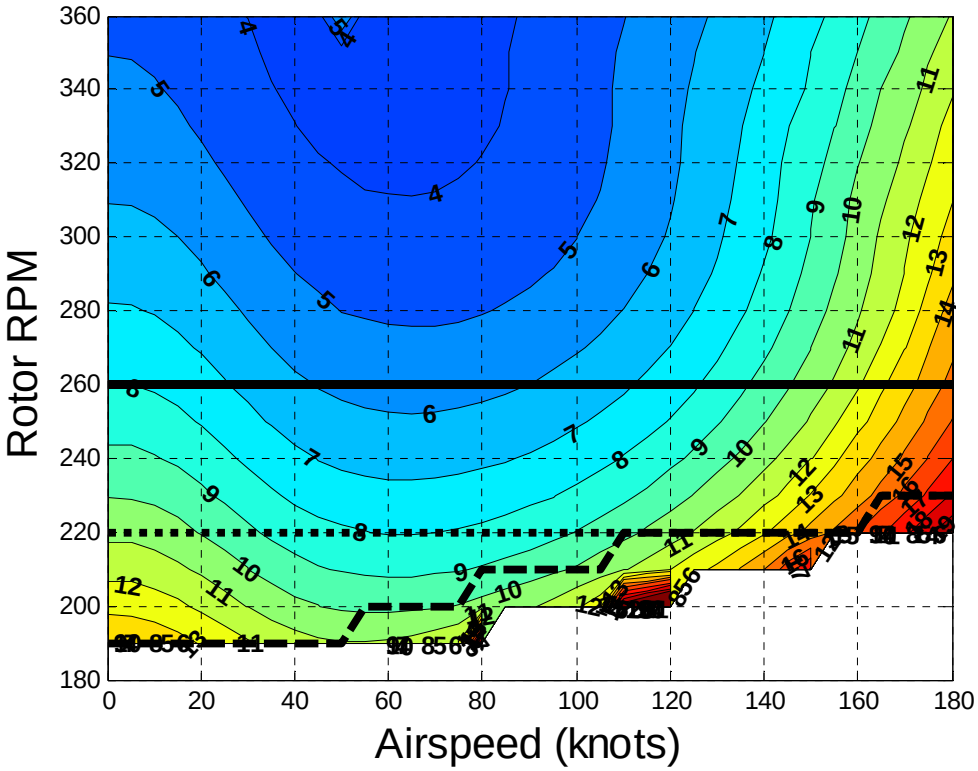

Figure 3.9: Collective Pitch Contours, 18,300 lbs Gross Weight, Sea Level

There is an additional effect of increasing rotor collective pitch: rotor coning increases. Coning is a result of the balance of centrifugal (or inertial) forces on the blade to the aerodynamic loads. Since the centrifugal loads are proportional to the square of the rotor speed, and rotor lift does not change appreciably, a decreasing rotor speed will result in the blade coning more. This is shown in Figure 3.10. Notice that the trend closely resembles the shapes from Figure 3.9.

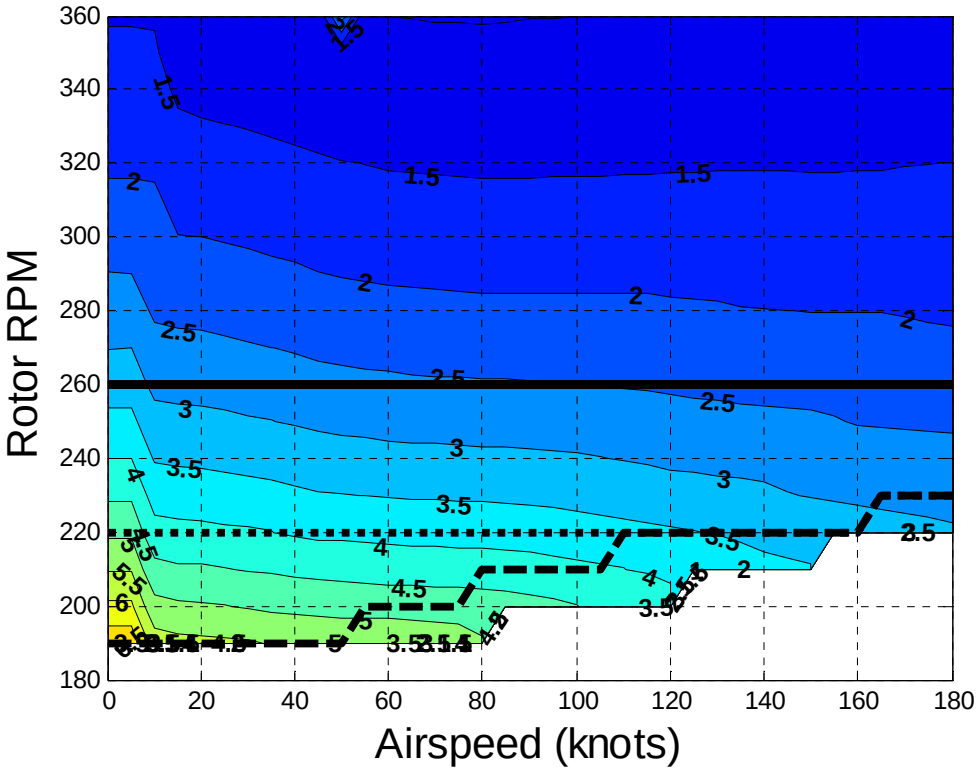

Figure 3.10: Rotor Coning Angle Contours, 18,300 lbs Gross Weight, Sea Level

Propulsive and side forces must also stay roughly the same to maintain trim in forward flight regardless of rotor speed. To this effect, the cyclic flapping angles must remain the same, since side and propulsive force can be viewed as the combination of total rotor thrust, determined by collective, and angle from the rotor mast, determined by blade flapping angles. In this case, the cyclic components of blade pitch had to increase in magnitude to maintain flapping angles. The contour plots for longitudinal flapping, β_{1C}, and the corresponding cyclic pitch, θ_{1S}, can be seen in Figure 3.11 and Figure 3.12.

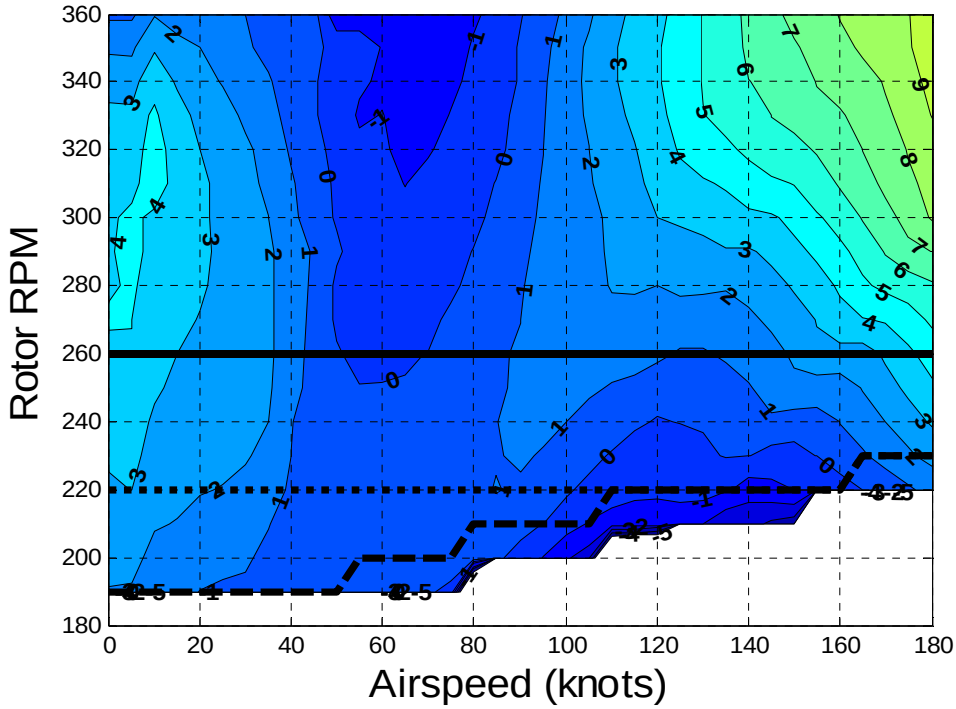

Figure 3.11: Longitudinal Flapping Contours, 18,300 lbs Gross Weight, Sea Level

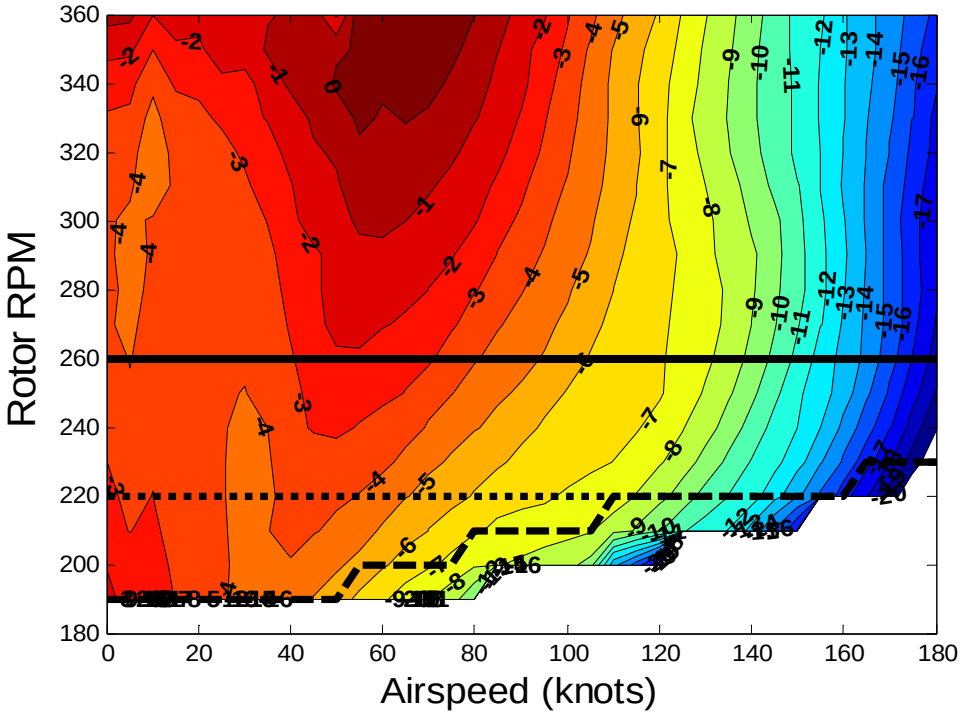

Figure 3.12: Longitudinal Cyclic Pitch Contours, 18,300 lbs Gross Weight, Sea Level

The same can be said of the lateral flapping and pitch, though these terms generally have a much smaller impact in helicopter operation. The primary need for lateral flapping is for negating the side force generated by the tail rotor or for maneuvering. Since this thesis deals only with propulsive trim and not maneuvering responses, the latter is not discussed. As was expected, the lateral flapping angles stayed relatively the same with respect to rotor speed, shown in Figure 3.13**.** The corresponding lateral cyclic pitch contour is found in Figure 3.14 and shows that reducing rotor speed results in an increase in pitch angle to maintain flapping angle.

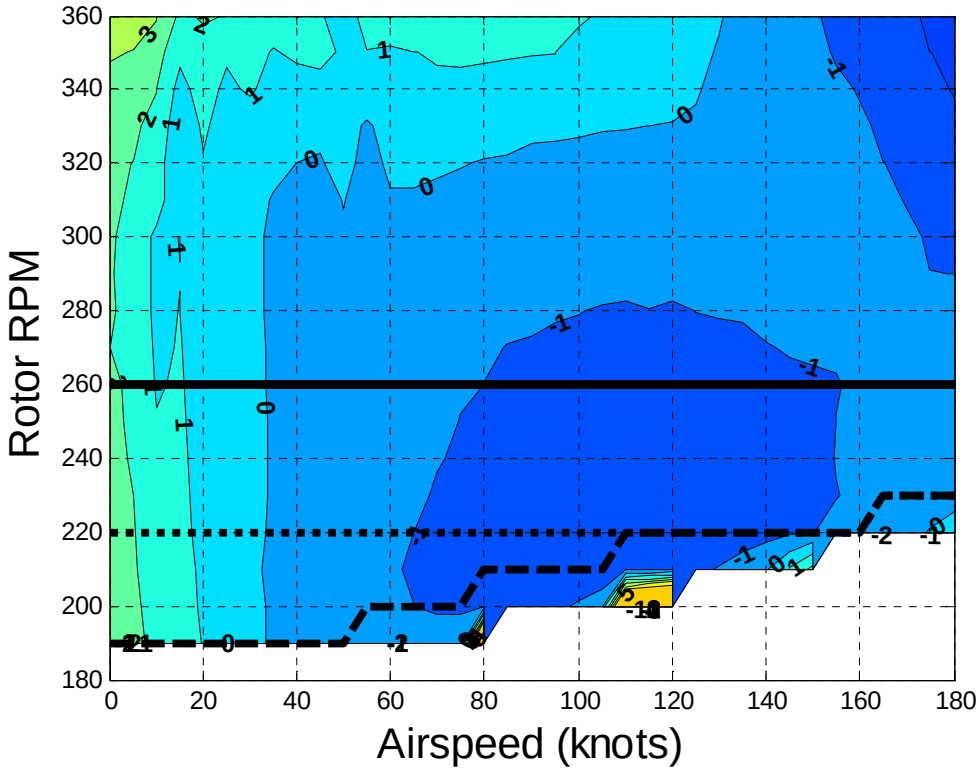

Figure 3.13: Lateral Flapping Contours, 18,300 lbs Gross Weight, Sea Level

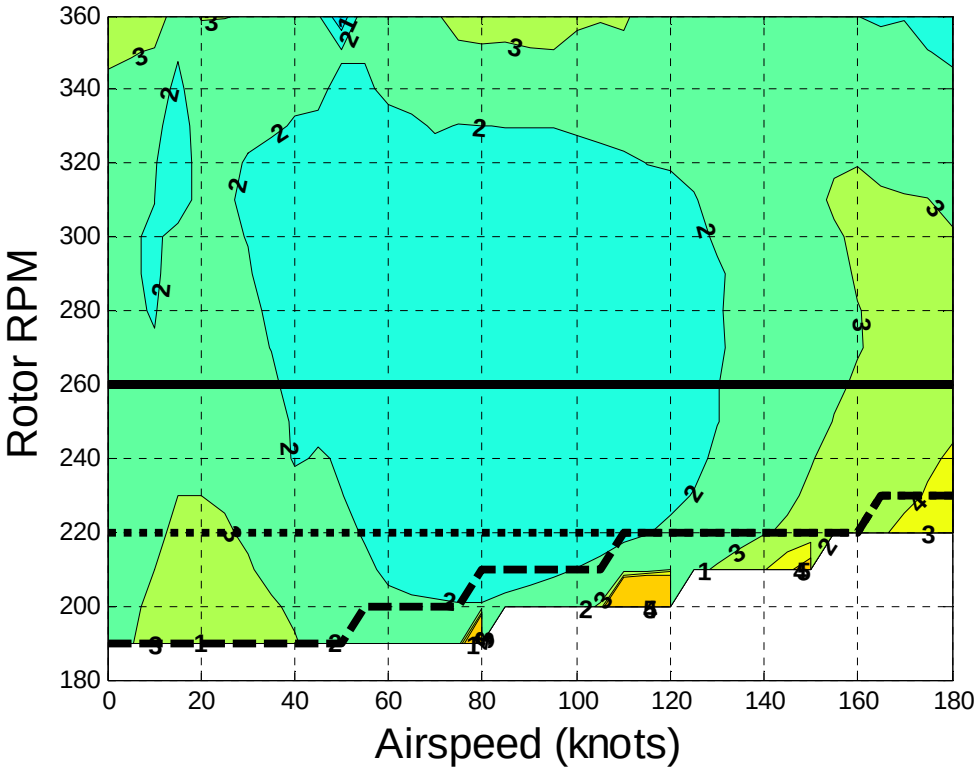

Figure 3.14: Lateral Cyclic Pitch Contours, 18,300 lbs Gross Weight, Sea Level

The remaining trim parameters that have not been discussed fully are vehicle attitude and tail rotor collective. The pitch and roll attitudes of the aircraft show little sensitivity to rotor speed, instead remaining solely a function of the airspeed of the helicopter. This is shown in Figure 3.15 and Figure 3.16.

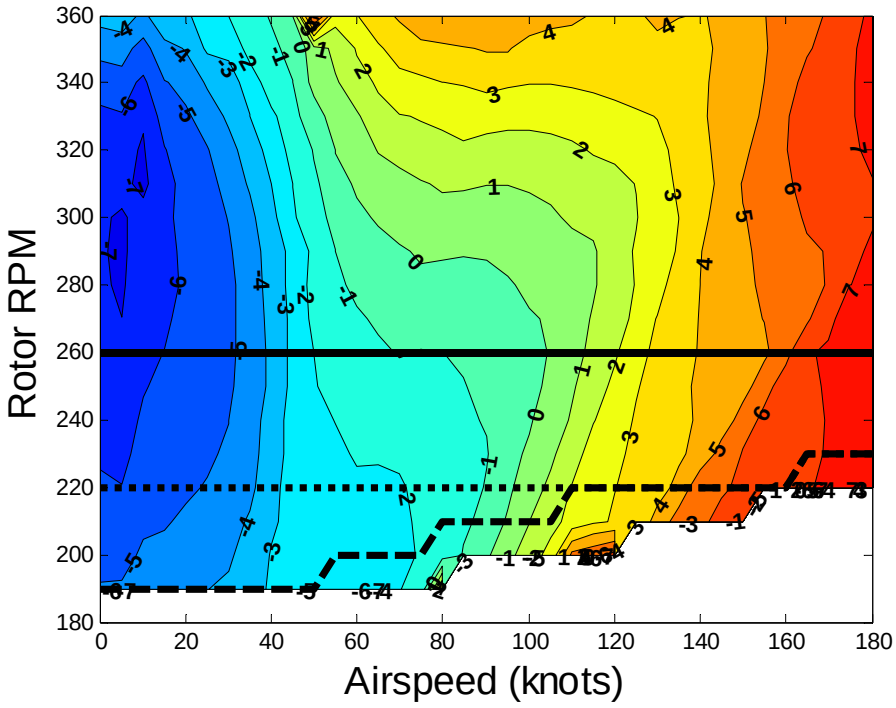

Figure 3.15: Vehicle Pitch Attitude Contours, 18,300 lbs Gross Weight, Sea Level

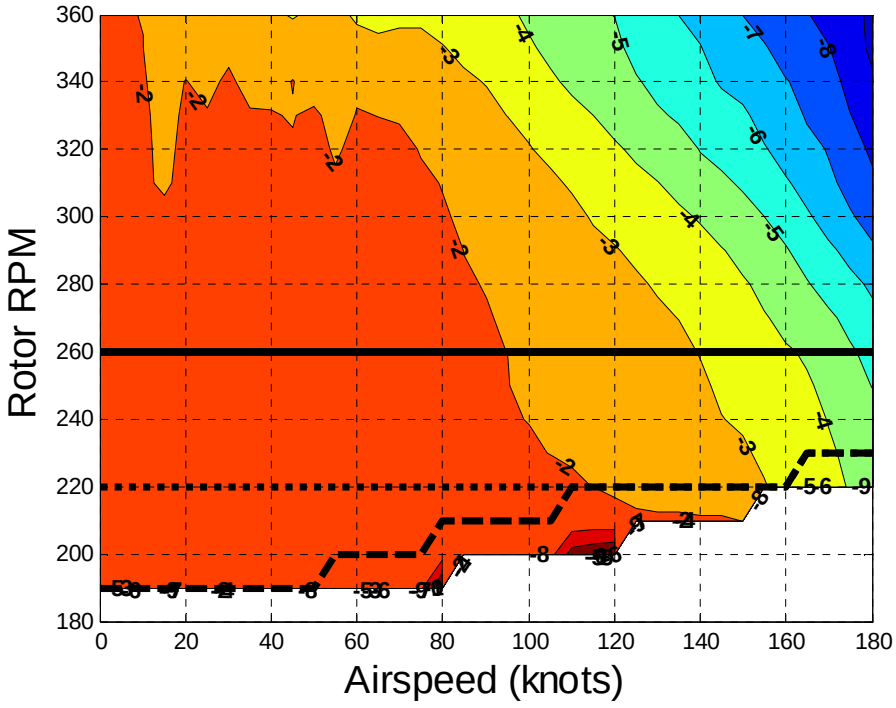

Figure 3.16: Vehicle Roll Attitude Contours, 18,300 lbs Gross Weight, Sea Level

Tail rotor collective directly relates to shaft torque. As discussed above, torque is dependent on rotor power and rotor speed, such that the torque requirements of the aircraft with a variable rotor speed are more complex than those encoutnered in a conventioanl, constant rotor speed, helicopter. For constant power, the torque value will increase linearly with a reduction in rotor speed. However, as seen in Figure 3.1, main rotor power does not remain constant, in general, for a change in rotor speed. It has been generally seen from the contour plots, like Figure 3.1**,** that rotor power decreases as rotor speed decreases. If the rate of power reduction is greater than the rate of speed decrease, rotor torque will decrease. Figure 3.17 shows a contour plot of rotor torque as a function of airspeed and rotor speed. For low speed flight there is a higher sensitivity of torque. This is due to the power reductions seen above being of smaller order. The rotor speed decreases more rapidly than the power, resulting in increased torque.

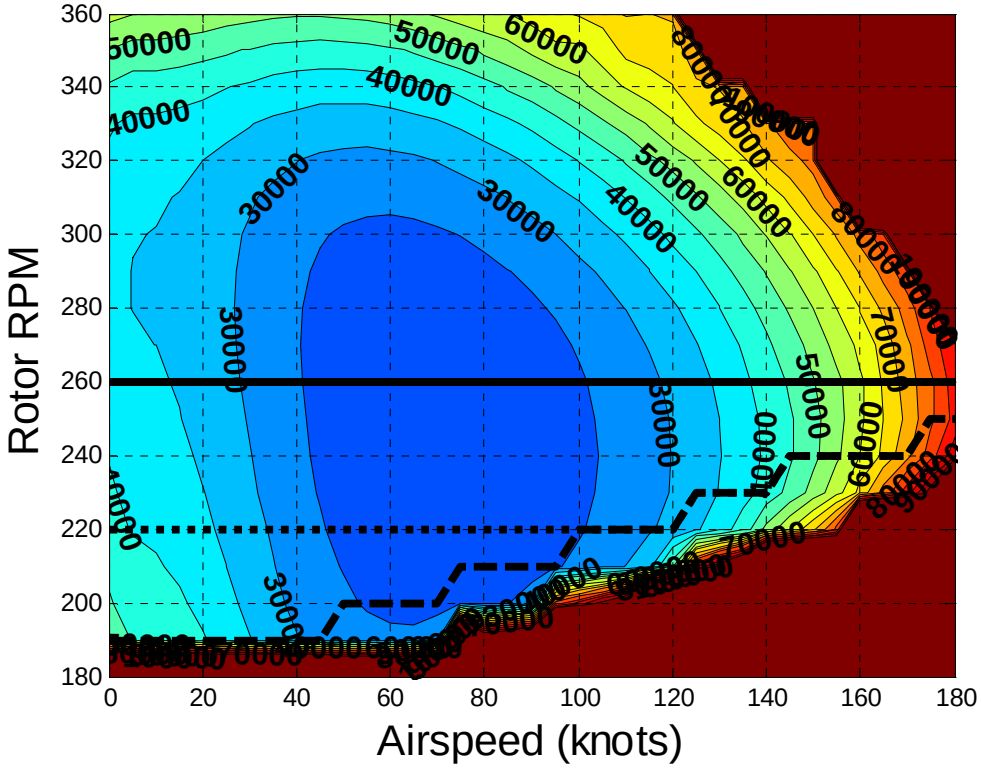

Figure 3.17: Shaft Torque Contours, 18,300 lbs Gross Weight, Sea Level

Results at Altitude

Since most helicopter operations occur above sea level the simulations were performed for altitudes up to 12,000 feet. Since the UH-60 does not have a pressurized cabin, this altitude is an appropriate upper limit for feasible operation. In this range, however, the effects of air temperature, which changes the Mach number, and density, which primarily effects dynamic pressure, are significant enough to show some very interesting behaviors. Obviously rotor stall becomes a more prominent concern as higher effective lift coefficients are required. Engine performance also begins to suffer, with decreasing ambient air density reducing the available power of a turboshaft engine, as discussed in Leishman [**Error! Not a valid link.**]. For conciseness, only three different altitudes will be discussed at length: 4000, 8000 and 12,000 feet.

Figure 3.18 shows power contours at an altitude of 4000 feet. This figure is similar to Figure 3.1, except that the stall boundary is at a higher rotor speed, and the maximum contour, resulting from a reduction in available engine power, has a smaller value than that of the sea level simulation. This plot, as with the sea level plots, includes the limited and unlimited optimum RPM schedules. The optimum rotor speed, within the 15% margin for engine control, starts out at 85% (220 RPM) as does the sea level case. However, the optimum RPM increases at lower airspeeds, and continues to be greater than or equal to the sea level case for the rest of the airspeed range. This shows that an increase in altitude, and thus a reduction in air density and temperature, necessitates a faster rotor to maintain the same thrust and moment values.

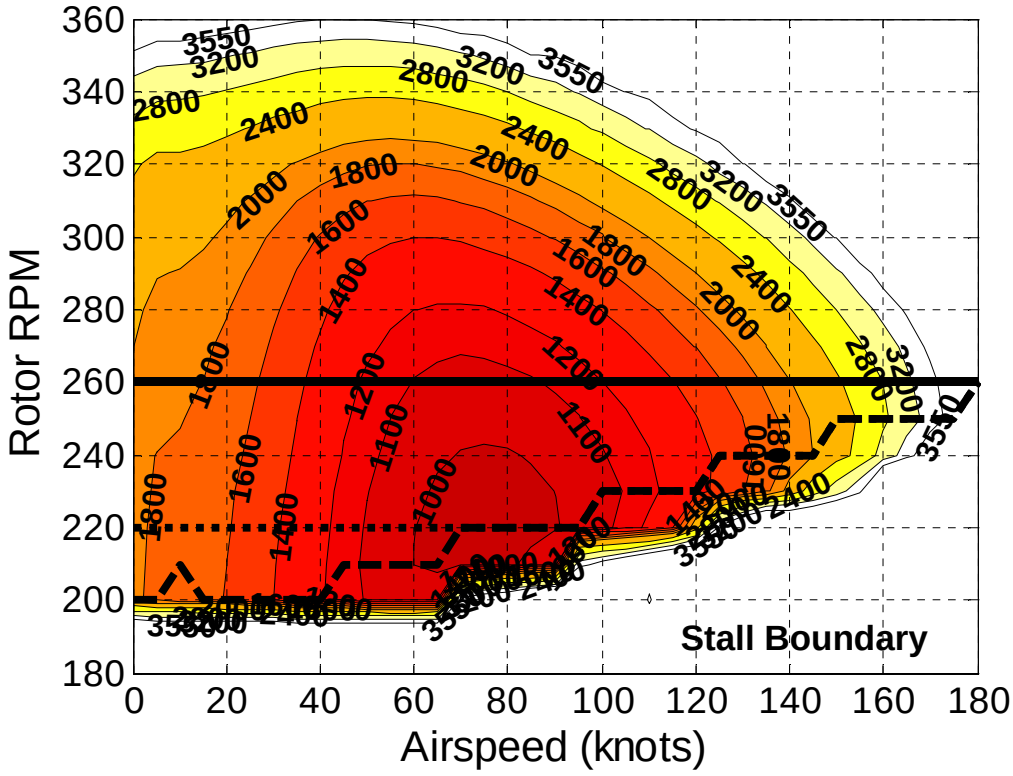

Figure 3.18: Main Rotor Power Contours, 18,300 lbs Gross Weight, 4000 Feet

When the operating altitude is again increased, this time to 8000 feet, the same thing happens, as seen in Figure 3.19. The flight envelope shrinks with respect to maximum airspeed, and the rotor stall speed increases to 220 RPM up to 80 knots, then increases further up to 260 RPM at 165 knots. This means the power-optimal rotor speed is also higher than the sea level or 4000 feet case. In fact, since the stall boundary is at 220 RPM, or 85% of the baseline, the imposed engine control limited rotor speed results in the same optimum as the unlimited case. Figure 3.20 shows the power contours at 12,000 feet. The maximum airspeed reduces to 140 knots for the baseline RPM. When using the optimal rotor speed, this airspeed limit increases to 155 knots as a result of *increasing* the rotor speed. This is contrary to the previous results which showed that rotor speed reduction was the cause of rotor power reduction. This is due to the fact that by increasing rotor speed slightly, in this case by 10 RPM, rotor stall can be

averted, reducing the power requirements that come with airfoils near stall. For low- and moderate-speed flight, the reduced RPM yields a reduced power since the rotor is not particularly close to encountering stall.

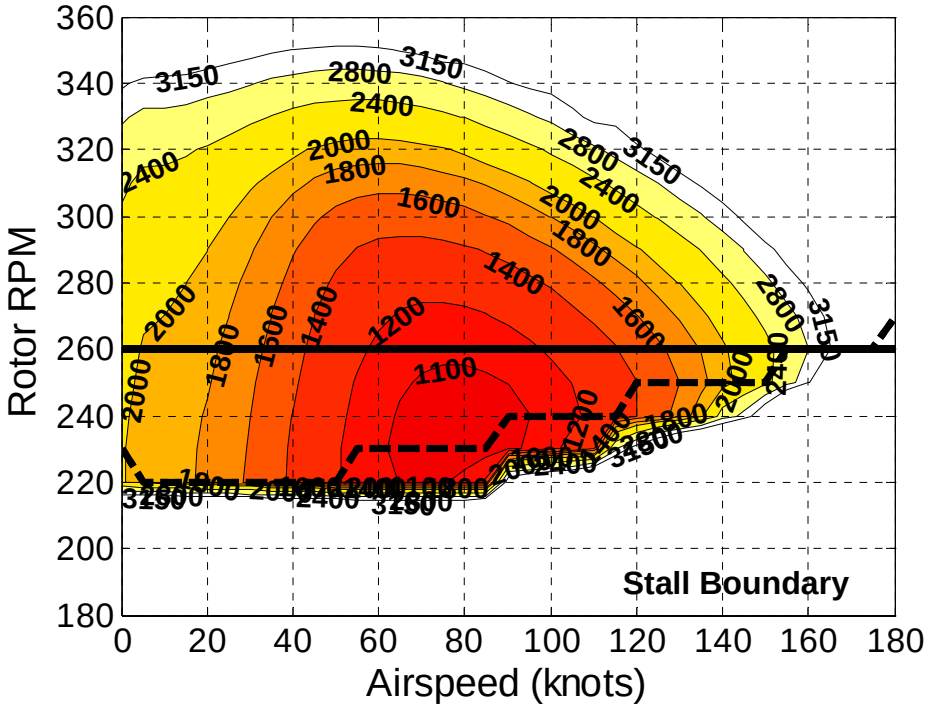

Figure 3.19: Main Rotor Power Contours, 18,300 lbs Gross Weight, 8000 Feet

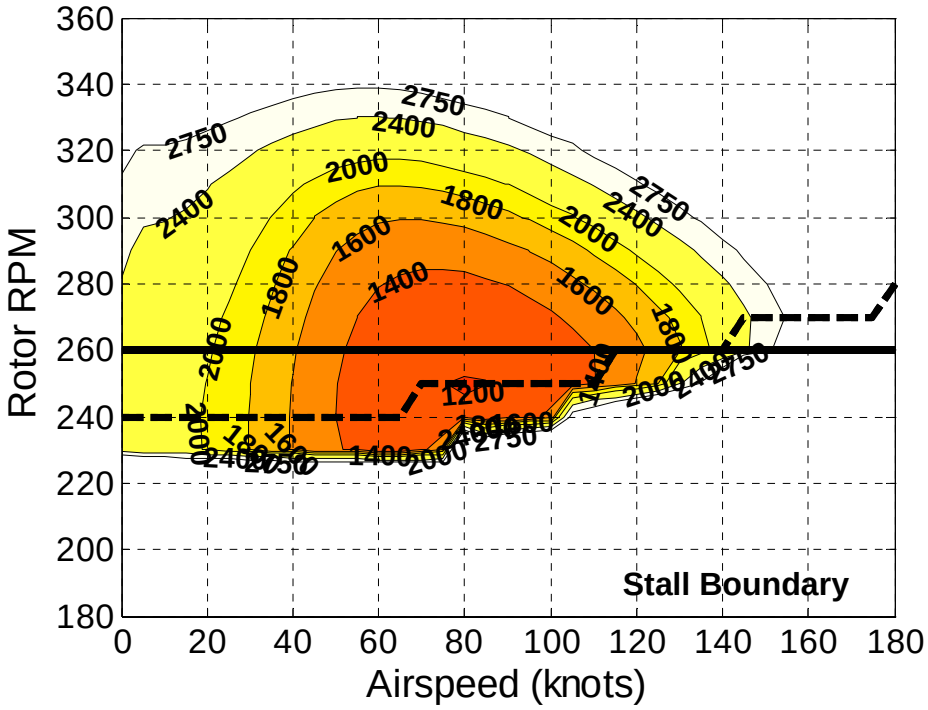

Figure 3.20: Main Rotor Power Contours, 18,300 lbs Gross Weight, 12000 Feet

Figure 3.21 shows the rotor RPM schedules for all of the aforementioned altitudes at 18,300 lbs gross weight. This gives a solid look at how altitude changes the effect of rotor speed on the vehicle. Figure 3.22 shows the corresponding reduction in rotor power for the optimum rotor schedules.

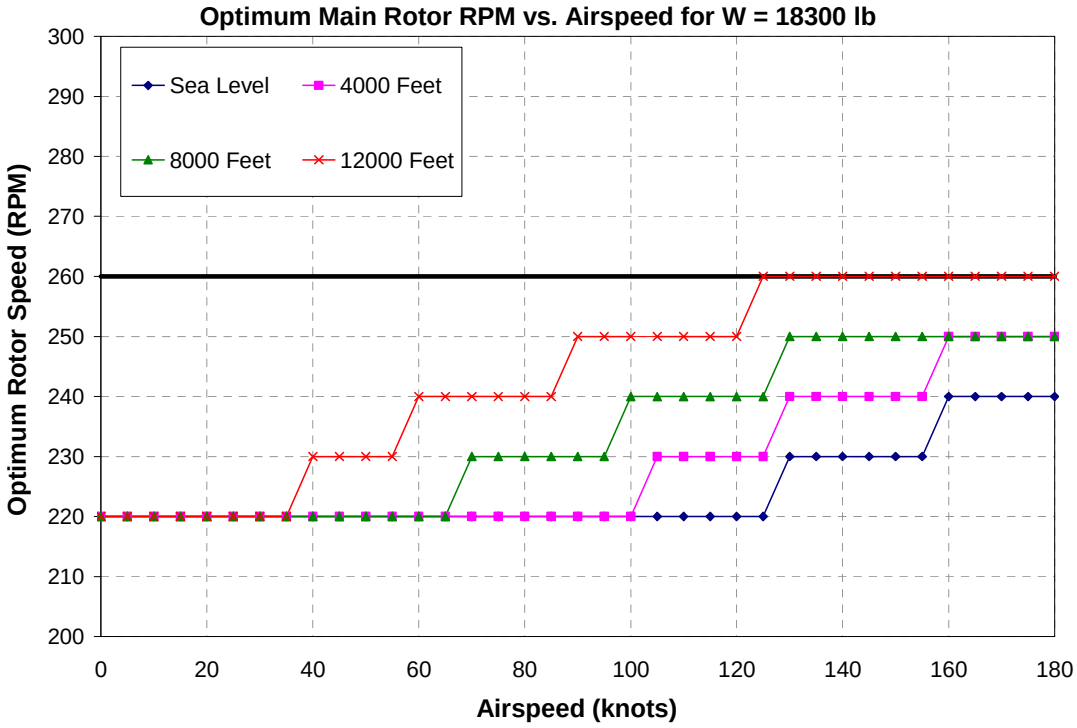

Figure 3.21: Optimal Rotor Speed Schedules, 18,300 lbs Gross Weight

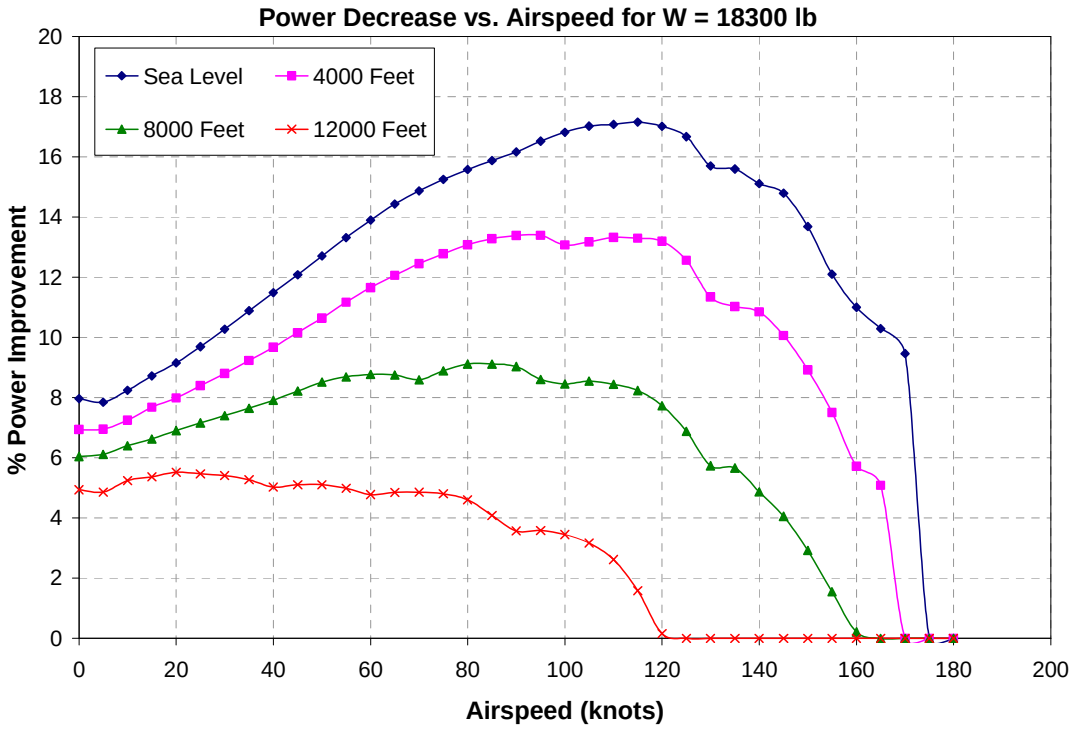

Figure 3.22: Power Reductions at Optimal Rotor Speed, 18,300 lbs Gross Weight

Variation in Gross Weight

All of the previous work was carried out using a gross weight in the middle of the UH-60 range. To gauge the impact of changing gross weights of the helicopter, two additional weights were examined: 16,000 lbs and 22,000 lbs. These correspond to the lowest useful gross weight and the maximum usable weight. The reasons for this are twofold. The first reason is to see how sensitive a variable rotor is to a parameter change and how it would scale. The second reason is to determine the benefits with an increased weight, since a variable speed transmission would likely add to vehicle gross weight. These weight variations were simulated over the same speed and altitude ranges as the baseline case. For the heavier case, there were additional limits encountered as the higher thrust requirements raised the rotor speed of rotor stall compared to the baseline.

Reduced Gross Weight

Sea Level

As with the baseline case, the simulations for the 16,000 lb case were first run for a sea level case. In general, results were similar to the results of the baseline case. The power requirements were lower across the board, as was expected, as the thrust requirements were lower, thus reducing the induced power. It is also apparent that the helicopter can operate at a lower RPM than the baseline weight as rotor stall happens with a lower rotor speed. Figure 3.23 shows the main rotor profile power contours as a function of airspeed and rotor RPM, as in Figure 3.1. The rotor stall boundary for the lightweight case is noticeably lower in the high speed range than that of the baseline case. For this weight, the helicopter can operate down to 180 RPM in the low and cruise speed

ranges. For high speed flight, the stall limit RPM is roughly 20 RPM lower than the baseline weight, and the corresponding optimum RPM for minimum power is lowered by the same amount.

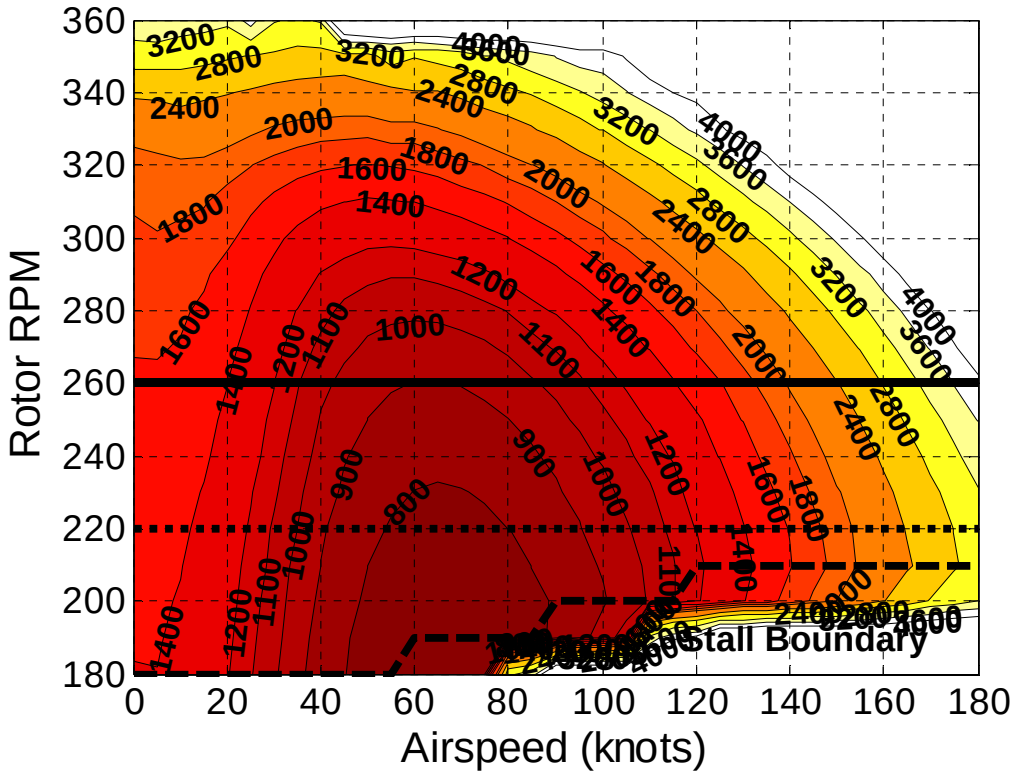

Figure 3.23: Main Rotor Power Contours, 16,000 lbs Gross Weight, Sea Level

The breakdown of induced and profile power does change when the weight is reduced. Induced power is reduced; however, as the thrust requirements correlate directly to a reduced induced power, as illustrated in Figure 3.24. Profile power, being largely driven by the local airspeeds and not, when far from the stall angles, by the angle of attack, stays close to that of the baseline case. This behavior is shown in Figure 3.25. Since the profile power, being roughly the same as before, makes up a larger portion of the total power, and since the profile power is responsible for the reduction in power with reducing rotor speed, the power reductions are more pronounced.

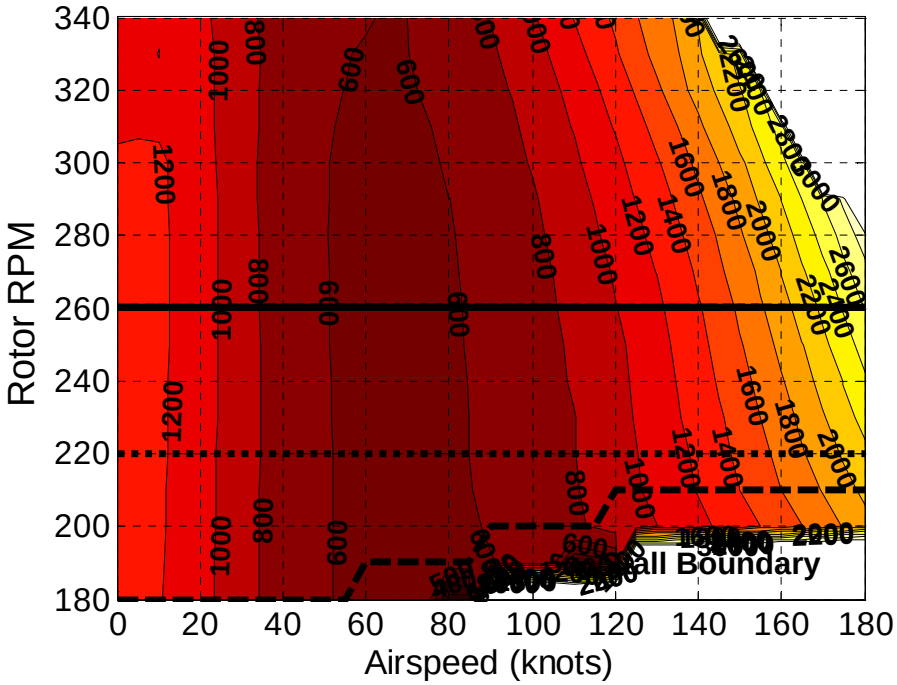

Figure 3.24: Main Rotor Induced Power Contours, 16,000 lbs Gross Weight, Sea Level

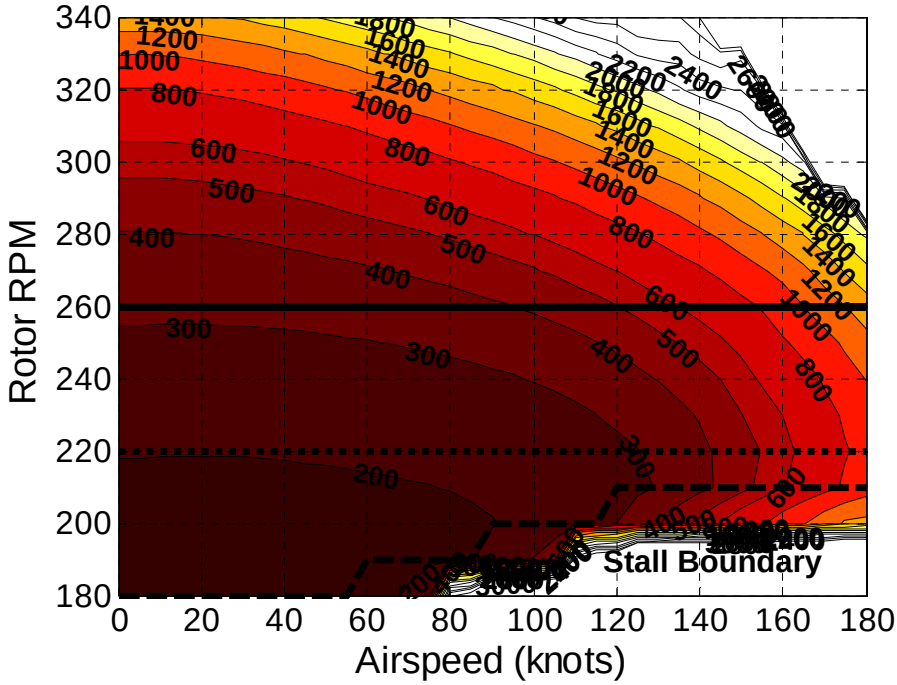

Figure 3.25: Main Rotor Profile Power Contours, 16,000 lbs Gross Weight, Sea Level

Like the baseline gross weight, the effects of optimizing rotor speed with respect to both torque and power were examined. Figure 3.26 shows the optimum rotor speed profiles for the sea level case. As expected, the power optimum signified by a 0% torque weighting showed that reducing rotor speed was the best approach. Like the baseline weight at sea level, the impact of torque resulted in the optimum rotor speed increasing, suggesting that the power reductions from reduced rotor speed were of smaller magnitude than the linear variation of rotor speed. When compared to Figure 3.5, the optimum rotor speeds for the 16,000 lb case tend to drop below the baseline rotor speed for high torque-weighted values more quickly to a lower value overall at moderate- and high-speeds.

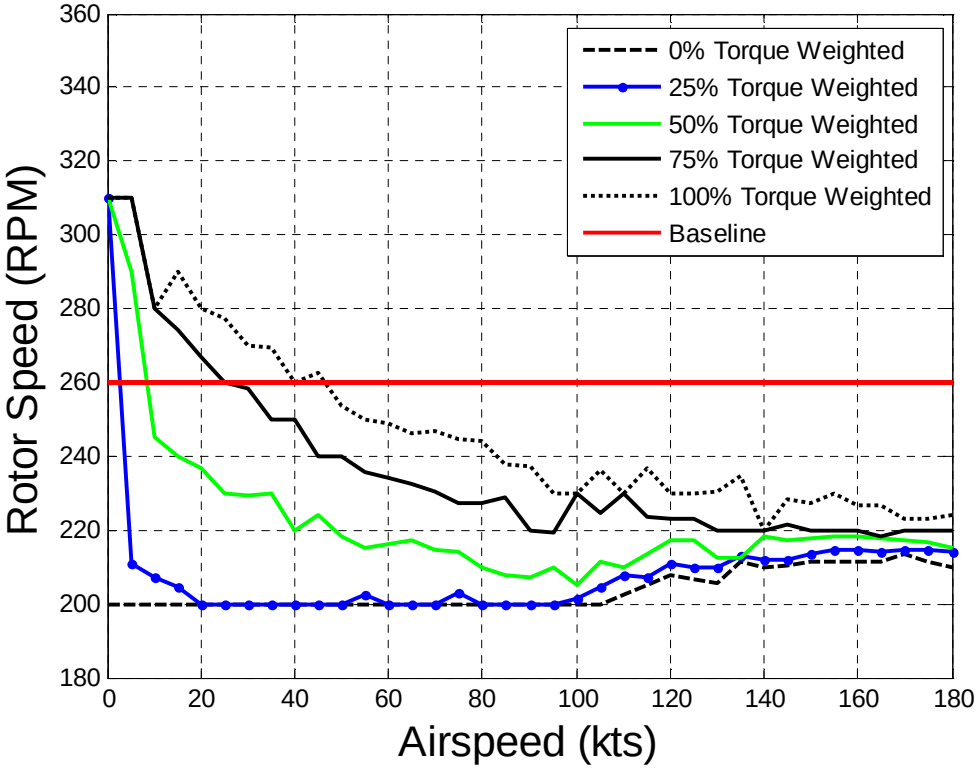

Figure 3.26: Torque Weighted Optimum RPM Schedules, 16,000 lbs Gross Weight, Sea Level

The corresponding power curve can be found in Figure 3.27. As before, the power is higher when torque is a more important consideration at low speeds,

but as airspeed increases, the torque weighted optimum, like the power optimum, yields a lower power. The rotor torque profiles, as seen in Figure 3.28, show the reverse trend: power-weighted optimums yield higher torque values at low speed, quickly reducing to sub-baseline levels as airspeed increases.

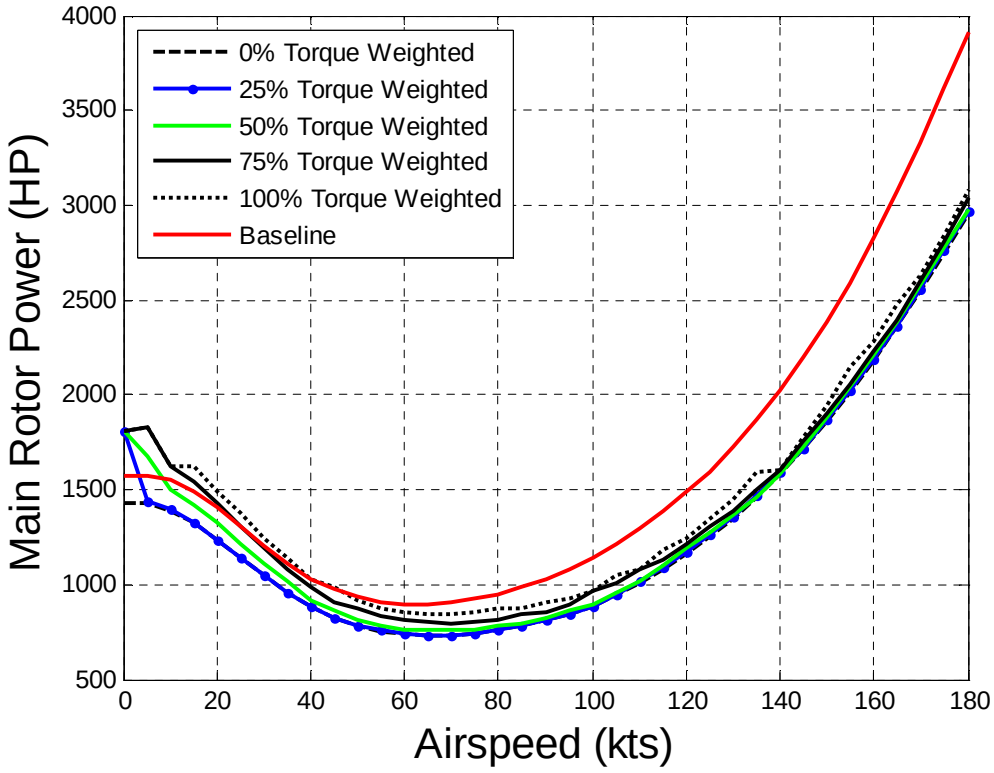

Figure 3.27: Torque Weighted Optimum Power Profiles, 16,000 lbs Gross Weight, Sea Level

The trim requirements for this reduced weight are similar to the requirements for the higher gross weight, with the exception that, since less thrust was required, the pitch and flap magnitudes are slightly lower than the baseline. Since the trends appear the same as the above case, the figures are omitted from this chapter and can be found in Appendix A.

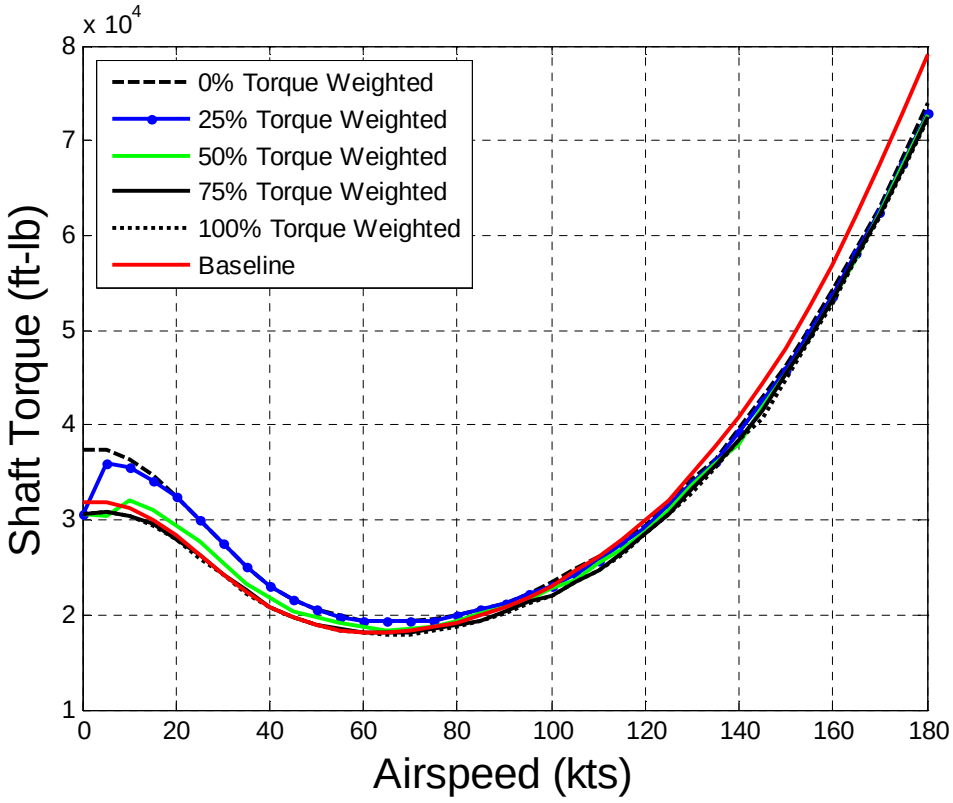

Figure 3.28: Torque Weighted Optimum Torque Profiles, 16,000 lbs Gross Weight, Sea Level

Results at Altitude

When this lower gross weight model was simulated at higher altitudes, the same trends followed as with the slightly heavier case above. Optimum rotor speed was higher compared to the sea level case. It is interesting to note that for an altitude of 12,000 feet, which is the practical limit for a non-pressurized cabin, the power optimal rotor speed is 250 RPM even at the maximum airspeed, as shown in Figure 3.29. This is smaller, albeit only slightly, than the baseline rotor speed. Thus, when the helicopter weight is reduced to this lightweight configuration, it is *never* better to operate at the baseline speed from a performance standpoint.

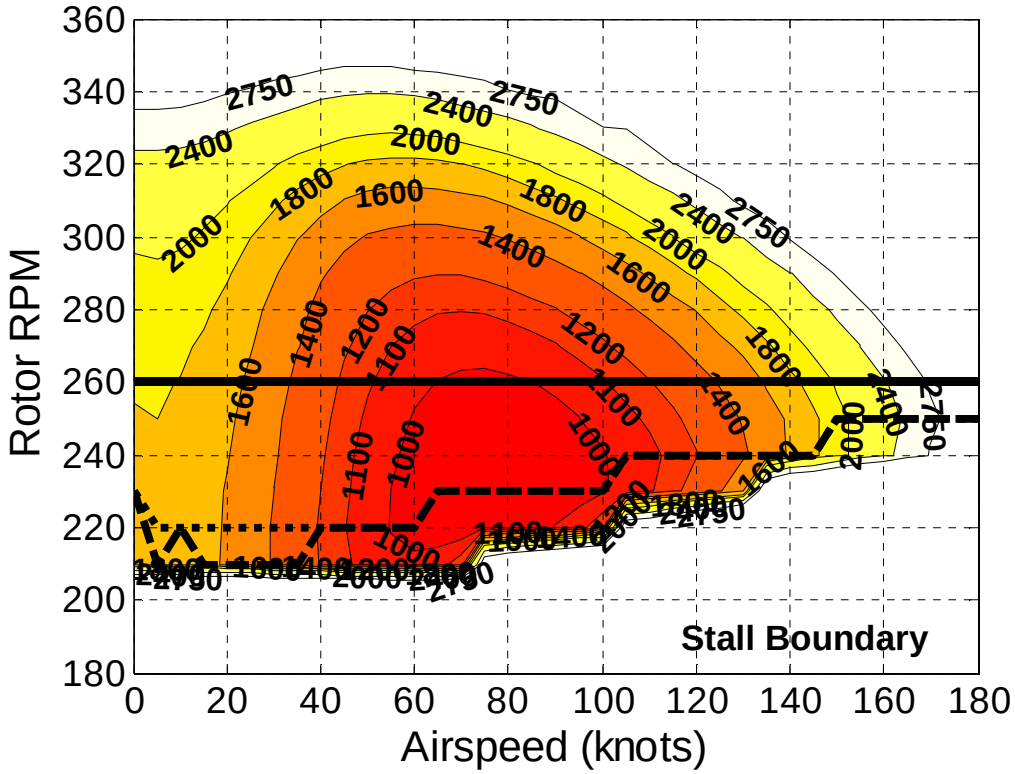

Figure 3.29: Main Rotor Power Contours, 16,000 lbs Gross Weight, 12,000 Feet.

A comparison of the power optimum rotor speed schedules for altitudes between sea level and 12,000 feet is shown in Figure 3.30. This figure uses the limited rotor speed, simulated engine control. Re-affirming the previous point, the rotor speed never reaches the baseline rotor speed even at high speed flight as was seen in the 18,300 lb case. The performance benefits that arise from following this discrete optimum are shown in Figure 3.31. As with the baseline weight, the relative power benefits shrink as altitude increases, except that here, the benefits extend to higher airspeeds than before.

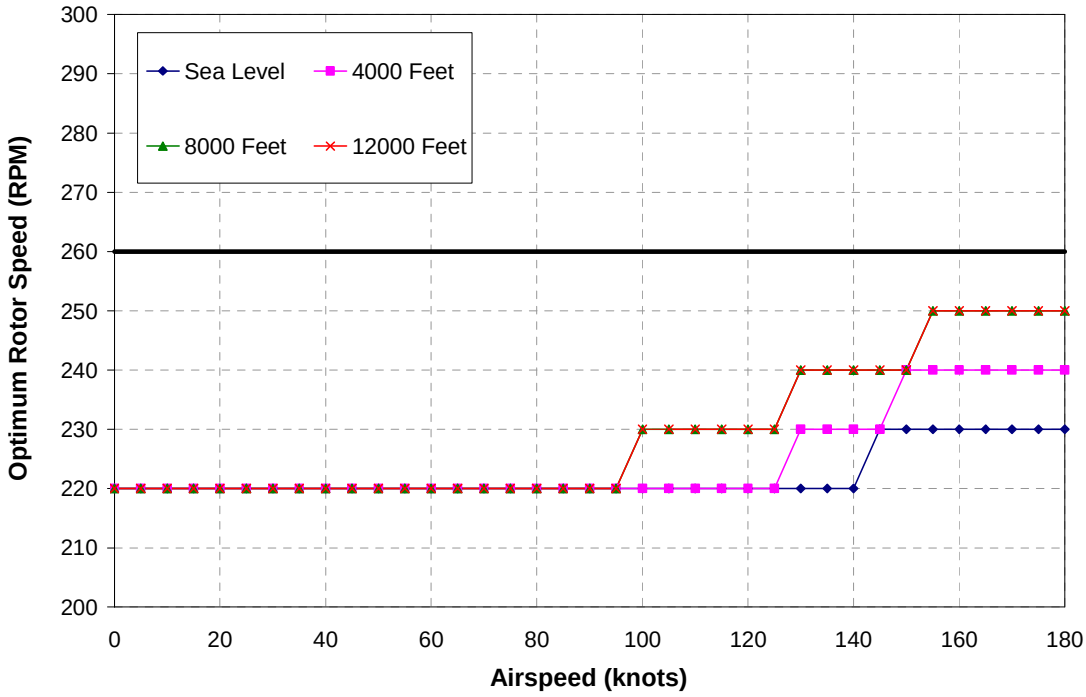

Figure 3.30: Optimal Rotor Speed Schedules, 16,000 lbs Gross Weight

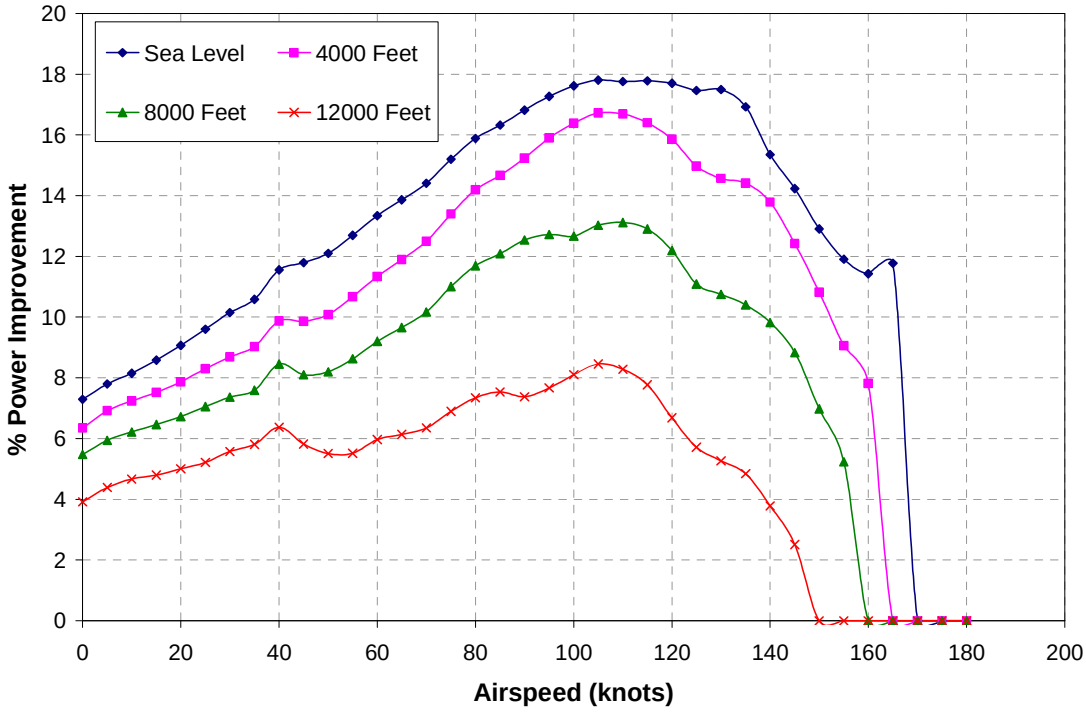

Figure 3.31: Power Reductions at Optimal Rotor Speed, 16,000 lbs Gross Weight

Increased Gross Weight

Sea Level

In addition to the baseline and lightweight case discussed above, trim simulations were performed for a heavy model corresponding to a fully loaded UH-60 helicopter with a gross weight of 22,000 lbs. As one would expect, the power requirements were higher for all conditions than for the baseline or lightweight model. The main rotor power contours shown in Figure 3.32 illustrate the higher power requirements, as well as the reduced maximum speed due to rotor stall. The power optimized rotor speed is higher than before, increasing towards the baseline at high speeds. Profile power, as with the other weights, is the prime culprit for power reductions. Figure 3.33 shows the main rotor profile power contours. Induced power becomes even larger for this weight, but continues to be nominally independent of airspeed, especially at low-speeds, as in Figure 3.34

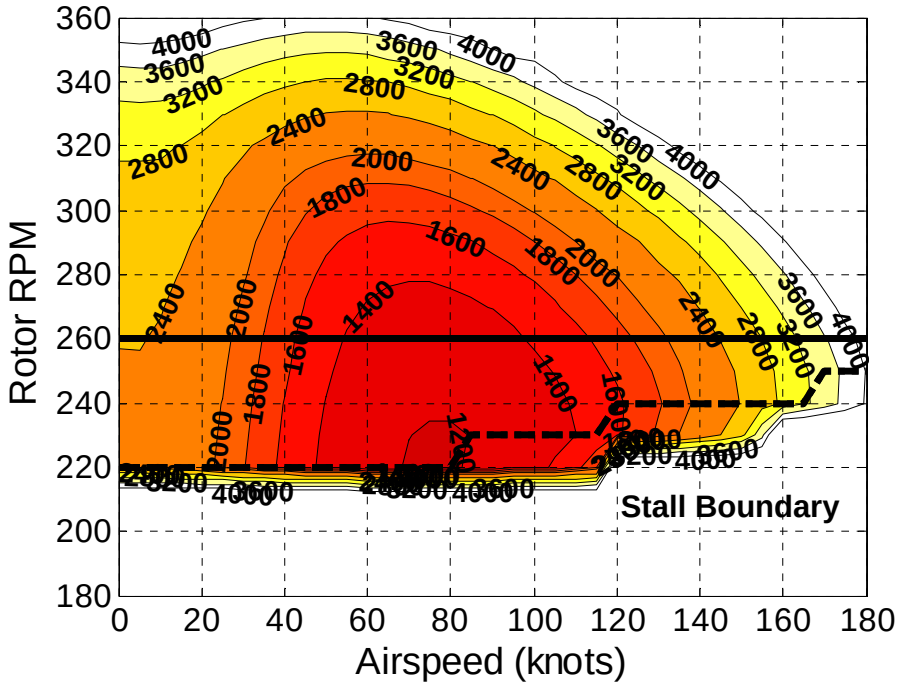

Figure 3.32: Main Rotor Power Contours, 22,000 lbs Gross Weight, Sea Level

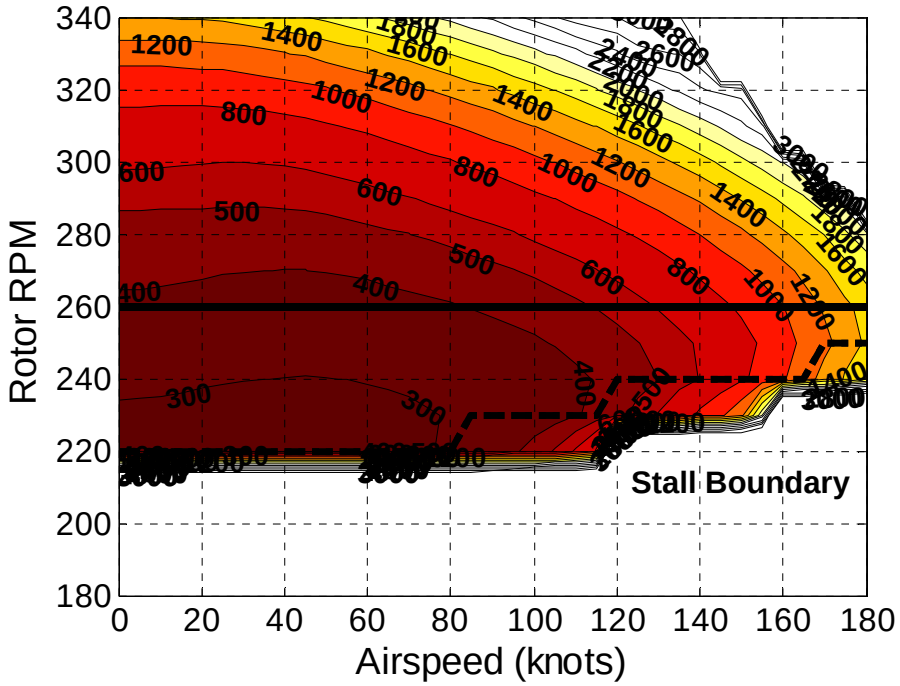

Figure 3.33: Main Rotor Profile Power Contours, 22,000 lbs Gross Weight, Sea Level

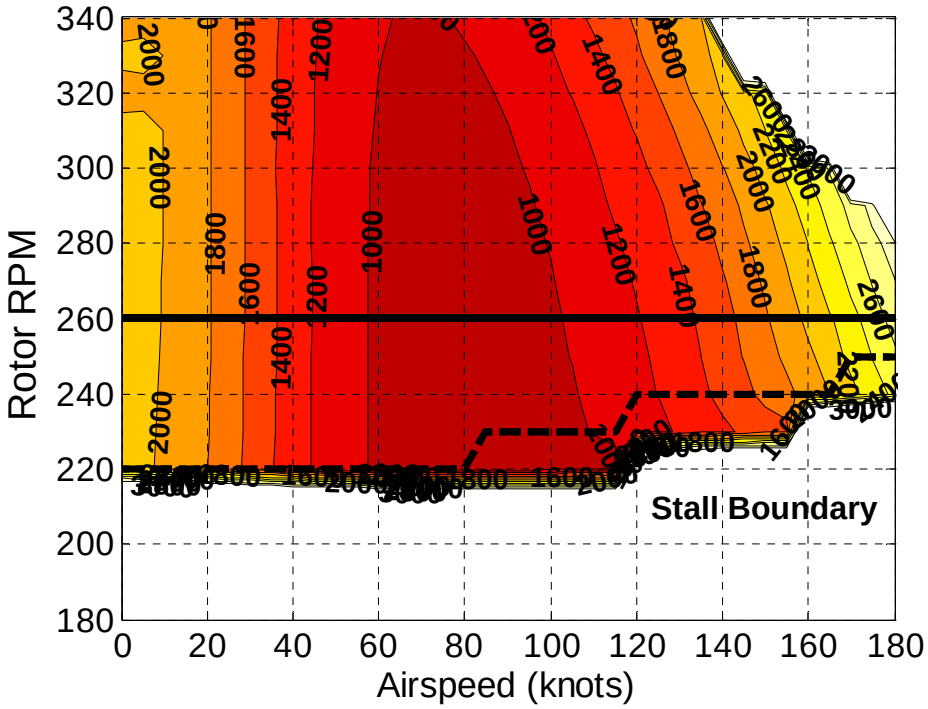

Figure 3.34: Main Rotor Induced Power Contours, 22,000 lbs Gross Weight, Sea Level

Results at Altitude

The heavyweight UH-60 model was trimmed for altitudes ranging from sea level to 12,000 feet. The trends in rotor power with respect to rotor speed and airspeed were similar to the other gross weights investigated. The maximum forward speed was reduced for the same altitudes, and in some cases, hover and low speed flight power requirements were higher than available power, thus meaning that the vehicle could not hover at altitudes above 8000 feet.

At 4000 feet, the power contours are similar to that of the sea level simulation. There are some significant differences, however. Figure 3.35 is the first case to show that near hover, the optimal rotor speed is higher than the optimal rotor speed in the cruise range. The optimum speed drops from 240 RPM

to 220 RPM (the 15% limit) at 20 knots, then slowly increases as airspeed increases. Between 135 and 160 knots the optimum rotor speed is actually the baseline rotor speed. The figure shows that an increase in rotor speed is optimal past 160 knots, however, engine power is not available to fly here, and thus it is not significant. At 8000 feet, as in Figure 3.36, the behavior is the same at lower speeds. The stall limit is of course higher, but the rotor speed dip is still evident, if to a lesser extent, around 20 knots. Again, the optimal rotor speed increases with airspeed, eventually equaling the baseline rotor speed of 260 RPM at 85 knots until 120 knots. At speeds higher than this, the power optimized rotor speed is actually higher than the baseline helicopter design. By increasing rotor speed to 270 RPM, the flight envelope, with a stall margin, expands from 130 to 150 knots. Obviously stall margin takes on a slightly different meaning when variable rotor speed is available, but power weighted stall margin, the ability to avoid stall and still operate relatively efficient, is still important. For speeds greater than 145 knots, the optimal approach would be to increase rotor speed again to 280 RPM. Since rotor power is limited, especially at altitude, this falls outside the flight envelope. For a larger engine, flight at these speeds is possible by avoiding rotor stall dependent on blade sizing.

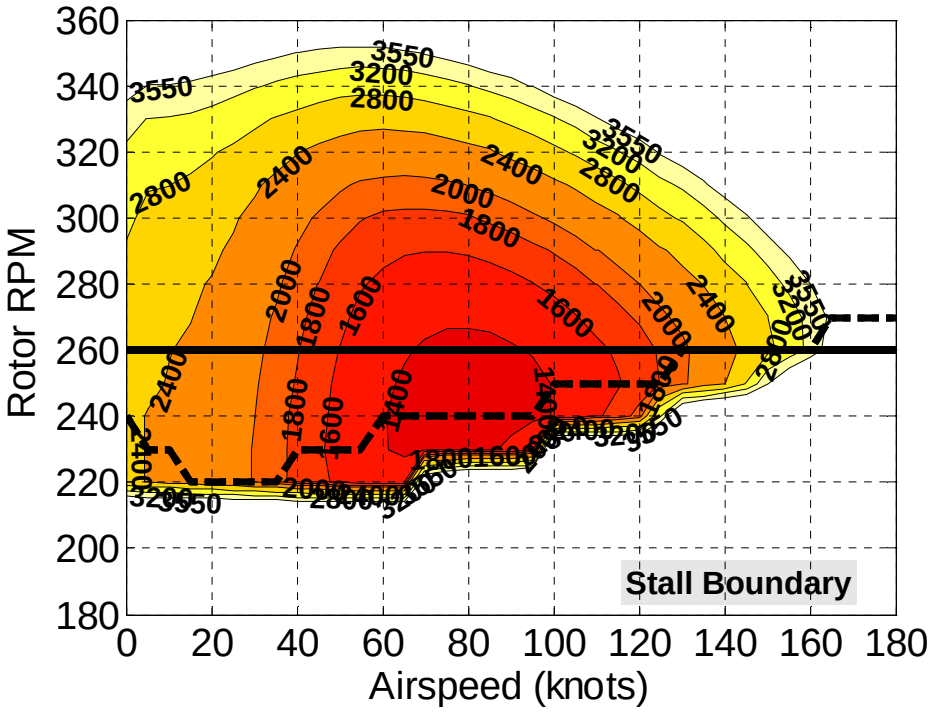

Figure 3.35: Main Rotor Power Contours, 22,000 lbs Gross Weight, 4000 Feet

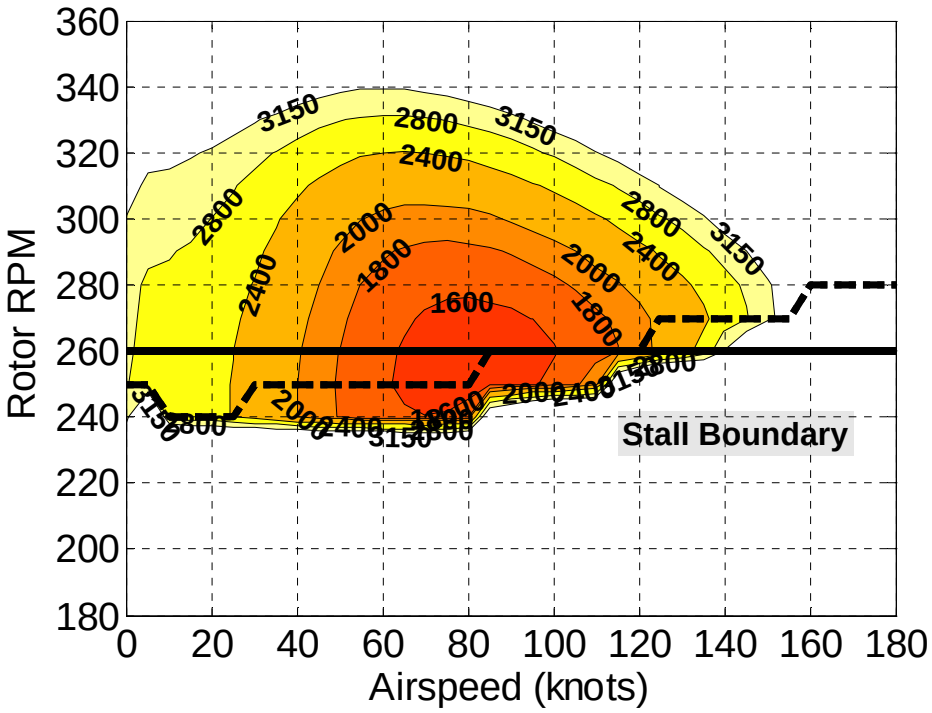

Figure 3.36: Main Rotor Power Contours, 22,000 lbs Gross Weight, 8000 Feet

The simulation at 12,000 feet further expanded on this increased RPM phenomenon. Figure 3.37 shows that at this altitude with a gross weight of 22,000 lbs, the optimal rotor speed is equal to or greater than the baseline rotor speed for the entire flight envelope. In fact, for most of the airspeed range, the baseline helicopter would not be able to fly due to rotor stall. Assuming that stall margin is not a concern, the flight envelope at this altitude increases from a maximum speed of 90 knots to a speed of 130 knots. If the safety of flying at the stall limit is questioned, the expansion encompasses the entire envelope, from 30 knots to 130 knots, even leaving a 10 RPM stall margin.

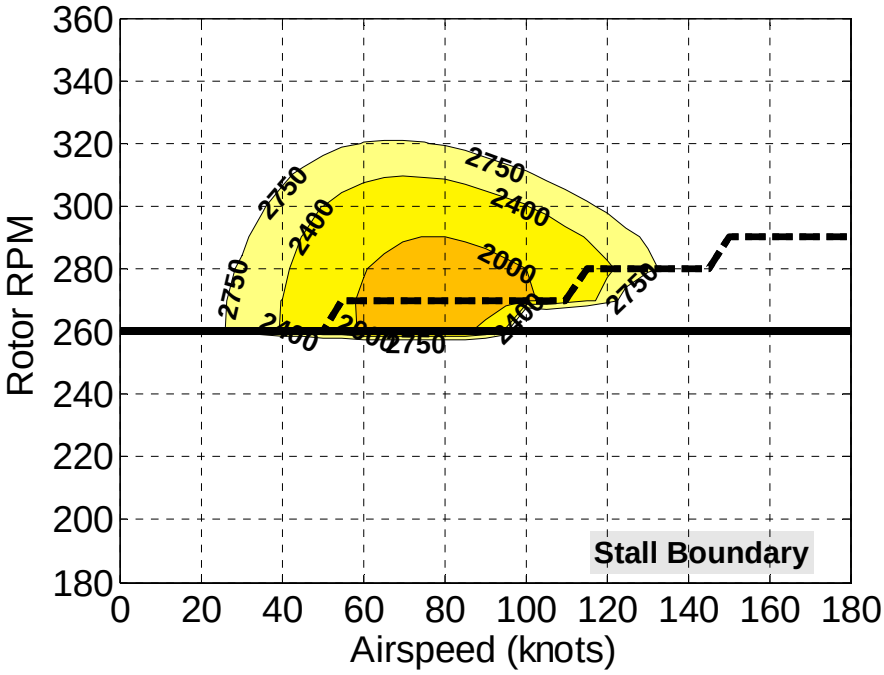

Figure 3.37: Main Rotor Power Contours, 22,000 lbs Gross Weight, 12,000 Feet

The optimum rotor speed schedules are shown in Figure 3.38. The rotor speeds at 4000 and 8000 feet demonstrate a “dip” in RPM at around 20 knots, then an increase up to and beyond the baseline rotor speed. The schedule for 12,000 feet shows that the entire flight envelope is optimal at or above the baseline speed. The power reductions for these rotor speeds can be seen in Figure 3.39. The high points correspond to the trim limits of the baseline rotor

speed, thus showing that flight is possible with a variable rotor speed, hence an apparent power reduction.

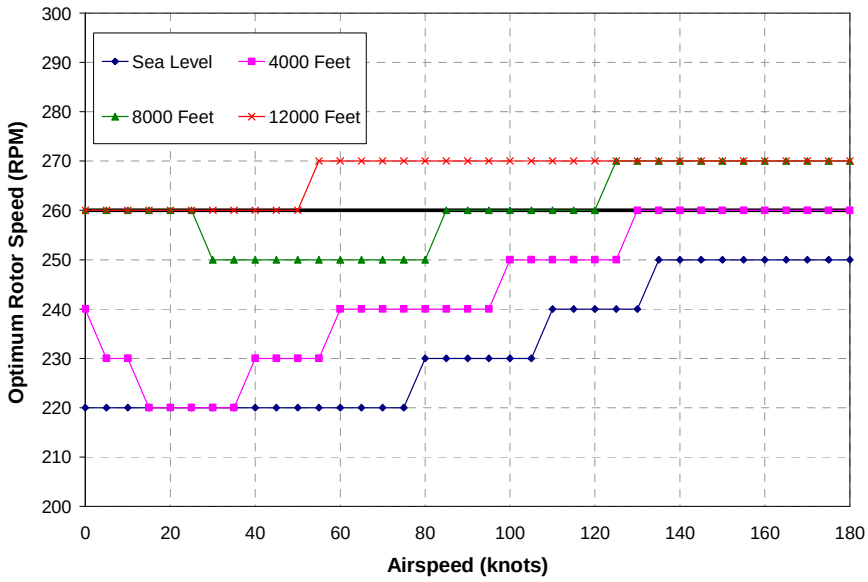

Figure 3.38: Optimal Rotor Speed Schedules, 22,000 lbs Gross Weight

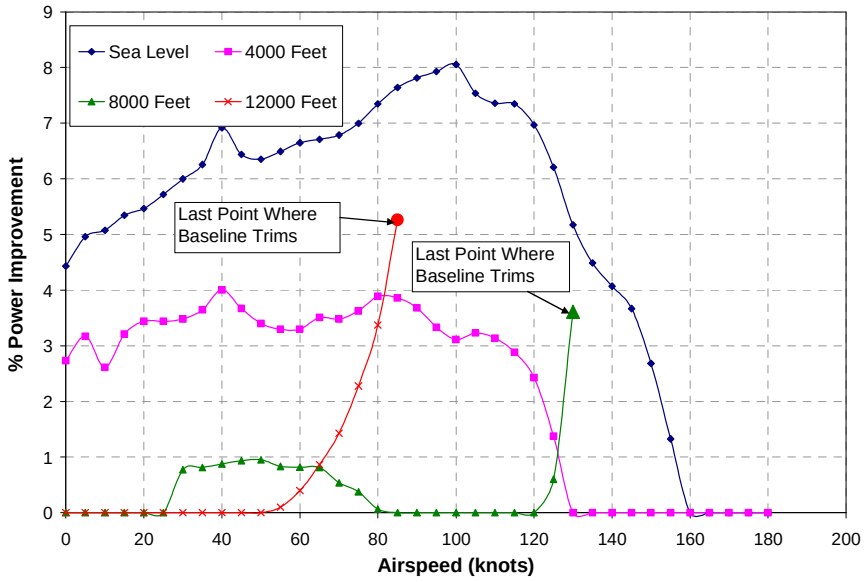

Figure 3.39: Power Reductions at Optimal Rotor Speed, 22,000 lbs Gross Weight

Chapter 4

Conclusions and Recommendations

Summary

This research was conducted to explore the concept of variable rotor speed throughout the flight envelope of a UH-60 helicopter. The primary goal was to investigate the possibility of power reduction. The requirements to trim the aircraft, namely blade collective and cyclic pitch, pitch and roll attitude of the aircraft, and shaft torque were also studied to ensure that reduction in power through rotor speed changes was still within the operating limits of the helicopter.

Sea level flight simulations of the UH-60 showed that power reductions could indeed be achieved through variable rotor speed while still maintaining the vehicle's ability to trim. Power reductions were seen when the rotor speed was reduced. A lower limit of 85% of the baseline rotor speed of 258 RPM was used to enforce a model that could be feasibly controlled through engine speed controls. By eliminating the need for a variable speed transmission, the weight and power estimates of the aircraft could be kept the same. Power reductions of up to 17% were observed in the cruise speed range, near 120 knots. Regardless of vehicle weight, sea level simulations showed power reductions through rotor speed reductions.

When torque was included as a factor for rotor speed optimization, the trends changed at low speeds. Instead of unilaterally decreasing rotor speed to optimize performance, some cases required an increased rotor speed. This was especially notable when torque was weighted the same as or greater than power. These cases showed that increasing the rotor speed of the helicopter above the

baseline from hover to 20 knots would reduce rotor torque without significant power penalties. This behavior was independent of vehicle weight as the hover and low-speed sensitivity to power was small; small increases in RPM decreased torque but left power relatively unchanged.

Through all of the simulations, the most significant limitation to helicopter performance with a variable speed rotor was rotor stall. In forward flight, regardless of gross weight or altitude, the lower RPM limit was defined by the onset of rotor stall. The location of rotor stall was significantly impacted by gross weight, but the fact that this border increased as airspeed increased shows that it is the most important limiting factor in using variable rotor speed to reduce power. As a result, for the baseline weight of 18,300 lbs, high speed flight corresponded with the rotor speed increasing towards the baseline of 258 RPM. The 16,000 lbs gross weight case showed that the upper limits of airspeed were reachable with a rotor speed of around 240 RPM, signifying that the rotor RPM could be decreased more before reaching stall. High gross weight, at 22,000 lbs, required even faster rotor speeds, equal to or greater than the baseline speed for high speed forward flight.

This trend became more evident as operating altitude increased. Since an increase in altitude results in a decreased air density, dynamic pressures decrease as well. Reducing the dynamic pressure for a given rotor speed will then require increased rotor pitch to provide the same amount of lift. Since the blades are limited to the stall limit of the SC-1095 airfoil, the minimum rotor speed will increase. This results in less rotor power reduction as nearly all of the power reductions were the result of profile power, and dynamic pressure, reductions. By stalling at higher speeds, the profile power component does not decrease as much.

For these reasons, in some conditions it was shown that the best rotor speed for power was an increase over the baseline. This was most prominent for

the 22,000 lbs gross weight at 8,000 and 12,000 feet. The 8,000 feet simulation showed that for high speed flight, rotor power could be decreased by increasing rotor speed, since this allowed the airfoils to operate farther from the stall region, and thus with less profile drag. There was also a small increase in maximum airspeed, though not significant. These effects were magnified when the altitude increased to 12,000 feet. Here, the entire airspeed range yielded reduced power, or increased envelope, by increasing rotor speed. Hover was still not possible, but, for a moving helicopter, the required power for high altitude flight was decreased. For high speed flight, increasing the rotor speed resulted in expanding the flight envelope, with a maximum speed increase of 40 knots, from 90 to 130 knots.

Throughout the airspeed and altitude simulation ranges, variable rotor speed showed noteworthy reductions in rotor power. Some areas, especially cruise speed, show large reductions in power though the use of variable rotor speed. High altitude flight envelope expansion through increased rotor speed shows that varying the speed throughout the operating envelope is important. Simply reducing rotor speed from the baseline will not help high altitude or high speed performance; a controllable variation is needed for these conditions.

Recommendations for Future Work

The research discussed in this thesis is important in that it sets the stage for a long-term serious look into implementing variable rotor speed in helicopters. There is still a large body of research yet to be undertaken in this field, including different vehicle models, improved inflow models, advanced blade dynamics, elastic blade models, and acoustic analysis.

This thesis only addresses a medium weight, conventional helicopter design. While it is an important component of the overall helicopter fleet, especially in the military, there are other areas that could potentially benefit. Expanding this basic analysis to lightweight and heavy lift helicopters with conventional tail rotor layouts could show even more benefits of variable rotor RPM. Applying this to a tandem or coaxial helicopter could show different benefits, since rotor torque becomes a different concern for this design. Conventional tail rotors are designed for a certain torque load that does not account for variable RPM. This layout is the limiting factor in implementing a variable speed rotor system on a conventional helicopter platform.

The effects of reduced takeoff weight due to reduced fuel are also out of the scope of this study. It must be mentioned as reduced power, especially in the cruise speed range, will result in reduced fuel requirements to achieve the same range and operational capability as the baseline aircraft. Fuel is an important component of gross weight early in the flight plan, so a reduction in this need would yield an even more pronounced power reduction. Detailed mission and flight plan analysis would need to be conducted to fully realize this benefit and would be an important part of any variable speed rotor design.

This study is also inherently limited by the choice of a production helicopter for the model. In practice, any serious integration of variable rotor speed in a new helicopter will be the result of an integrated design approach. The A-160 Hummingbird is an example of this approach, though it has much room to grow. The use of a variable speed drive system will show larger improvements than an engine speed control system would. Next generation variable rotor speed aircraft would likely be designed around a multiple rotor system. As mentioned in the paper, rotor torque is an important issue that must be understood. Significant power gains can be made by reducing rotor speed, but this can entail an increase in torque at low speeds. The easiest way to negate this problem is to use a coaxial or tandem configuration with counter-rotating rotors. In this case, a

vehicle designed to take advantage of the performance benefits of variable RPM can do so without major torque repercussions.

As mentioned in Chapter 1, the use of a momentum based inflow model is not sufficient for low airspeed power predictions. Future work should include use of a free vortex wake inflow model. This will improve the accuracy of low speed power predictions. Another area for research is using advanced dynamic blade models, including lag and torsion, and implementing finite element analysis methods. One concern with varying rotor speed is the possibility of exciting a fuselage or rotor mode, thus resulting in instabilities or increased vibration levels. If this is indeed true, blade tailoring and isolation devices may be necessary to fully utilize the performance gains from a variable speed rotor safely. For a variable speed engine and driveline, vibration characteristics could, and most likely will, change due to the increased periodicity of the rotor forcing. Since the advance ratio for the rotor increases at a given airspeed as rotor speed is reduced, the vibratory loads will increase in magnitude. This adds another level of complexity to the helicopter modeling. If these vibrations interfere with operation, another layer of isolation and damping devices could be necessary. Even so, the performance benefits achievable with a variable speed system are significant enough that the added complexity could be worth it.

Finally, the acoustic properties of a variable speed rotor warrant further investigation. General understanding links reduced rotor speed to reduced acoustic energy. However, the increase in lift coefficients with reduced rotor speeds could lead to increased vortex strength. This could lead to an increased in Blade-Vortex interaction noise.

Bibliography

1 Karem, Abraham E., 1999. *Optimum Speed Rotor*. U.S. Patent Application No. 60/075,509, Feb. 20, 1998.

2 Prabhakar, Tushar, "A Centrifugal Force Actuated Variable Span Morphing Helicopter Rotor." *Proceedings of the American Helicopter Society 63rd Annual Forum*, Virginia Beach, VA, May 1 – 3, 2007.

3 Floros, M. and Johnson, W. "Performance Analysis of a Slowed-Rotor Compound Helicopter Configuration." *Proceedings of the American Helicopter Society 4th Decennial Specialists Conference on Aeromechanics*, San Francisco, CA, January 21-23, 2004.

4 Carter, Jay Jr, "Carter Copter Aircraft," *Proceedings of the American Helicopter Society 59th Annual Forum*, Phoeniz, AZ, May 6-8, 2003.

5 Chen, Robert T. N. "An Exploratory Investigation of the Flight Dynamics Effects of Rotor RPM Variations and Rotor State Feedback in Hover." National Aeronautics and Space Administration. Ames Research Center, Moffet Field, CA. September 1992.

6 Iwata, Takanori and Rock, Stephen. "Benefits of a Variable Rotor Speed in Integrated Helicopter/Engine Control." *Proceedings of the American Institute of Aeronautics and Astronautics, Guidance Navigation and Control Conference*, Monterey CA. August 9 – 11, 1993.

7 Yoshizaki, Yuji. *Swashplateless Control of a Rotary Wing UAV Using Variable RPM and Movable CG.* MS Thesis, The Pennsylvania State Universtiy, 2007.

8 Jenkins, J.L. "Wind Tunnel Investigation of a Lifting Rotor Operating at Tip-Speed Ratios from 0.65 to 1.45." National Aeronautics and Space Administration. Langley Research Center, Langley, VA, February 1, 1965.

9 Floros, Matthew and Johnson, Wayne. "Stability Analysis of the Slowed Rotor Compound Helicopter Configuration." *Proceedings of the American Helicopter Society 60th Annual Forum*, Baltimore, MD, June 7-10, 2004

10 Bluman, James E. *Reducing Trailing Edge Flap Deflection Requirements in Primary Control through a Moveable Horizontal Tail*. MS Thesis, The Pennsylvania State University, 2006.

11 Yeo, H., Bousman, W., Johnson, W., “Performance Analysis of a Utility Helicopter with Standard and Advanced Rotors,” *Journal of the American Helicopter Society*, January 2005.

12 Belegundu, Ashok D. and Chanbrupatla, Eirupathi R., *Optimization Concepts and Applications in Engineering.* Prentice Hall, Upper Saddle River, NJ, 1999.

13 Leishman, J. Gordon, *Principles of Helicopter Aerodynamics.* Cambridge University Press, New York, NY, 2006.

Appendix A

Additional Figures

18,300 lbs Gross Weight

This gross weight was the baseline model for the study, since it lies in the middle of the helicopters weight range. Additional trim results are shown here for higher altitude simulations. These results were not of critical importance to the understanding of the concept, but are useful for showing that the trends continue to apply as altitude increases, such as increasing stall boundary, predominance of profile power in power reductions and increase in required collective.

At 4000 feet, the induced and profile power contours looks very similar to the sea level case. Induced power in Figure A.1 shows sensitivity to operating altitude by increasing as altitude increases. The profile power does not show any appreciable change with respect to altitude in Figure A.2 when you compare the 4000 ft. case with the sea level case in Chapter 3. Figure Figure A3 shows an increase in main rotor collective with altitude. In most cases near the baseline rotor speed, the collective angle increases between 0.5 and 0.7 degrees.

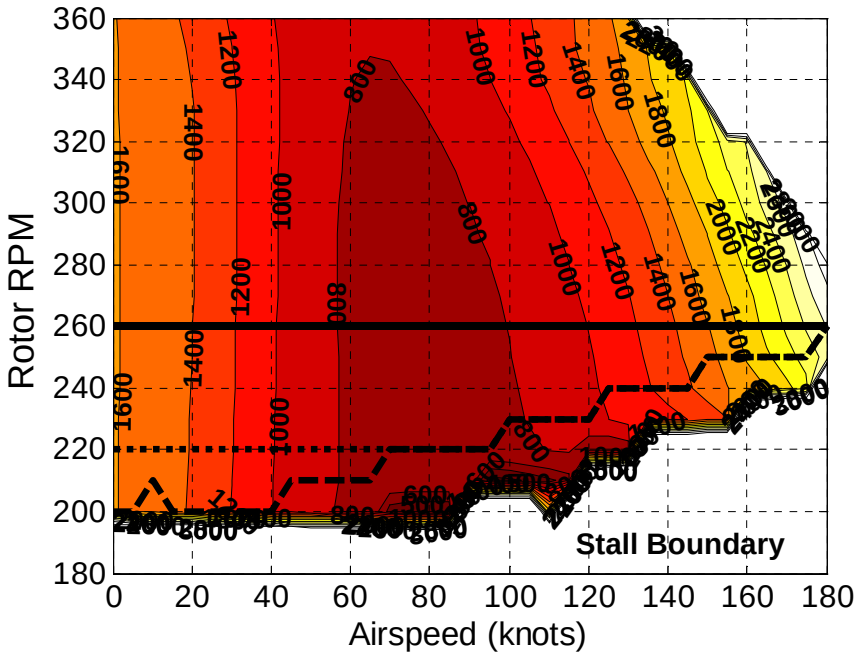

Figure A.1: Induced Power Contours, 18,300 lbs Gross Weight, 4000 feet

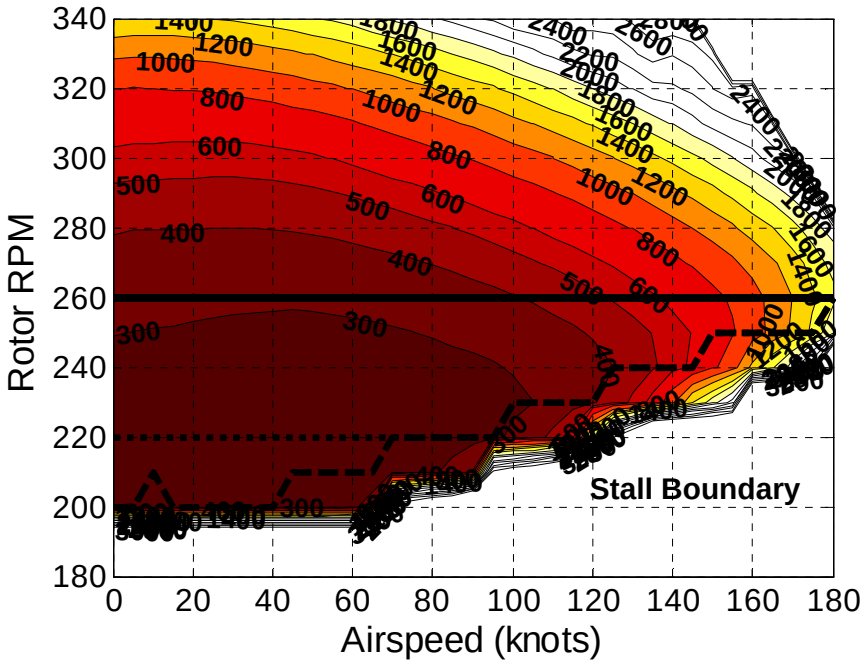

Figure A.2: Profile Power Contours, 18,300 lbs Gross Weight, 4000 feet

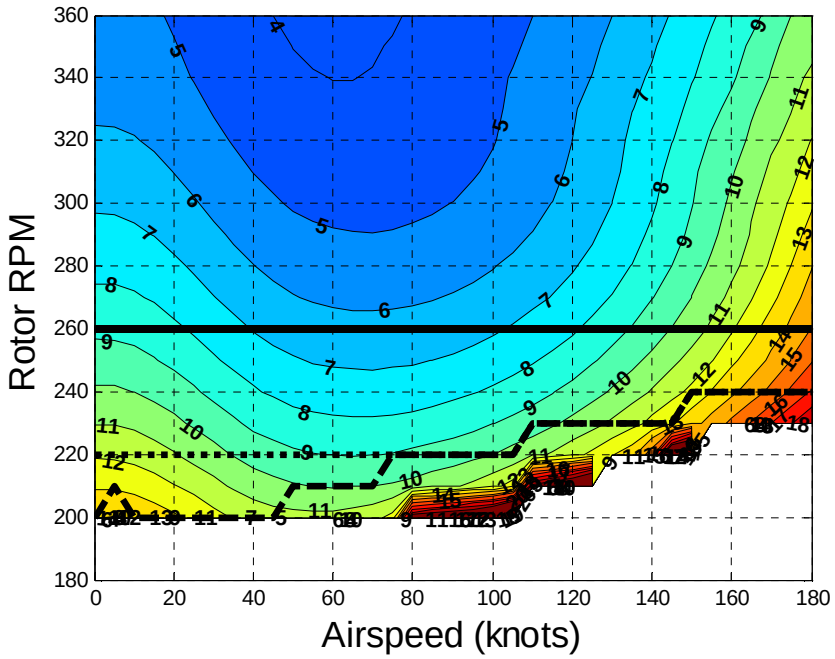

Figure A3: Main Rotor Collective Pitch, 18,300 lbs Gross Weight, 4000 feet

As the altitude increases further to 8000 feet, induced power again increases. Figure A.4 shows this increase, especially near hover. Figure A.5 shows that profile power begins to increase as airspeed increases, but for the cruise speed range it remains the same. This slight increase in profile power occurs because the decreased air density results in rotor blade pitch close to stall for high speeds. This is evident in the upward movement of the stall boundary when compared to the 4000 ft. case. Figure A.6 shows that rotor collective continues to increase by approximately 0.7 degrees across the airspeed range.

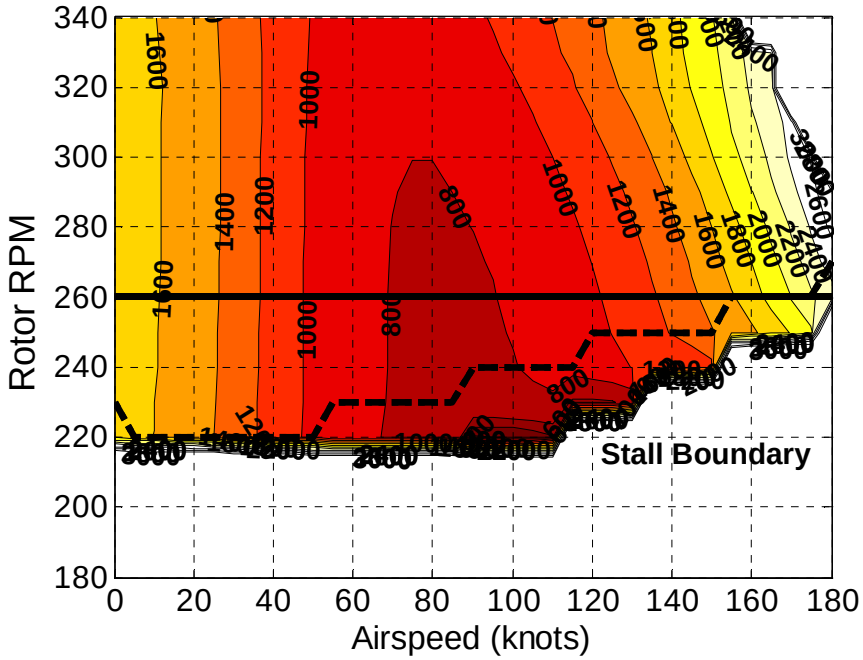

Figure A.4: Induced Power Contours, 18,300 lbs Gross Weight, 8000 feet

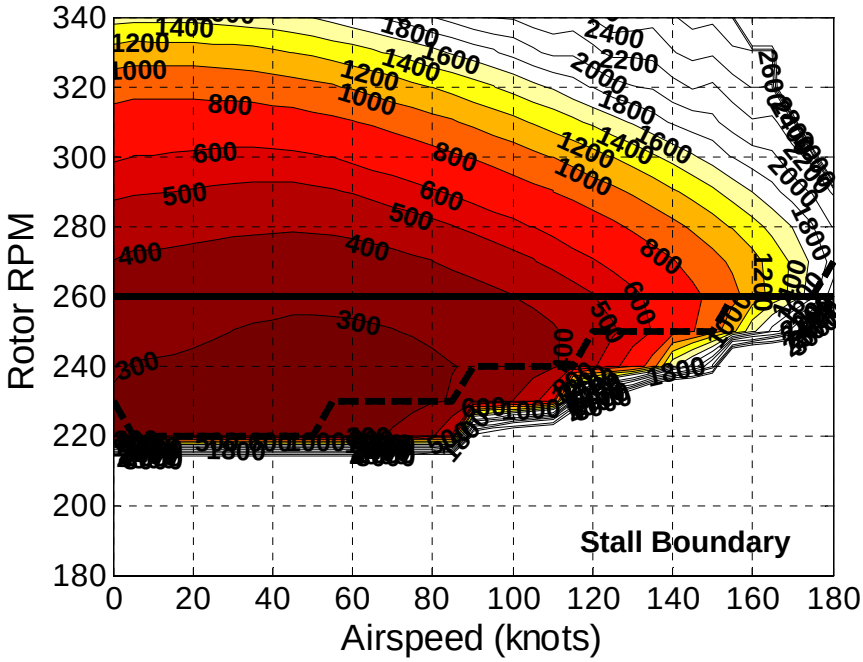

Figure A.5: Profile Power Contours, 18,300 lbs Gross Weight, 8000 feet

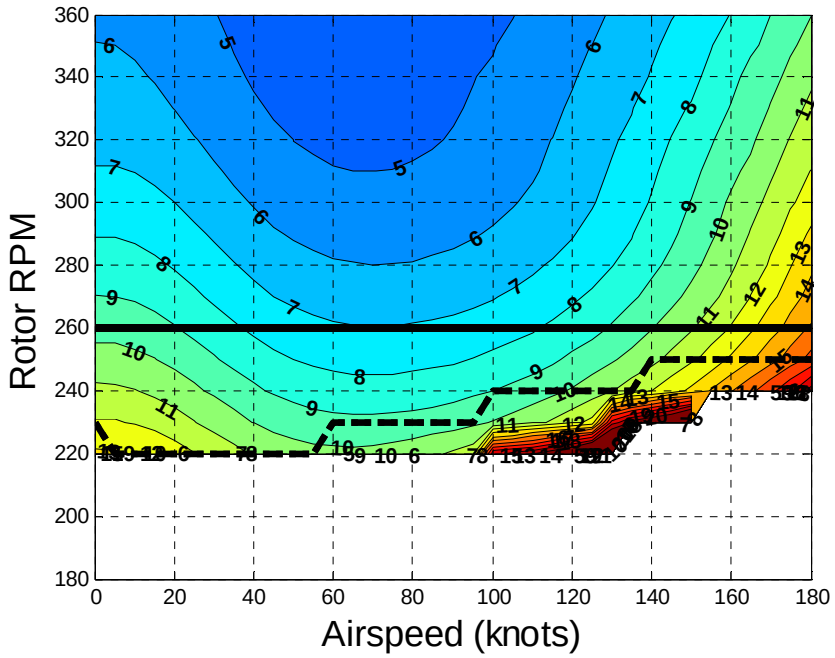

Figure A.6: Main Rotor Collective, 18,300 lbs Gross Weight, 8000 feet

At 12,000 feet altitude, the rotor speed stall boundary has increased again. For airspeeds greater than 150 knots, the stall boundary is equal to or greater than the baseline rotor speed of 258 RPM. Figure A.7 shows that the induced power requirements are now over 800 HP across the whole range, with low speed and high speed flight requiring up to 2400 HP, if such power were available. The profile power in Figure A.8 shows that the rotor is closer to stall. The minimum profile power nearly 400 HP, with no significant decreases due to rotor speed reduction. For high speed flight, profile power is reduced by increasing the rotor as is shown in the optimal rotor speed schedule.

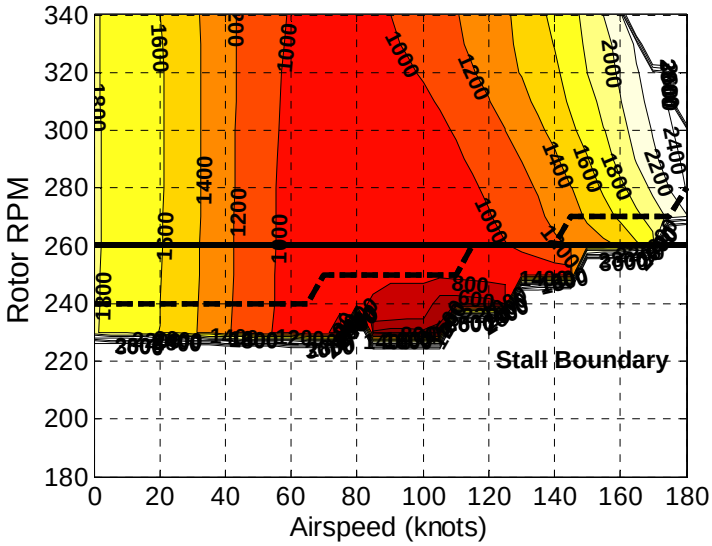

Figure A.7: Induced Power Contours, 18,300 lbs Gross Weight, 12000 feet

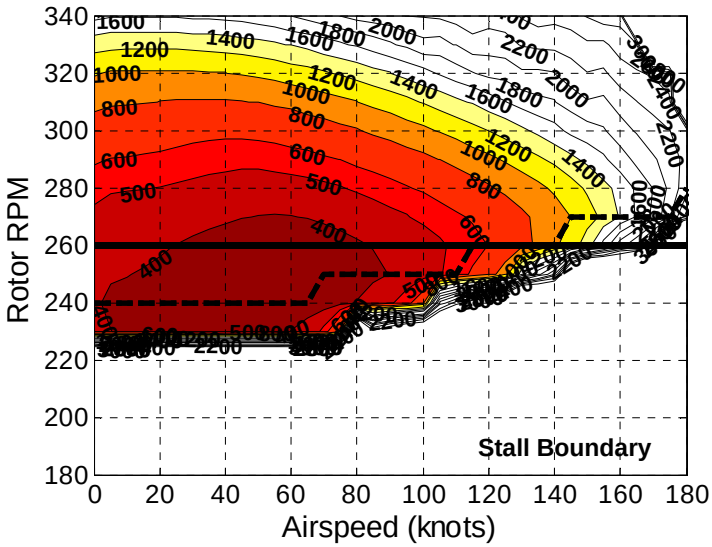

Figure A.8: Profile Power Contours, 18,300 lbs Gross Weight, 12,000 feet

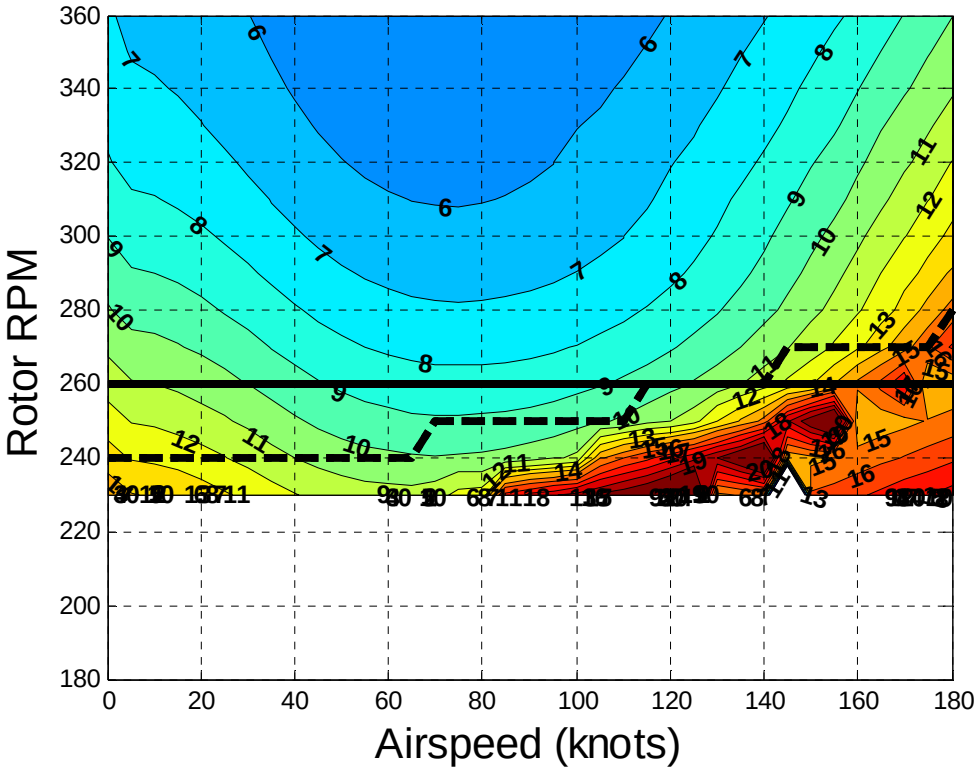

Figure A.9: Main Rotor Collective Pitch, 18,300 lbs Gross Weight, 12,000 ft

16,000 lbs Gross Weight

The altitude simulations with a gross weight of 16,000 lbs show very similar trends to the baseline case above. The power levels are lower than the baseline speed due to the reduction in required thrust. Profile power is lowered slightly as the rotor blades are operating farther from stall than for the heavier case. The most important note is that the optimum rotor speeds for this gross weight are never higher than the baseline RPM. The stall boundary is lower for this gross weight as well.

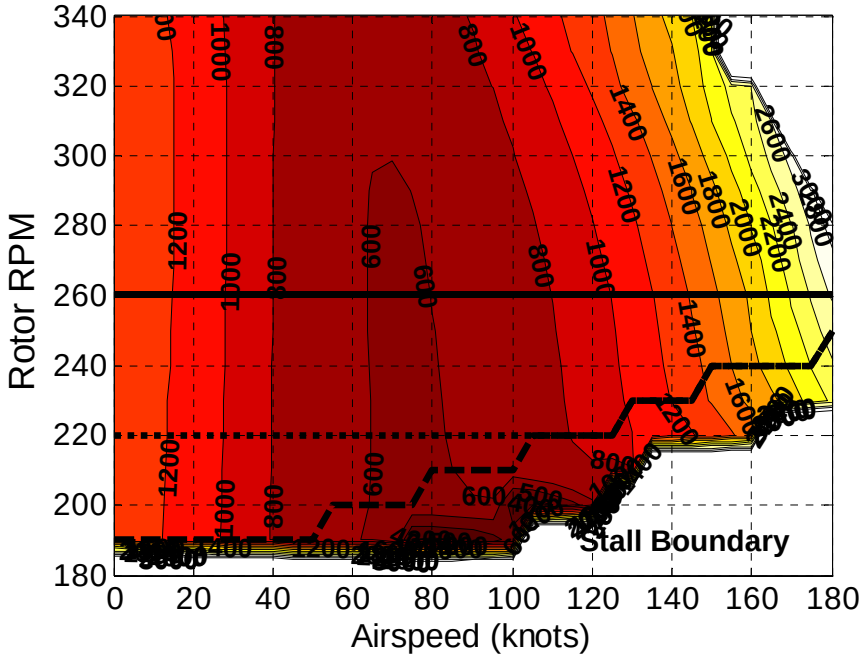

Figure A.10: Induced Power Contours, 16,000 lbs Gross Weight, 4000 feet

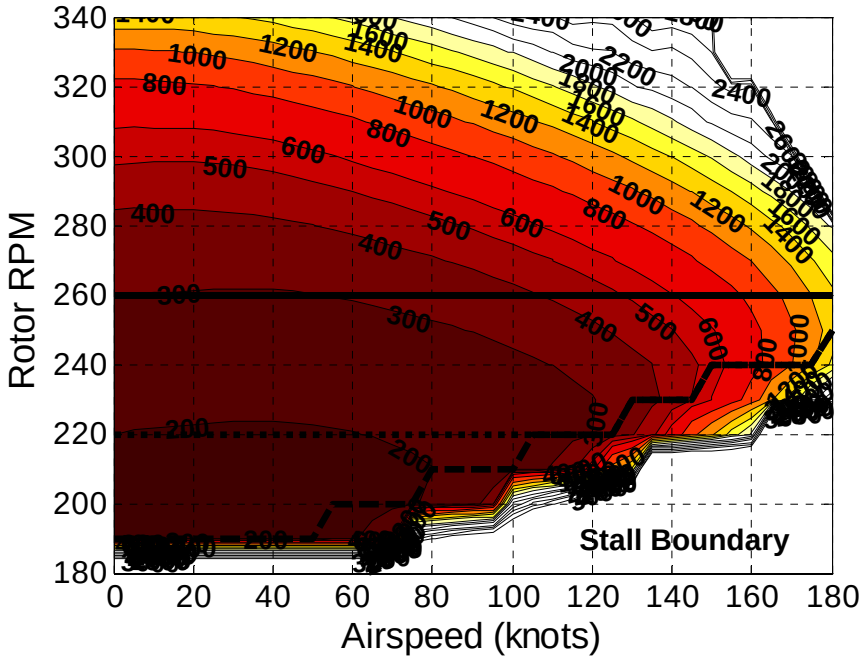

Figure A.11: Profile Power Contours, 16,000 lbs Gross Weight, 4000 feet

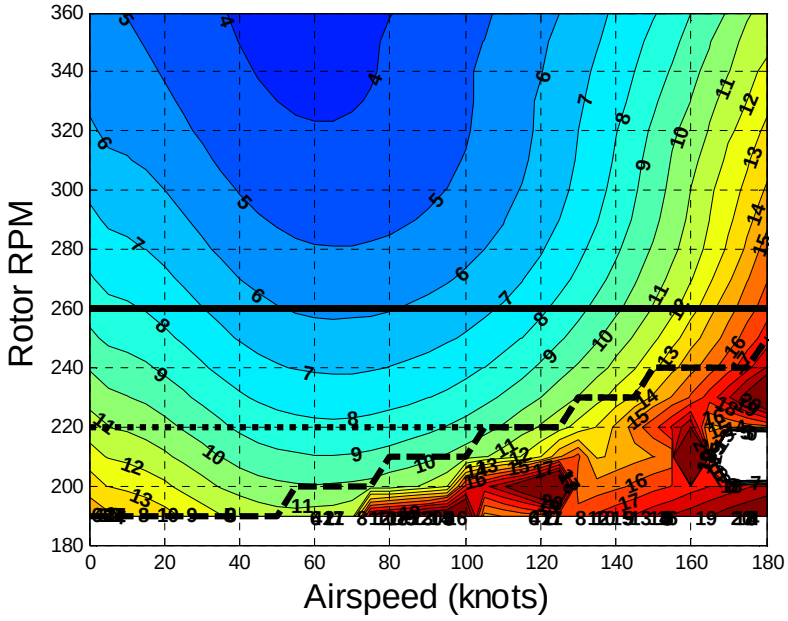

Figure A.12: Main Rotor Collective Pitch, 16,000 lbs Gross Weight, 4000 ft

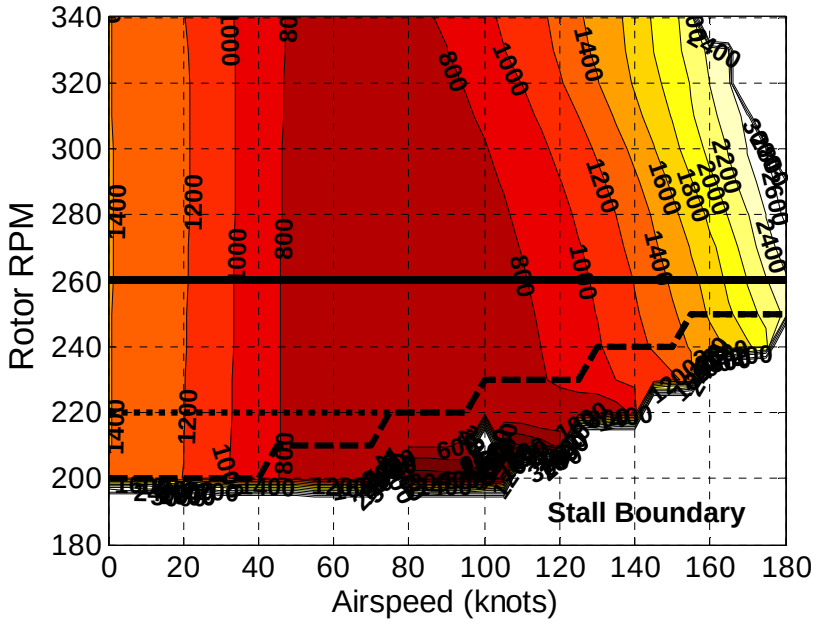

Figure A.13: Induced Power Contours, 16,000 lbs Gross Weight, 8000 feet

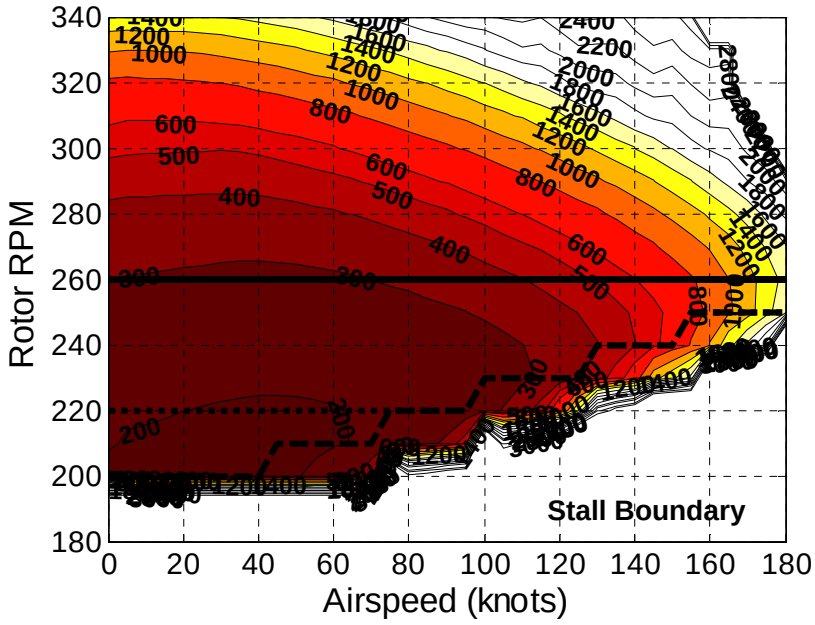

Figure A.14: Profile Power Contours, 16,000 lbs Gross Weight, 8000 feet

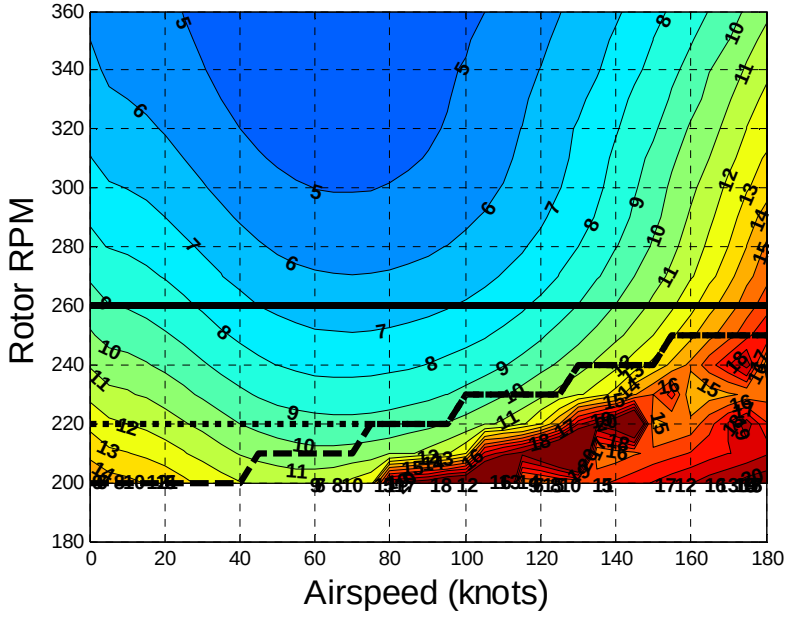

Figure A.15: Main Rotor Collective Pitch, 16,000 lbs Gross Weight, 8000 ft

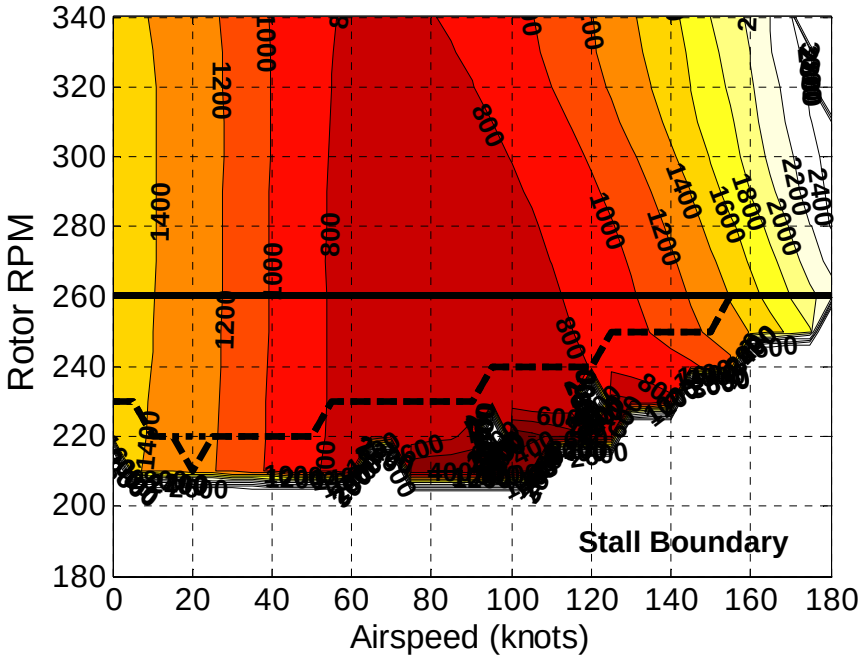

Figure A.16: Induced Power Contours, 16,000 lbs Gross Weight, 12000 feet

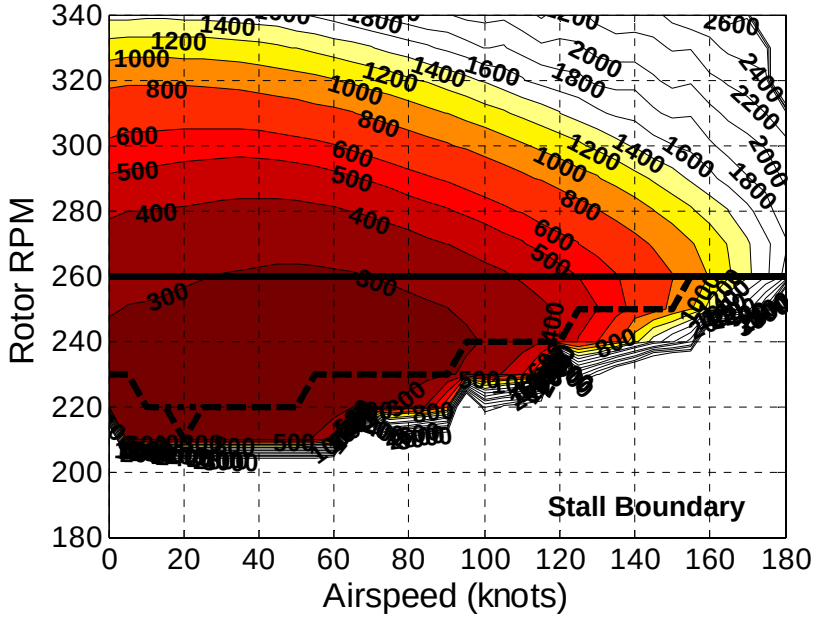

Figure A.17: Profile Power Contours, 16,000 lbs Gross Weight, 12,000 feet

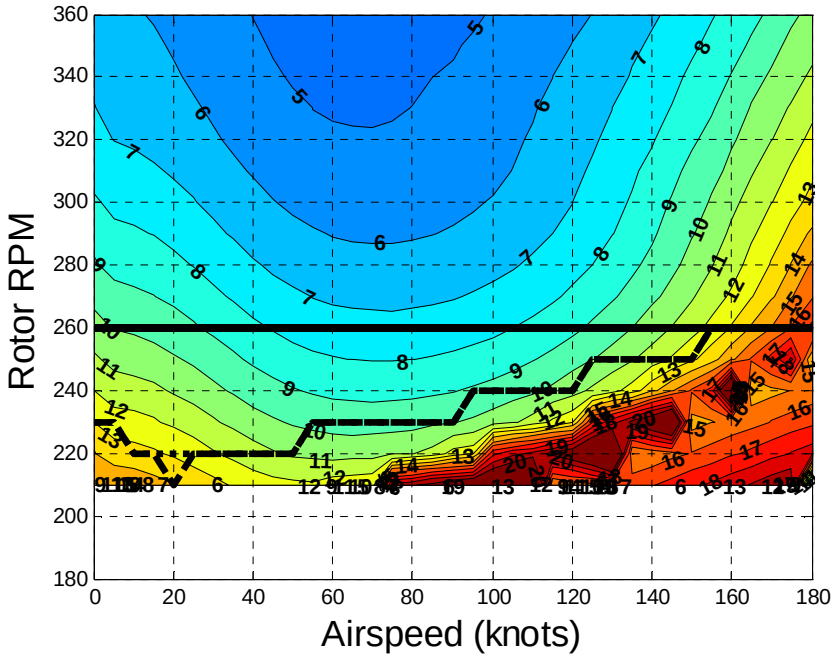

Figure A.18: Main Rotor Collective Pitch, 16,000 lbs Gross Weight, 12,000 ft

22,000 lbs Gross Weight

When vehicle gross weight is increased to 22,000 lbs, power increases significantly. The rotor has to provide more thrust, thus increasing induced power, but this requires that the blades operate closer to stall, resulting in more profile power. As altitude increases, this becomes even more evident. Figure A.20 shows that profile power at 4000 feet is nearly always greater than 400 HP, whereas at the same altitude with a gross weight of 16,000 lbs, the profile power was around 200 HP.

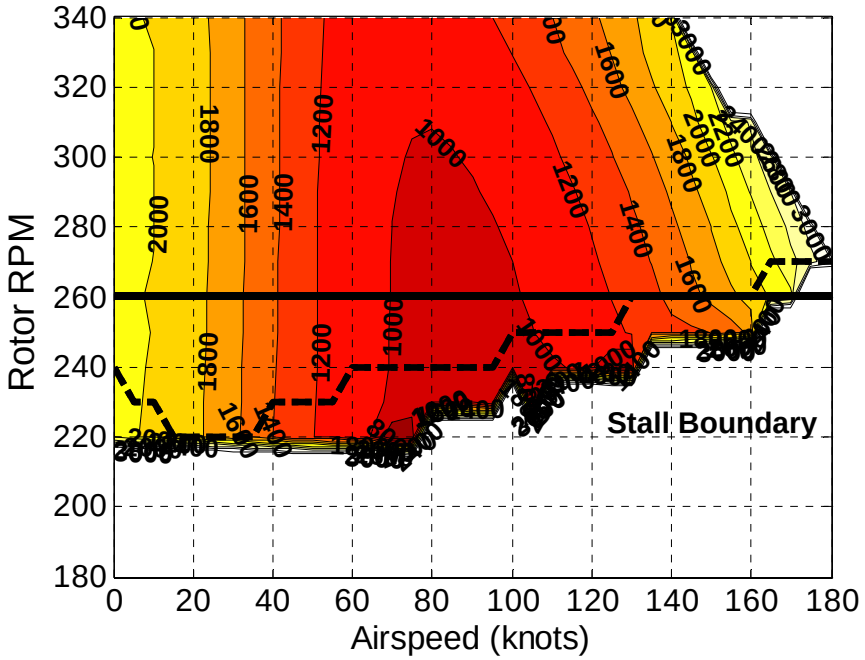

Figure A.19: Induced Power Contours, 22000 lbs Gross Weight, 4000 feet

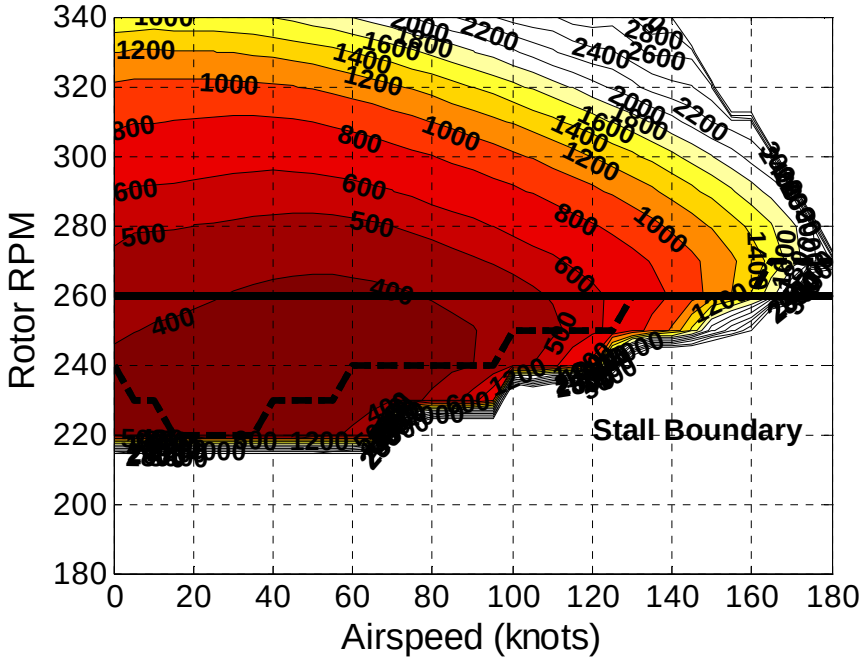

Figure A.20: Profile Power Contours, 22,000 lbs Gross Weight, 4000 feet

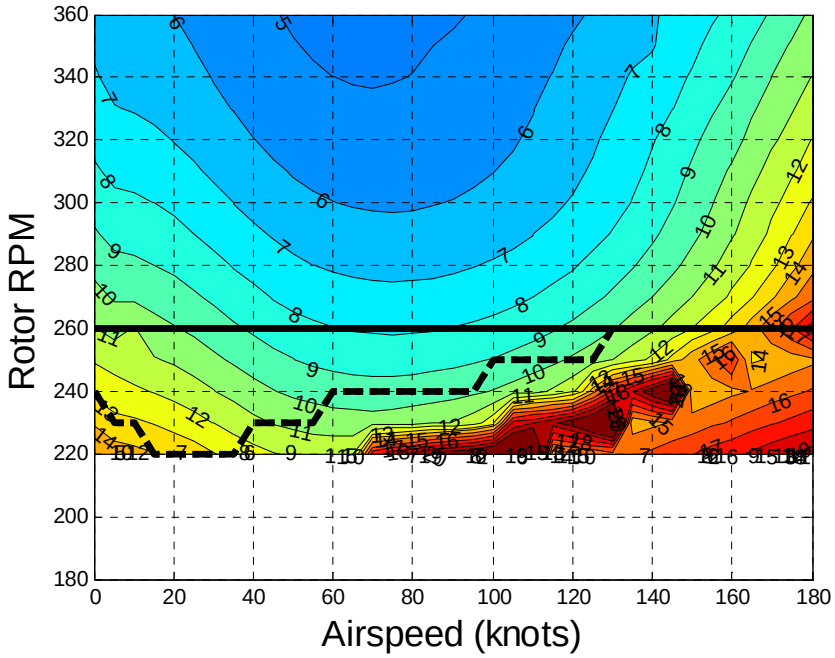

Figure A.21: Main Rotor Collective Pitch, 22,000 lbs Gross Weight, 4000 ft

As altitude and airspeed increase, the rotor speed begins to climb. After 120 knots, the rotor speed increases above the baseline. Main rotor induced power, as seen in Figure A.22, is relatively independent of rotor speed except near stall. Figure A.23 shows that the optimum rotor speed corresponds to the minimum values of profile power for that airspeed.

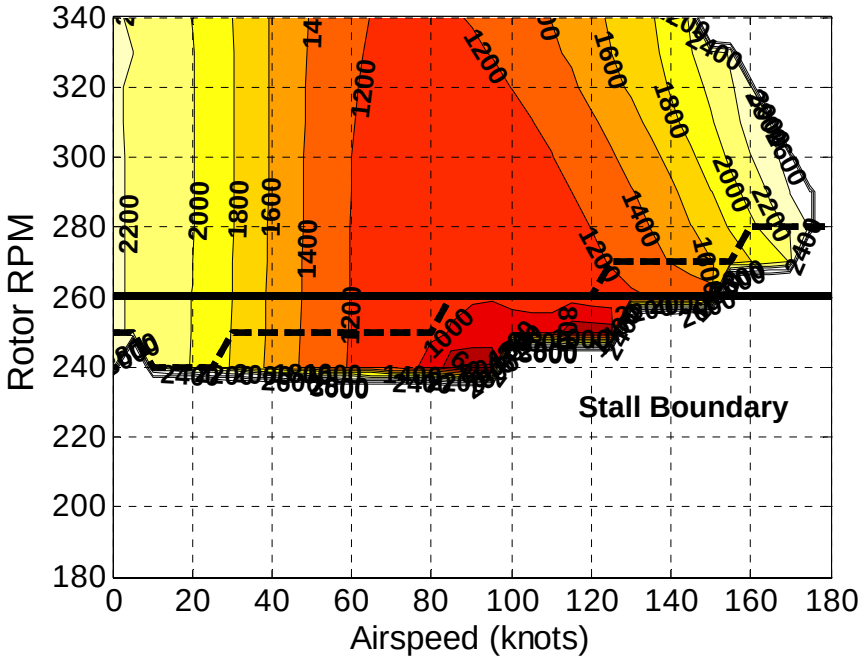

Figure A.22: Induced Power Contours, 22,000 lbs Gross Weight, 8000 feet

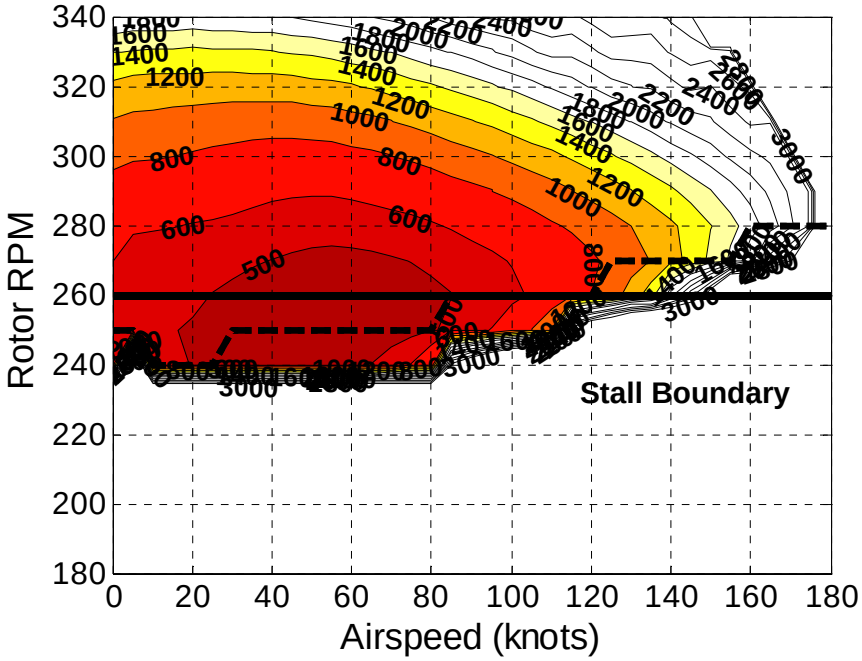

Figure A.23: Profile Power Contours, 22,000 lbs Gross Weight, 8000 feet

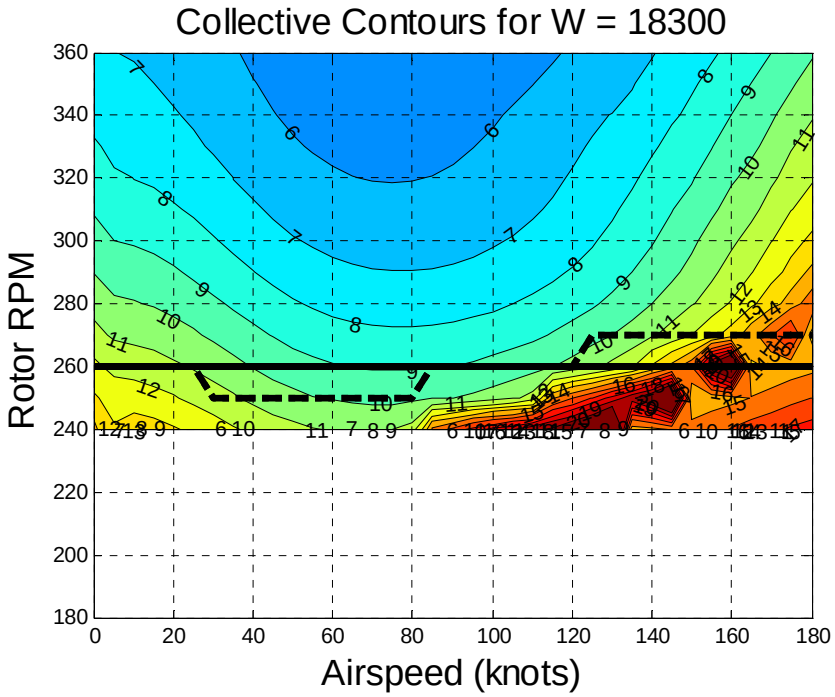

Figure A.24: Main Rotor Collective Pitch, 22,000 lbs Gross Weight, 8000 ft

As altitude increases to 12,000 feet, the optimal rotor speed is greater than the baseline value of 258 RPM for all airspeeds. This rotor speed increase, which would be detrimental for lower weights and altitudes, actually serves to reduce rotor power and increase the operating envelope. The rotor stall boundary is around 258 RPM, so the increase allows the rotor to operate away from stall, resulting in a reduction in profile power.

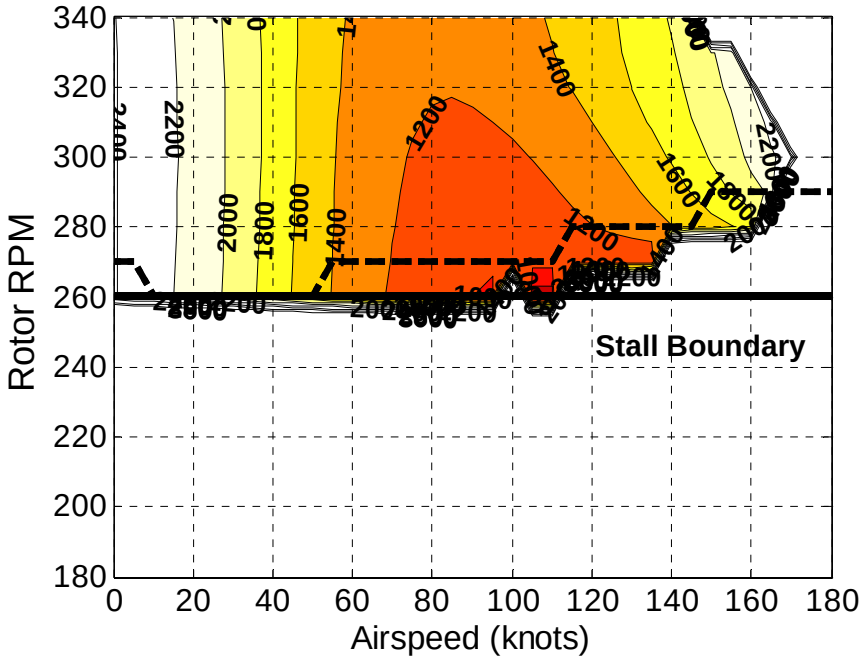

Figure A.25: Induced Power Contours, 22,000 lbs Gross Weight, 12000 feet

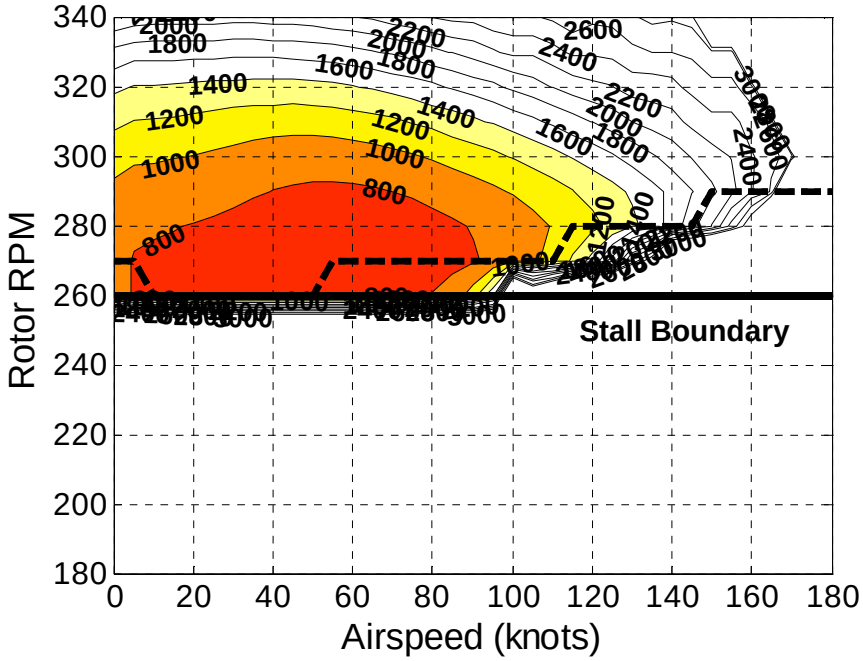

Figure A.26: Profile Power Contours, 22,000 lbs Gross Weight, 12,000 feet

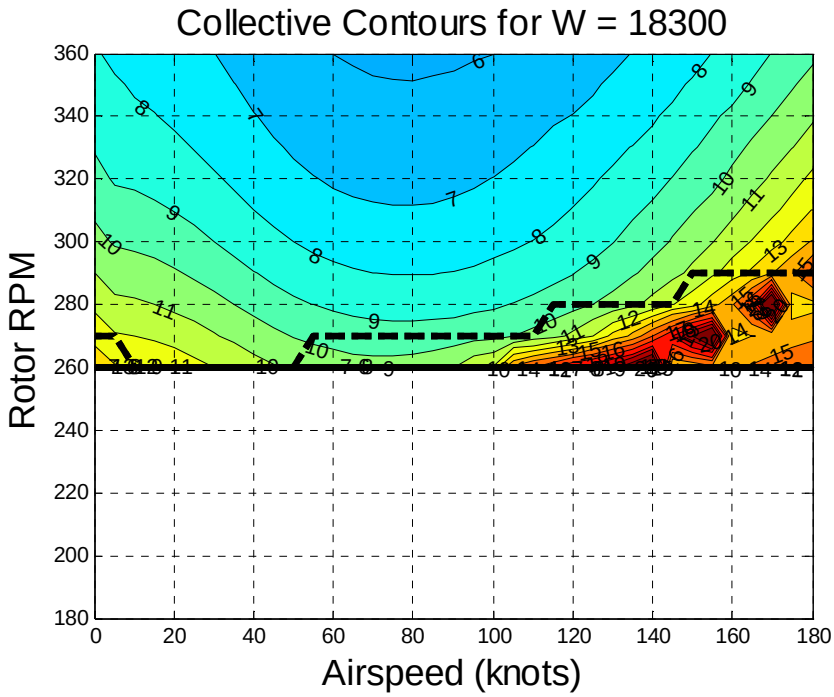

Figure A.27: Main Rotor Collective Pitch, 22,000 lbs Gross Weight, 12,000 ft

Appendix B

Helicopter Properties

As stated in the thesis, the helicopter model used for this simulation was based on the UH-60A for rotor and fuselage geometry. This model includes the non-linear twist distribution of the rotor blades. The model also calculates the blade chord and airfoil profile at each blade station as this is not constant across the blade. The horizontal tail, or stabilator, is modeled as a NACA 0012 airfoil with a an airspeed dependent slew schedule and effective downwash from the rotor.

Table B.1: Helicopter Properties

Weight	W	18300	lbs
Longitudinal CG Offset	x_cg	1.525	ft
Lateral CG Offset	y_cg	0	ft
Vertical CG Offset	z_cg	5.825	ft
Lon. Stabilator offset	x_ht	29.925	ft
Lat. Stabilator offset	y_ht	0	ft
Vert. Stabilator offset	z_ht	5.915	ft
Lon. Tail Rotor offset	x_tr	32.565	ft
Lat. Tail Rotor offset	y_tr	0	ft
Vert. Tail Rotor offset	z_tr	-0.805	ft
distances with respect to the hub			

Table B.2: Rotor Properties

Number of blades	Nb	4	
Radius	R	26.8	ft
Chord	c	1.73*	ft
twist	θtw	varies	
angular velocity	Ω	258	RPM
Shaft tilt	α	3 forward	
Lift Slope		5.73	1/rad
airfoil section		SC1095*	
Lock Numer	γ	6.5344	
Solidity	σ	0.0822	
cd0		0.0076	
kappa	κ	1.15	
blade mass		7.79	slugs
e_B		1.25	ft
e_Z		1.25	ft
root CU		3.83	ft
	*varies spanwise		

Table B.3: Rotor Motion Parameters

Nondimensional Rotating Frequencies		
1st Flap	υ_β	1.04
1st Lag	υ_ζ	2.71
1st Torsion	υ_θ	4.27
Moments of Inertia (slug-ft^2)		
Flapping	I_β	1861
Lag	I_ζ	1861
torsion	I_f	0.978
inertial flap-torsion coupling	I_x	1.5147

Table 2.4: Tail Properties

Horizontal Tail Properties

Area	45	sq. ft.
Reference Lift Coefficient Slope	5.3	
ref Drag coeff	0.04	
index angle	varies	
Airfoil Section	NACA0014	

Tail Rotor Properties

angular Vel	Ωtr	1290	RPM
Radius	R	5.5	ft
Ref. lift curve slope	atr	2pi()	/radian
Cant Angle	φtr	20	degrees

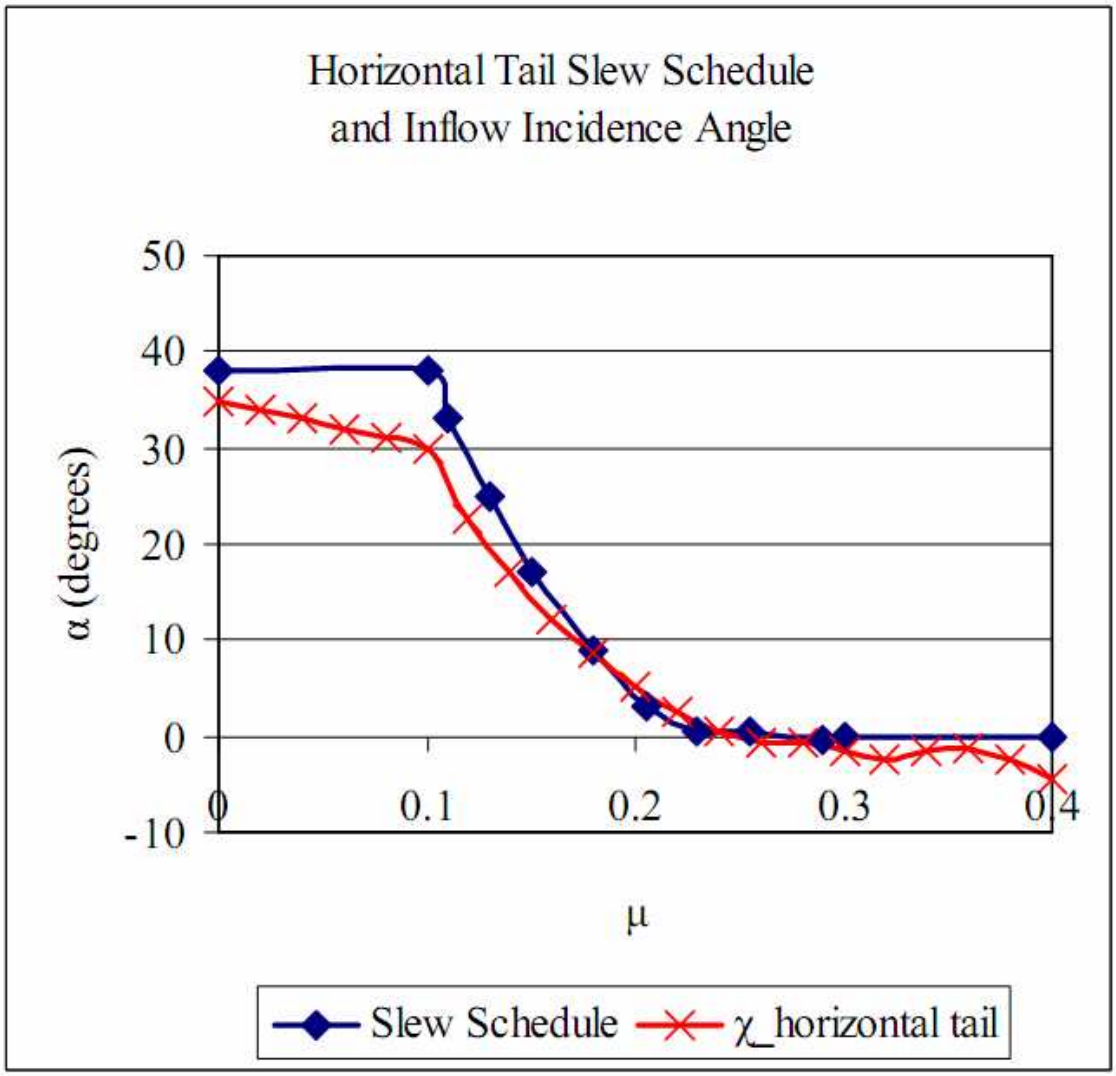

Figure B.1: Horizontal Tail Slew Schedule and Inflow Incidence Angle
(Courtesy of Bluman [10])